

ISTANBUL TECHNICAL UNIVERSITY ★ INFORMATICS INSTITUTE

**SPACE TIME ADAPTIVE PROCESSING (STAP)
IN MULTI INPUT MULTI OUTPUT (MIMO) RADAR**



M.Sc. THESIS

Meysam BEHNAM KHAJEHPASHA

**Department of Communication Systems
Satellite Communication & Remote Sensing Program**

JUNE 2016

ISTANBUL TECHNICAL UNIVERSITY ★ INFORMATICS INSTITUTE

**SPACE TIME ADAPTIVE PROCESSING (STAP)
IN MULTI INPUT MULTI OUTPUT (MIMO) RADAR**



M.Sc. THESIS

Meysam BEHNAM KHAJEHPASHA

705101013

Department of Communication Systems

Satellite Communication and Remote Sensing Programme

Thesis Advisor: Assoc. Prof. Dr. Mesut Kartal

JUNE 2016



İSTANBUL TEKNİK ÜNİVERSİTESİ ★ BİLİŞİM ENSTİTÜSÜ

**ÇOK GİRİŞLİ ÇOK ÇIKIŞLI (ÇGÇÇ)
RADAR LARDA
UZAY ZAMAN ADAPTİF İŞLEME**

YÜKSEK LİSANS TEZİ

Meysam BENAM KHAJEHPAHS

705101013

**İletişim Sistemleri Anabilim Dalı
Uydu Haberleşme ve Uzaktan Algılama Programı**

Tez Danışmanı: Assoc. Prof. Dr. Mesut Kartal

HAZİRAN 2016



Meysam Behnam Khajehpasha, a **M.Sc.** student of ITU **Institute of Informatics** student ID **705101013**, successfully defended the **thesis** entitled **SPACE TIME ADAPTIVE PROCESSING (STAP) IN MULTI INPUT MULTI OUTPUT (MIMO) RADAR**”, which he/she prepared after fulfilling the requirements specified in the associated legislations, before the jury whose signatures are below.

Thesis Advisor: **Assoc. Prof. Dr. Mesut KARTAL**
İstanbul Technical University

Jury Members : **Prof. Dr. Sedef K.PINAR**

Assist. Prof. Dr. Hamid TORPI

Yıldız Technical University

Date of Submission : **02 May 2016**

Date of Defense : **10 June 2016**





To my parents,



FOREWORD

I would like to gratefully acknowledge the enthusiastic supervision of Assoc. Prof. Dr. Mesut Kartal during this work. This research project would not have been possible without your support. Thank you for offering different ideas and perspectives that have enriched the study. Despite lack of time, you have been so caring and supportive, providing guidance and critical insight when I needed.

Foremost, I would like to thank to my beloved Parents for their blessings. I am forever indebted to my parents for their understanding, endless patience and encouragement when it was most required and my sisters for their boundless love, giving me all the support I needed. You are my life's angels, encouraging and supporting me both physically and morally in difficulties. I dedicate this project to you as you are my invaluable precious persons in the world.

My friends have provided much encouragement, support, and laughter over the years. I would like to express my heartfelt thanks to my friends for their help and wishes for the successful completion of this project and for their understandings and morally supports on me in Istanbul.

May 2016

Meysam BEHNAM KHAJEHPASHA



TABLE OF CONTENTS

FORWARD	ix
TABLE OF CONTENT	xi
ABBREVIATIONS	xiii
LIST OF TABLES	xv
LIST OF FIGURES	xvii
SUMMARY	xix
ÖZET	xxi
1. INTRODUCTION	1
1.1 Detection and Ranging.....	1
1.2 Estimation of the Velocity.....	5
1.3 Beamforming.....	9
1.4 Types of RADAR	12
1.4.1 Multistatic radar.....	13
1.4.2 Phased array systems.....	17
1.4.3 Phased-MIMO systems.....	19
2. MIMO RADARS	21
2.1 Coherent MIMO.....	22
2.1.1 Signal scheme.....	23
2.1.2 Improvement of coherent MIMO.....	24
3. SPACE TIME ADAPTIVE PROCESSING IN MIMO RADAR	31
3.1 Overview of STAP and Airborne Clutter.....	31
3.2 STAP in MIMO Radar.....	36
3.2.1 Signal scheme.....	36
3.2.2 Totally adaptive MIMO STAP.....	40
3.2.3 Clutter subspace in MIMO.....	43
3.2.4 Estimation of the clutter subspace (PSWF).....	46
3.3 Novel Stap For Mimo Radar.....	48
3.3.1 Complexity of the novel technique.....	49
3.3.2 Zero-forcing technique.....	50
3.4 Range Recursive Space Time Adaptive Processing (Stap).....	51
3.5 Fast and stable YAST algorithm.....	52
4. SIMULATION RESULTS	57
4.1 Optimum Fully Adaptive STAP.....	62

4.2 FAPI Algorithm in STAP	67
4.3 Fast and stable YAST algorithm Algorithm in STAP	71
REFERENCES	77
CURRICULUM VITAE	79



ABBREVIATIONS

MIMO	:Multiple Input Multiple Output
RCS	:Radar Cross Section
LFM	:Linear Frequency Modulated
ULA	:Uniform Linear Antenna Array
MISO	:Multiple Input Single Output
SIMO	:Single Input Multiple Output
ICM	:Internal Clutter Motion
SINR	:Signal-To-Interference-Plus-Noise Ratio
CNR	:Clutter-To-Noise Ratio
JNR	:Jammer-To-Noise Ratio
GMTI	:Ground Moving Target Indicator
CPI	:Coherent Processing Interval
STAP	:Space Time Adaptive Processing
MVDR	:Minimum Variance Distortionless Response
SMI	:Sample Matrix Inversion
EC	:Eigencanceller
PAST	:Projection Approximation Subspace Tracking
SP	:Subspace Projection
FAPI	:Fast Approximated Power Iteration
YAST	:Yet Another Subspace Tracker



LIST OF TABLES

Page

TABLE.3.1: Parameters list which used in the signal scheme.....	38
TABLE.3.2: FAPI Algorithm.....	52
TABLE.3.3: YAST Algorithm.....	54
TABLE.4.1: Assumption in this model.....	58
TABLE.4.2: Airborne radar system parameters, platform and interference scenario	59





LIST OF FIGURES

	<u>Page</u>
Figure 1.1: Basic radar for detection and ranging.	1
Figure 1.2: Matched filter in the radar receiver.	2
Figure 1.3: LFM signal.....	4
Figure 1.4: Illustration of the Doppler Effect.	5
Figure 1.5: The pulse train.....	6
Figure 1.6: Doppler processing.....	8
Figure 1.7: Range r , azimuth angle θ , and elevation angle \emptyset	9
Figure 1.8: A uniform linear antenna array (ULA).....	10
Figure 1.9: Configuration of Multistatic Radar (Multiple Bistatic).....	13
Figure 1.10: Configuration of Multistatic Radar (Multiple Monostatic).....	14
Figure 1.11: Configuration of Multistatic Radar (Fully Multistatic).....	14
Figure 1.12: Phased Array systems.....	16
Figure 1.13: Transmitter Construction of Phased MIMO Radars	19
Figure 2.1: 4 x 4 MIMO and channel between the transmitter and the receiver example...	21
Figure 2.2: Construction of MIMO Radar receiver.....	22
Figure 2.3: Configuration of Coherent MIMO Radar	23
Figure 2.4: Round trip delays are the same for the Tx/Rx pair and the phantom element....	25
Figure 2.5: One dimensional synthesised linear array of phantom elements.....	26
Figure 2.6: Two dimensional synthesised planar array of phantom elements.....	26
Figure 2.7: Three dimensional synthesised cylindrical array of phantom elements.....	26
Figure 2.8: Configuration of Virtual Receiver Array.....	27
Figure 2.9: Configuration of Virtual Receiver Array.....	27
Figure.3.1: Airborne clutter [17].....	31
Figure.3.2: Geometry of airborne antenna arrays [16].....	32
Figure.3.3: Isodops [16].....	33
Figure.3.4: Isodops and circles of Isorange.....	34
Figure.3.5: Space-time construction of clutter [37].....	35
Figure.3.6: MIMO radar structure with M transmitter and N receiver. The velocity of radar platform motion is v	36
Figure.3.7: Data cube.....	41
Figure.3.8: Range cell.....	42
Figure.3.9: Estimating the space-time interference covariance matrix.....	42
Figure.3.10: An Example of Real part and Magnitude response of Fourier transform of a signal.....	46
Figure 4.1: Platform geometry.....	56
Figure.4.2: optimum fully adaptive STAP of SIMO radar $N=18, M=1, L=18$	60

Figure.4.3: optimum fully adaptive STAP of MIMO radar $N=6, M=3, L=18$	61
Figure.4.4: Principal plane cuts at target azimuth and Doppler of SIMO radar $N=18, M=1, L=18$	62
Figure.4.5: Principal plane cuts at target azimuth and Doppler of MIMO radar $N=6, M=3, L=18$	62
Figure.4.6: optimum fully adaptive STAP of MIMO radar $N=9, M=9, L=18$	63
Figure.4.7: Principal plane cuts at target azimuth and Doppler of MIMO radar $N=9, M=9, L=18$	64
Figure.4.8: optimum fully adaptive STAP of MIMO radar $N=6, M=3, L=36$	64
Figure.4.9: Principal plane cuts at target azimuth and Doppler of MIMO radar $N=6, M=3, L=36$	65
Figure.4.10: FAPI algorithm STAP of SIMO radar $N=18, M=1, L=18$	66
Figure.4.11: FAPI algorithm STAP of MIMO radar $N=6, M=6, L=18$	66
Figure.4.12: Principal plane cuts at target azimuth and Doppler of FAPI algorithm SIMO radar $N=18, M=1, L=18$	67
Figure.4.13: Principal plane cuts at target azimuth and Doppler of FAPI algorithm MIMO radar $N=6, M=3, L=18$	67
Figure.4.14: FAPI Algorithm STAP of MIMO radar $N=9, M=9, L=18$	68
Figure.4.15: Principal plane cuts at target azimuth and Doppler of FAPI algorithm MIMO radar $N=9, M=9, L=18$	68
Figure.4.16: fast and stable YAST algorithm STAP of SIMO radar $N=18, M=1, L=18$	69
Figure.4.17: fast and stable YAST algorithm STAP of MIMO radar $N=6, M=3, L=18$	70
Figure.4.18: Principal plane cuts at target azimuth and Doppler of YAST algorithm SIMO radar $N=18, M=1, L=18$	70
Figure.4.19: Principal plane cuts at target azimuth and Doppler of YAST algorithm MIMO radar $N=6, M=3, L=18$	71
Figure.4.20: YAST Algorithm STAP of MIMO radar $N=9, M=9, L=18$	71
Figure.4.21: Principal plane cuts at target azimuth and Doppler of YAST algorithm MIMO radar $N=9, M=9, L=18$	72
Figure.4.22: SINR for the optimum and FAPI STAPs.....	73
Figure.4.23: SINR for the optimum and YAST STAPs.....	73

SPACE TIME ADAPTIVE PROCESSING (STAP) IN MULTI INPUT MULTI OUTPUT (MIMO) RADAR

SUMMARY

A system that uses electromagnetic waves to detect, locate and measure the velocity of reflecting objects like aircraft, ships, spacecraft, automobile, people, weather formations and terrain, called RADAR. It broadcast the electromagnetic waves into territory and receives the repetition reflected from objects. Applying signal processing algorithms on the reflected waveform, detected the reflecting objects. Furthermore, the position and the velocity of the objects can also be approximate. Initial radar development was particularly driven by military and military is still the prevalent user and planner of radar technology. Military utilization include surveillance, navigation, and weapon guidance. However, now extended radar applications include meteorological precipitation, measuring ocean surface waves, air traffic control, police detection of speeding traffic, sports radar speed guns, and preventing car or ship collisions.

The original contribution of this thesis is a multiple-input multiple-output (MIMO) generalization of space-time adaptive processing (STAP) to mitigate spread Doppler clutter returns in radar. Multi input multi output (MIMO) radar is a radar system with multiple receive and transmit antennas, that can transmit independent waveforms on each transmit elements. Although many traditional multi-antenna radar concepts such as phased- array, receive beamforming, synthetic aperture radar (SAR), polarimetry and interferometry can be seen as special cases of MIMO radar, the distinct advantage of a multi-antenna radar system with independent transmit waveforms is the increased number of degrees of freedom leading to improved resolution and performance in detection and parameter estimation tasks.

MIMO radar obtains important potentials for fading reduction, resolution augmentation, and interference and jamming elimination. Exploiting these potentials can reaction in greatly improved target detection, parameter estimation, target tracking and recognition performance. Uses MIMO technology in RADAR has quickly drawn remarkable attention from many researchers. Various advantages of MIMO radar have been recognized by many different scientists like enhanced diversity of the target data, superior interference rejection sufficiency, improved parameter identifiability, and increase flexibility for transmit beampattern layout. The degrees of freedom introduced by MIMO radar develop the performance of the radar schemes in many distinct aspects. Although, it also turn out some issues. It increases the number of dimensions of the received signals. As a consequence, this increases the complexity of the receiver. Furthermore, the MIMO radar transmits an incoherent waveform on each of the transmitting antennas. This approximately reduces the processing gain related to the phased array radar. The numerous ideal waveforms also affects the range and Doppler resolution of the radar system.

A promising application of MIMO radar is the identification of slowly moving targets using airborne MIMO radar platforms. The advantage of using MIMO in this configuration is its ability to synthesize a larger virtual array with relatively fewer antennas. This allows higher spatial resolution and better separation of returns from ground clutter and targets. The space-time adaptive processing (STAP) methods originally developed for Single-input, Multiple-output (SIMO) radar are applicable to

MIMO radar systems after proper pre-processing of the received signals. The performance of STAP algorithm critically hinges on the structure of the clutter covariance matrix; therefore, MIMO STAP methods will benefit greatly from theoretical and empirical study of the clutter statistics.

Of specific concern is clutter subject to multipath distribution between receive and transmit arrays. Considerable multipath clutter can appear in over-the-horizon (OTH) radar info when ocean or ground surface reflects undergo multiple ionospheric scattering that cause significant wavenumber spreads and Doppler frequency. In such situation, traditional single-input multi-output (SIMO) STAP cannot relieve Doppler spread mainlobe clutter without repressing the target.

With a little remodeling, space time adaptive processing methods expanded basically for the single input multiple output radar systems (phased array radar) can also be utilized in multiple input multiple output radar system. Although, in the MIMO radar system, the rank of the interference subspace becomes extra-large, particularly the jammer and clutter subspace. It impress both the convergence and complexity the of the STAP performance.

After reconsidering the advantages and drawbacks of the extended MIMO-STAP, namely the sample matrix inversion (SMI) and eigencanceller (EC), fast approximated power iteration (FAPI) algorithms, we propose fast and stable YAST algorithm the range recursive algorithm as an alternative to resolve the convergence and complexity problems.

YAST algorithm novelty is the lower computational cost and the extension to minor subspace tracking. Although, the initial performance of the YAST algorithm suffered from a numerical balance issue (the subspace weighting matrix moderately loses its orthonormality). Hence in this thesis we applied a novel execution of YAST, whose stability is fixed theoretically and tested via computer simulation in space time adaptive processing in MIMO radar. This algorithm fuses all the favor confidants for a subspace tracker: significantly linear complexity, lowest steady state error, high convergence rate and numerical stability concerning the orthonormality of the subspace weighting matrix.

The contribution of this work can be summarized in four parts. First, we present the basic review of the detection and ranging in radar system. Multistatic and Phased Array Radar scheme are explained and covered to compare those systems with MIMO Radar. Then, we totally covered the coherent MIMO radar systems and its difference with phased array radar or SIMO, signal model and advancement that coherent MIMO radar systems offer such as high resolution and parameter identifiability. In the third part we briefly explain space-time adaptive processing (STAP) in MIMO radar. Then we discuss about different algorithms of STAP in MIMO radar as if sample matrix inversion (SMI), eigencanceller (EC), fast approximated power iteration (FAPI) and fast and stable YAST. Ultimately we introduced outcomes of the simulations which have been performed in this thesis study and these simulations present STAP efficiency of various MIMO radar composition.

ÇOK GİRİŞLİ ÇOK ÇIKIŞLI RADAR LARDA UZAY ZAMAN ADAPTİF İŞLEME

ÖZET

Radar elektromanyetik dalgaları kullanarak, uçaklar, gemiler, uzay araçlar, arabalar, insanlar, hava oluşumları, ve arazi gibi nesnelere tespit eden, konumunu ve hızını belirleyen bir sistemdir. Radar belirli bir alana elektromanyetik dalgalar iletir ve nesnelere yansıyan yankı sinyalini alır. yansıyan dalgaya sinyal işleme algoritmaları uygulayarak, yansıyan nesnelere tespit edilebilir. Bundan başka, nesne hızını ve konumunu da tahmin edilebilir. Başlangıçta radar sadece askeri amaçla geliştirildi, ve hala en yaygın kullanıcı ve radar teknoloji geliştiricisi askeri birimlerdir. Askeri uygulamalara gözetim, navigasyon ve silah rehberliği dahildir. Ancak, radar artık meteorolojik yağış tespiti, okyanus yüzey dalgalarını ölçme, hava trafik kontrolü, trafik hızın polisi tespiti ve araç veya gemi çarpışmaları önleyen uygulamalar gibi daha geniş bir yelpazeye sahiptir.

Bu tezin asıl katkısı çoklu giriş çoklu çıkış (MIMO) radarlarda yansıyan yayılmış doppler yığılmayı hafifletmek için uzay-zaman adaptif işleminin (STAP) geliştirilmesidir. Çok girişli çok çıkışlı (MIMO) radar, birden fazla alıcı ve verici antenlerden oluşan ve her iletim elemanları üzerinde bağımsız dalga formları iletebilen bir radar sistemidir. Birçok geleneksel çoklu anten radar kavramları, fazlı-dizi, sentetik açıklıklı radar (SAR), polarimetri ve enterferometre gibi, MIMO radarın özel bir tasarım şekli gibi gözüksede, Bağımsız dalga iletebilen çok antenli radar sisteminin belirgin avantajı, serbestlik derecesi sayısının artışından kaynaklanan algılama ve parametre tahmin görevlerinde çözünürlük ve performansın Geliştirilmesidir.

MIMO radar, solma azaltma, çözünürlük geliştirme, ve parazit bastırma gibi görevlerde önemli potansiyellere sahiptir. Bütün bu potansiyellerden faydalanarak hedef tespiti, parametre kestirimi, hedef izleme ve tanıma performansında önemli ölçüde geliştirilmeye neden olabilir. MIMO radar teknolojisi hızla birçok araştırmacının büyük ilgisini çekmiştir. MIMO radarın birçok avantajı, hedef bilgilerinin çeşitlilik artışı, mükemmel parazit ret yeteneği, parametre tanımlama gelişmesi ve gönderme beampattern tasarımı için esneklik sağlamak gibi birçok farklı araştırmacılar tarafından tespit edilmiştir. MIMO radar tarafından tanıtılan serbestlik dereceleri çok farklı yönlerde radar sistemlerinin performansını artırır. Ancak, aynı zamanda bazı sorunlar oluşturur. Bu alınan sinyaller boyutlarının sayısını artırır. Sonuç olarak, bu alıcının karmaşıklığını artırır. Ayrıca, MIMO radar vericisi antenlerinden birbirinden tutarsız bir dalga biçimi iletir. Buda genellikle işlem kazancı, faz dizili radar ile karşılaştırıldığında azaltır. Birden fazla keyfi dalga şekilleri de radar sisteminin menzil ve Doppler çözünürlüğü etkiler.

MIMO radarın umut verici bir uygulaması uçuşan MIMO radar platformları kullanarak yavaş hareket hedeflerin belirlenmesidir. Bu yapılandırmada MIMO kullanmanın avantajı, daha az antenler ile daha büyük bir sanal dizi sentezleme yeteneğidir. Bu yüksek uzaysal çözünürlüğü hemde zemin yığılma ile hedeflerden gelen yansımaların daha iyi ayrılmasını sağlar. başlangıçta Tek giriş, Çoklu-çıkış (SIMO) radar için geliştirilmiş uzay-zaman adaptif işleme (STAP) yöntemleri, alınan sinyallerin doğru işlendikten sonra MIMO radar sistemleri için geçerlidir. STAP algoritmasının performansı kritik esas noktası kovaryans matrisinin yapısıdır; Bu nedenle, MIMO STAP yöntemleri dağınkılık istatistiklerinin teorik ve deneysel çalışmalarından büyük ölçüde yararlanacaktır.

Özel ilgi konusu, dağınkılığın iletim ve alıcı dizilereden çok yönlü yayımlara maruz kalmasıdır. Zemin ya da okyanus yüzeyinden yansıyan çoklu ionosferik saçılmaları ile, en önemli ufuk ötesi (OTH) çoklu dağınkılık radar verileri elde edilebilir buda önemli yayılmış Doppler frekansı ve dalga sayılarına neden olur. Bu durumda, geleneksel tek-giriş çoklu çıkış (SIMO) STAP doppler yayılım mainlobunu belirli hedefi bastırmadan azaltamıyor.

Hafif bir değişiklik yaparak başlangıçta tek giriş çoklu çıkış (SIMO) radar (faz dizili radar) da geliştirilen STAP yöntemleri MIMO radar da bile kullanılabilir. Ancak, MIMO radar da, jammer-ve-clutter altuzayın rütbesi, çok büyük olur. Özellikle jammer alt uzay. Bu STAP algoritmasının karmaşıklığı ve yakınsamasını etkiler. Genişletilmiş MIMO-STAP avantaj ve dezavantajları tekrar ele aldıktan sonra yani örnek matris dönüşümü (SMI) ve eigencanceller (EC), hızlı yaklaştırılır güç iterasyon (FAPI) algoritmaları, Biz yakınsama ve karmaşıklığı sorunlarını çözmek için bir alternatif aralığı özyinelemeli algoritması olarak hızlı ve istikrarlı YAST algoritmasını önermişiz.

YAST algoritması özelliği, düşük hesaplama maliyet (lineer eyer veri korelasyon matrisi son zamanlarda adlandırılan shift-değişmezlik özelliğini tatmin ediyorsa) ve küçük alt uzay izleme uzantısı idi. Ancak, YAST algoritmasının orijinal uygulanması sayısal stabilite probleminden rahatsızdı. (Alt uzay ağırlık matrisi yavaşça orthonormalite kaybeder). Biz bu nedenle bu tezde istikrarlığı kurulmuş, teorik olarak ve sayısal simülasyonlar ile test edilmiş, yeni bir YAST uygulaması kullandık. Bu algoritma, bir alt uzay izci için istenen tüm özellikleri birleştiriyor: oldukça yüksek yakınsama hızı, düşük kararlı hal hatası, lineer karmaşıklığı ve alt uzay ağırlık matrisi ortonormallik ile ilgili sayısal stabiliti.

Bu çalışmanın katkısı dört bölümden özetlenebilir. İlk olarak biz radar da hedef algılama va menzil belirleme temel değerlendirmesini sunucuz. Multistatik Radar Sistemleri incelenir ve okuyuculara MIMO Radar ve Phased Array Radar sistemlerini karşılaştırmak için Phased Array Radar anlatılacak. İkincisi, biz tamamen tutarlı MIMO radar konseptini ve onun SIMO veya faz dizi radarı ile farkını, Sinyal modeli ve tutarlı MIMO radar sistemlerin, yüksek çözünürlük ve parametre tanımlanabilir gibi

özellikleri sunucuz. Üçüncü bölümde ise kısaca MIMO radar uzay-zaman uyarlamalı işlemi (STAP) açıklanacak. Sonra biz MMO radar larda farklı STAP algoritmalarını, örnek matris dönüşümü (SMI), eigencanceller (EC), hızlı yaklaşırlır güç iterasyon (FAPI) ve hızlı ve istikrarlı YAST, tartışcaz. En sonda Bu tez çalışmasında yapılan simülasyonların sonuçları tanıtılacak ve simülasyonlar farklı MIMO radar yapılandırmaların performansını sunmak için yapılmaktadır.





1. INTRODUCTION

In this part, we survey essential ideas from radar and quickly portray the real aftereffects of every section. The chapter is organized as follows: Section 1.1 gives the fundamental audit of the detection and ranging in radar system. Section 1.2 reviews estimation of the velocity in radar. Section 1.3 we will talk about beamforming. In Section 1.4 Multistatic Radar Systems are analyzed, and Phased Array Radars are covered to give the peruser the chance to contrast those frameworks and MIMO Radar.

1.1 Detection and Ranging

Detection and Recognition is the most crucial capacity of a radar framework. In the wake of radiating the electromagnetic waveform, the radar gets the reflected sign. To identify the objective, it is important to recognize the signal reflected from the objective, from the signal containing just noise. In the wake of recognizing the objective, one can further calculate the range. In the radar community the word range is utilized to demonstrate the separation between the radar framework and the objective.

Consider a monostatic radar system with one antenna as shown in Fig. 1.1. The radar emits a waveform $u(t)$ into the space. The waveform hits the objective situated in range r and returns to the receiving antenna. After demodulation, the received signal can be represented as [1]

$$\alpha u\left(t - \frac{2r}{c}\right) + v(t). \quad (1.1)$$

Where c is the velocity of wave propagation, r is the range of the objective, $v(t)$ is the additive noise, and α indicates the amplitude response of the objective. The amplitude response α is defined by the radar cross section (RCS) of the target, the range r of the target, the angle of the target and the beampattern of the antenna. In the receiver, a matched filter is generally connected to improve the signal to-noise ratio (SNR). Output of matched filter can be expressed as

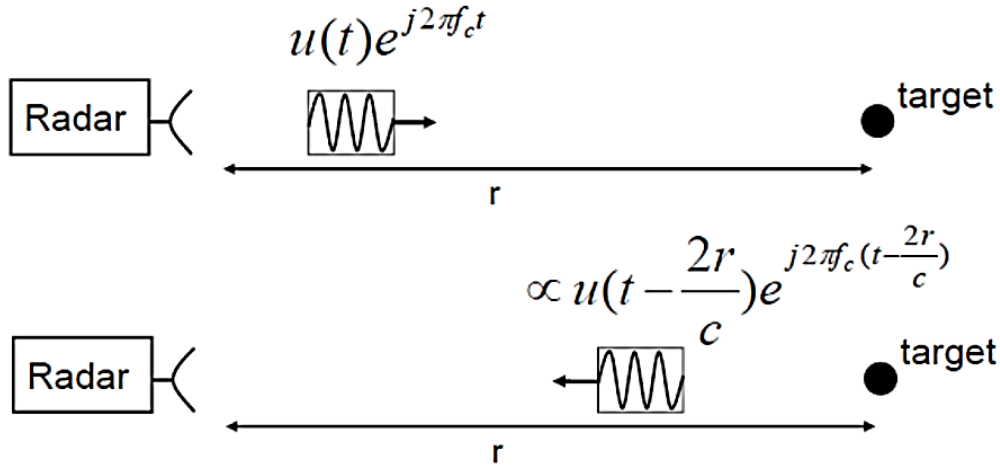


Figure 1.1: Basic radar for detection and ranging.

$$\begin{aligned}
 y(\tau) &= \int_{-\infty}^{+\infty} a u\left(t - \frac{2r}{c}\right) u^*(t - \tau) dt + \int_{-\infty}^{+\infty} u(t) u^*(t - \tau) dt \\
 &= a r_{uu}\left(t - \frac{2r}{c}\right) + \int_{-\infty}^{+\infty} u(t) u^*(t - \tau) dt.
 \end{aligned} \tag{1.2}$$

Where the autocorrelation function of $u(t)$ is $r_{uu}(\tau) = \int_{-\infty}^{+\infty} u(t) u^*(t - \tau) dt$. The input output relation is displayed in Fig.1.2. To figure out if there is an objective, the matched filter yield sign is checked at a particular time moment τ_0 . If $r_{uu}(\tau) > \eta$ for a predetermined threshold η , at that point the radar framework reports that it has found an objective. There is a trade-off between false alarm rate and detection rate when choosing the threshold η [2]. Small threshold η enhances the discovery rate additionally increases the false alarm rate. Then again, large threshold reduces the false alarm rate additionally diminishes the discovery rate. In the wake of identifying the objective, one can encourage decides the range of the objective. For a simple point target, the range of the objective can be obtained by

$$r = \frac{1}{2} \tau_0 c. \tag{1.3}$$

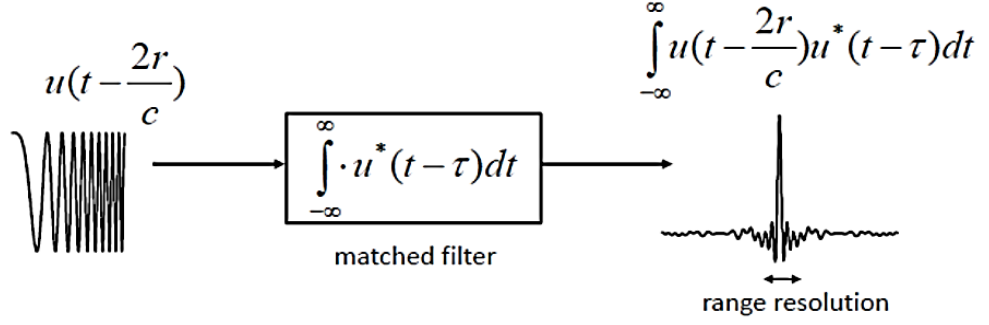


Figure 1.2: Matched filter in the radar receiver.

Where τ_0 is the time moment at which the matched filter yield surpasses the threshold. For the case of numerous objectives, the matched filter output signal can be written as

$$y(\tau) = \sum_{i=0}^{N_t-1} \alpha_i r_{uu} \left(\tau - \frac{2r_i}{c} \right) + \int_{-\infty}^{+\infty} u(t) u^*(t - \tau) dt. \quad (1.4)$$

While N_t is the number of targets, α_i is the reflected signal amplitude of the i th target and r_i is the range of the i th target. To have the capacity to recognize these targets, the autocorrelation function $r_{uu}(\tau)$ has to be a narrow pulse in order to diminish the interferences coming from different targets. A narrow pulse in time-domain has a widely spread energy in its Fourier transform and vice versa. Accordingly to get a thin pulse $r_{uu}(\tau)$, one can elect the waveform $u(t)$ so that the energy of the Fourier transform of $r_{uu}(\tau)$ is widely spread. We can express Fourier transform of the autocorrelation function $r_{uu}(\tau)$ as

$$S_{uu}(j\omega) = |U(j\omega)|^2. \quad (1.5)$$

Where $U(j\omega)$ is the Fourier transform of the waveform $u(t)$. Hence, one can elect $u(t)$ so that its energy is broadly spread over various frequency segments.

Another critical attractive property of the transmitted waveform is the consistent modulus property. The consistent modulus property permits the antenna to always work at the same power. This maintains a strategic distance from the utilization of costly amplifiers, and the nonlinear impact of the amplifiers. One great applicant that has widely spread energy in the frequency domain furthermore fulfills the consistent modulus property is the linear frequency modulated (LFM) waveform. It is also called the chirp waveform. We can express LFM waveform as

$$u(t) \propto \begin{cases} e^{j2\pi f_c t} e^{j\pi k t^2}, & 0 \leq t < T \\ 0, & \text{otherwise.} \end{cases} \quad (1.6)$$

Where f_c is the carrier frequency, T is the span of the signal and k is the parameter that defines the bandwidth of the signal. The instantaneous frequency of the LFM waveform obtains from derivative of the phase function

$$\frac{1}{2\pi} \frac{d(2\pi f_c t + \pi k t^2)}{dt} = f_c + kt. \quad (1.7)$$

So kT is the approximate bandwidth of the LFM signal. The autocorrelation function of the linear frequency modulated (LFM) waveform can be approximated as [3]

$$r_{uu}(t) \cong \begin{cases} \left| \frac{\sin(\pi k T \tau (1 - \frac{|\tau|}{T}))}{\pi k T \tau} \right|, & 0 \leq t < T \\ 0, & \text{otherwise.} \end{cases} \quad (1.8)$$

Fig.1.3 shows the linear frequency modulated (LFM) waveform and the corresponding autocorrelation. The first zero-crossing of the autocorrelation function $r_{uu}(t)$ appears at the point $1/kT$. So the waveform has been “compressed” after the matched filtering from the primary width T to $1/kT$. This effect is termed pulse compression. The proportion between the primary width and the compressed width is defined as the compression ratio. We can express it as

$$T / \frac{1}{kT} = kT^2. \quad (1.9)$$

We have previously specified that kT is the bandwidth of the LFM signal. Hence the time-bandwidth product of the LFM signal is $kT^2 = (kT) \cdot T$. T is the time-bandwidth product of the linear frequency modulated (LFM) signal. In this way the resolution of a radar system radiating LFM waveform is specified by the time-bandwidth product of the linear frequency modulated (LFM) waveform.

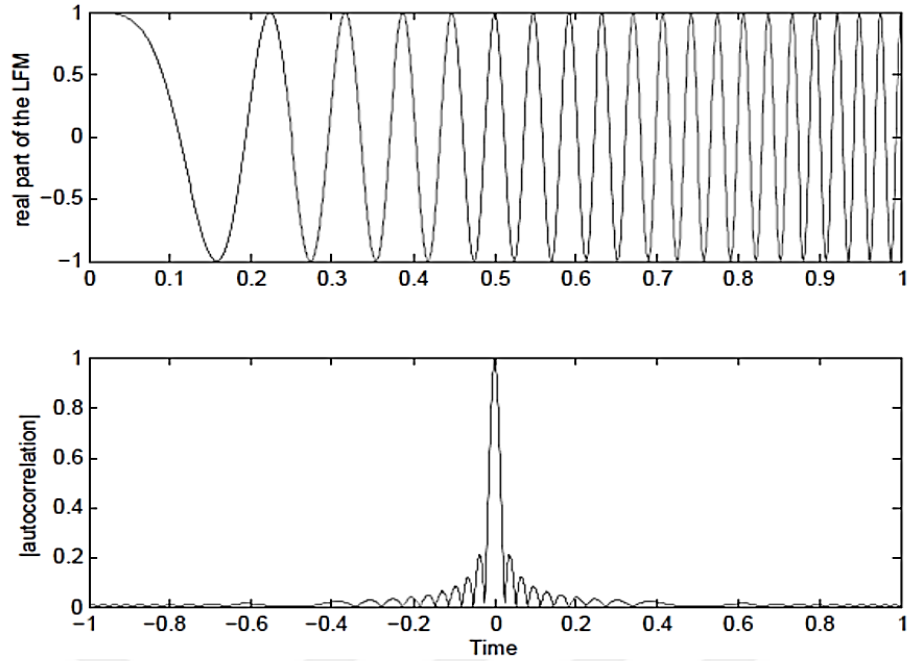


Figure 1.3: The LFM signal: (a) real part of an LFM waveform and (b) Fourier transform magnitude of the LFM waveform.

Another incredible advantage of the LFM sign is that it can be effortlessly created by circuits [4]. Indeed, LFM sign can even be found in some natural "radar framework, for example, the ultrasonic frameworks of bats and dolphins.

1.2 Estimation of the Velocity

Radar system can be utilized to further measuring the speed of an item besides detection and ranging. For instance, police speed radar measures the speed of moving vehicles. Also the radar systems can filter out the unwanted reflected signals by using the velocity information. For instance, for a radar system worked to distinguish flying items, for example, air ships or rockets, clouds will be the undesirable reflected signs. In radar community, this sort of undesirable sign is called clutter. In the majority of the case, the clutter can be very strong. Sometimes it may go up to 35 to 45 dB over the target signal. Fortunately, one can use the velocity information to filter it out because the clutter objects are usually still or moving slowly. We will clarify how radar frameworks acquire the velocity information.

Consider a monostatic radar system with one transmitter and receiver antenna and a moving target as appeared in Fig. 1.4. The target at an angle θ moves with the velocity v as shown in the figure. A narrowband waveform $u(t)e^{j2\pi f_c t}$ are emitted from radar

system. Here narrowband means the carrier frequency f_c is much larger than the bandwidth of the signal. The waveform hits the moving target at range r and returns to the antenna. After demodulation, the received waveform can be defined as

$$\alpha u\left(t - \frac{2r}{c}\right) e^{j2\pi f_D t} + v(t). \quad (1.10)$$

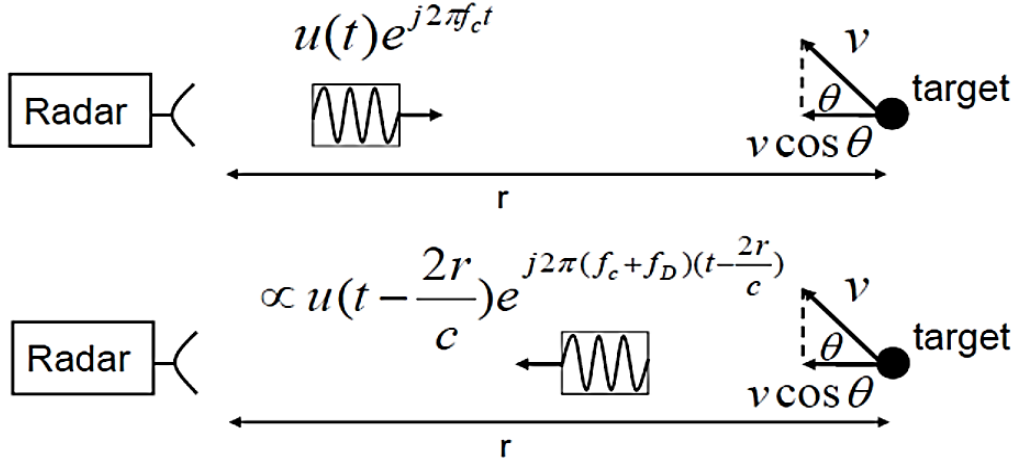


Figure 1.4: Illustration of the Doppler Effect.

Where $v(t)$ denotes the noise in the receiver, α is the amplitude response of the target and f_D is the Doppler frequency. We can express the Doppler frequency as [3]

$$f_D = \frac{c+v \cos\theta}{c-v \cos\theta} f_c \cong \frac{2v \cos\theta}{c} f_c. \quad (1.11)$$

Note that the carrier frequency f_c is much larger than f_D because the speed of light is usually much larger than the velocity of the object v . Along these lines, to viably evaluate the small Doppler frequency f_D , we will require a longer time window. One approach to accomplish this is to transmit various pulses. As shown in Fig. 1.5 these pulses can involve a longer time window. Along these lines they give better Doppler frequency resolution. Additionally, the computational complexity for processing pulses is much smaller than processing a long continuous waveform. In radar community the radar systems which transmit pulse trains are called pulse radar. Most advanced radar frameworks are pulse radars. We can express the transmitted signal in pulse radar as

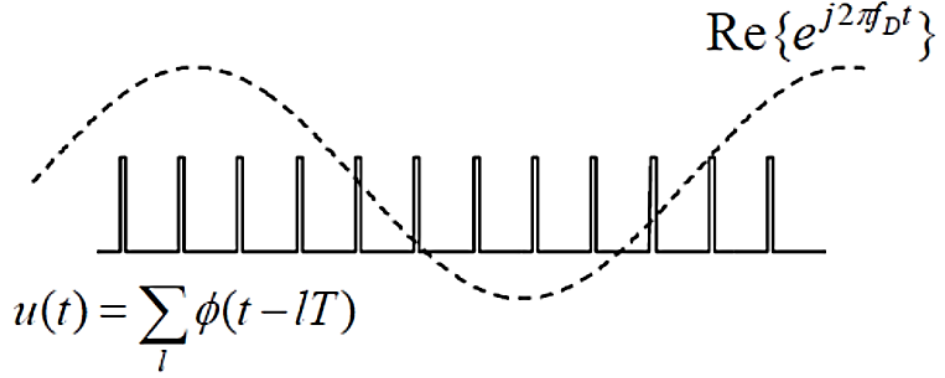


Figure 1.5: The pulse train.

$$u(t) = \sum_{l=0}^{L-1} \phi(t - lT). \quad (1.12)$$

Where $\phi(t)$ is the basic shape pulse, L is the number of the total transmitted pulses, T is the pulse repetition period and l is the pulse index. l and t are regularly called slow time index and fast time respectively, in radar community. The fast time is utilized to process the range data while the slow time is utilized to process the Doppler data. Fig. 1.5 shows the Doppler envelope and a pulse train signal. Using (1.12) and (1.10), the corresponding received signal becomes

$$\alpha \sum_{l=0}^{L-1} \phi\left(t - lT - \frac{2r}{c}\right) e^{j2\pi f_D t} + v(t). \quad (1.13)$$

Since the pulse $\phi(t)$ is narrow in time domain, one can estimated the Doppler expression $e^{j2\pi f_D t}$ as a consistent inside the pulse. Along these lines the above equation can be approximated as

$$\alpha \sum_{l=0}^{L-1} \phi\left(t - lT - \frac{2r}{c}\right) e^{j2\pi f_D lT} + v(t). \quad (1.14)$$

Recall that the matched filter is utilized as a part of receiver to carry out pulse compression and boosted the SNR. In the pulse radar case, it is adequate to utilize the matched filter which matches to the pulse $\phi(t)$. We can express the matched filter output as

$$\begin{aligned} y(\tau) &= \alpha \sum_{l=0}^{L-1} \left(\int_{-\infty}^{\infty} \phi\left(t - lT - \frac{2r}{c}\right) \phi^*(t - \tau) dt \right) e^{j2\pi f_D lT} + \int_{-\infty}^{\infty} v(t) \phi^*(t - \tau) dt \\ &= \alpha \sum_{l=0}^{L-1} r_{\phi\phi}\left(t - lT - \frac{2r}{c}\right) e^{j2\pi f_D lT} + \int_{-\infty}^{\infty} v(t) \phi^*(t - \tau) dt. \end{aligned} \quad (1.15)$$

Utilizing the above matched filter yield, one can perform detection and ranging as portrayed in the last segment. After acquiring the range r , we can extract the Doppler data, by sampling the matched filter output $y(\tau)$ associated with the range and acquire the peaks of the received signal as

$$\begin{aligned}
 y_q &= y\left(qT + \frac{2r}{c}\right) \\
 &= \alpha \sum_{l=0}^{L-1} r_{\emptyset\emptyset}((q-l)T) e^{j2\pi f_D l T} + \int_{-\infty}^{\infty} v(t) \emptyset^*(t - qT + \frac{2r}{c}) dt \\
 &\cong \alpha r_{\emptyset\emptyset}(0) e^{j2\pi f_D q T} + \int_{-\infty}^{\infty} v(t) \emptyset^*(t - qT + \frac{2r}{c}) dt.
 \end{aligned} \tag{1.16}$$

For $q = 0, 1, \dots, L-1$ Computing the discrete Fourier transform (DFT) $Y(f)$ of y_q , we access

$$\begin{aligned}
 |Y(f)| &= \left| \sum_{q=1}^{L-1} y_q e^{-j2\pi f q} \right| \\
 &= \left| \alpha r_{\emptyset\emptyset}(0) \sum_{q=1}^{L-1} e^{-j2\pi f q} + \text{noise term} \right| \\
 &= \left| \alpha r_{\emptyset\emptyset}(0) \frac{\sin(\pi L(f - f_D))}{\sin(\pi(f - f_D))} + \text{noise term} \right|.
 \end{aligned} \tag{1.17}$$

We can compute the Doppler frequency f_D from the peak of the magnitude. One can also utilize the Doppler processing to filter out the undesirable reflected signals. For instance, assume there are two targets at the same range r , but with various Doppler frequencies. Then we can express the received signal associated with the range r , as

$$y_q \approx \alpha_1 r_{\emptyset\emptyset}(0) e^{j2\pi f_{D1} q} + \alpha_2 r_{\emptyset\emptyset}(0) e^{j2\pi f_{D2} q} + \text{noise term}. \tag{1.18}$$

Where f_{D1} and f_{D2} are Doppler frequencies and α_1 and α_2 are the amplitude responses of the targets. To separate the two frequency components of signal y_q , one can utilize a bandpass filter to extract interest Doppler frequency as appeared in Fig. 1.6.

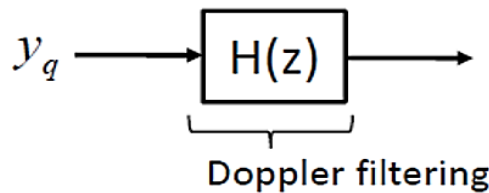


Figure 1.6: Doppler processing.

For instance, the signal reflected by clouds is one major source of interference when identifying the flying targets. However, aircraft or missiles usually move faster compared to the clouds. One can utilize a filter to eliminate the greater part of the undesirable reflected signs. We will remark more about Doppler processing in section 3.

1.3 Beamforming

We have talked about identification, ranging and measuring speed utilizing radar. Now we will discuss another vital parameter, angle, in this subsection. Along with the range data, the angle information gives us the entire information about the target location. The target location can be indicated by three parameters $(r; \theta; \phi)$, where ϕ is the elevation angle and θ is the azimuth angle. These three parameters are illustrated in Fig. 1.7. In this thesis, we usually deal with only one angle because the two angles θ and ϕ can be processed independently. The one-dimensional outcome presented in this thesis can be easily generalized to two dimensions.

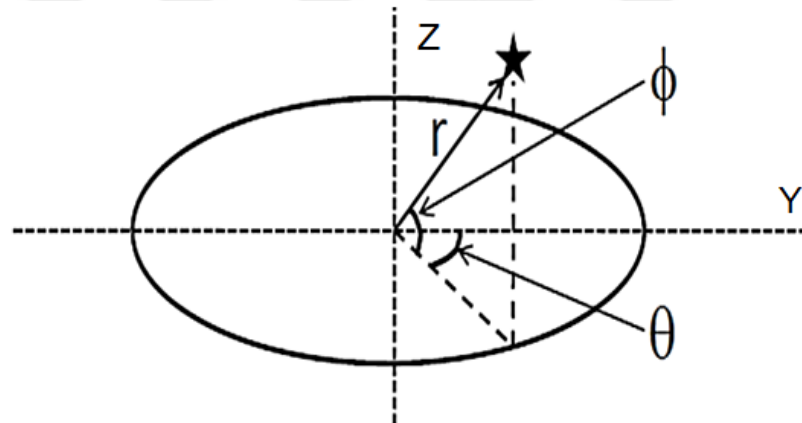


Figure 1.7: Range r , elevation angle ϕ and azimuth angle θ .

For signals received from different angles and signals transmitted to different angles, Antennas usually have different gain. The beam pattern $B(\theta)$ is defined the antenna gain as a function of angles. Think about an antenna with beam pattern $B(\theta)$ which has a great gain around angle 0° but has miniature gains at other angles. To detect a target at 0° we can use this antenna. However, to recognize targets at different sides, we have to mechanically spin the antenna to the side of interest. spinning the antenna mechanically is highly priced and usually generally.

In order to avoid mechanically spinning the antenna, we can utilize a technology called beamforming which allowed us to rotate the beampattern electronically. This requires numerous antennas and generally these antennas have more extensive beampatterns. For convenience, we assume the beampatterns of all antennas are omnidirectional. In simple terms, for every antenna, $B(\theta) = 1$ for all θ . These antennas are implanted uniformly on a straight-line. This is named a uniform linear antenna array (ULA). Such an antenna array are displayed in Fig. 1.8. Assume a narrowband plane wave with carrier frequency f_c hitting from angle θ . We can express the received signal of the n th antenna as

$$r_n(t) = \alpha s(t) e^{j\frac{2\pi}{\lambda} d_n \sin\theta} + v(t). \quad (1.19)$$

For $n = 0; 1; \dots; N - 1$; where N is the number of antennas, $s(t)$ is the signal envelope, α is the amplitude response, $\lambda = \frac{c}{f_c}$ is the wavelength of the signal, $v(t)$ is the additive noise and x is the range of the target. The phase difference item $e^{j\frac{2\pi}{\lambda} d_n \sin\theta}$ originates from various traveling distances to various antennas as illustrated in Fig. 1.8.

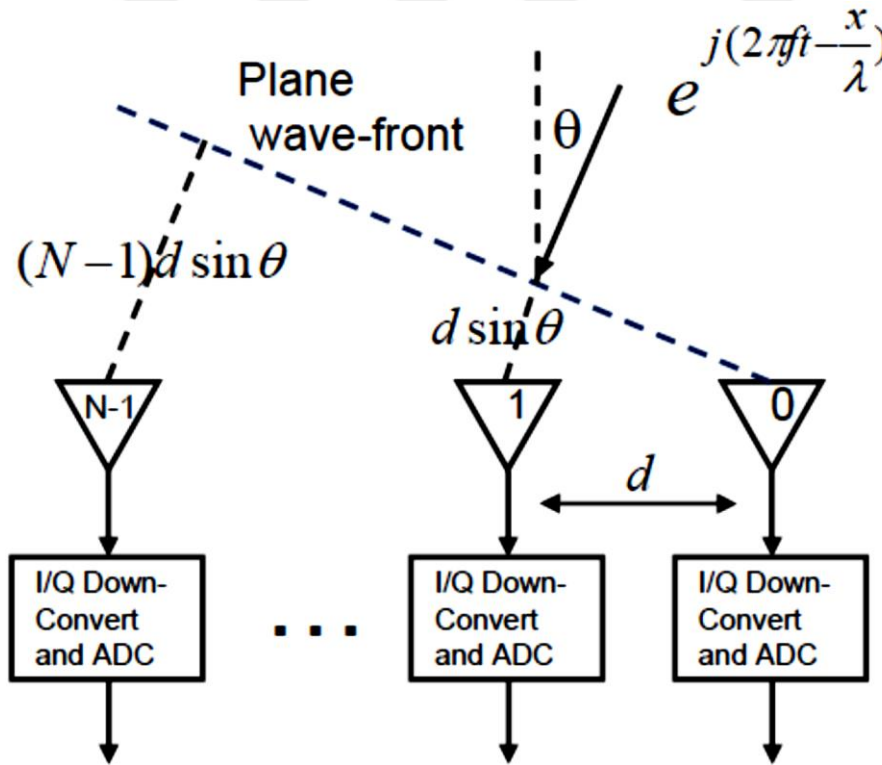


Figure 1.8: A plane wave hitting a uniform linear antenna array (ULA).

To extract signal from θ (to get obviously signal coming from θ), one can linearly combine the received signals and obtain

$$\begin{aligned} y(t) &= \sum_{n=0}^{N-1} \omega_n r_n(t) \\ &= \alpha s(t) \sum_{n=0}^{N-1} \omega_n e^{j\frac{2\pi}{\lambda} d_n \sin\theta} + \sum_{n=0}^{N-1} \omega_n v(t). \end{aligned} \quad (1.20)$$

Here ω_n is the weighting coefficient matching to the n th antenna. Considering the above formula, one can notice that $y(t)$ has a various gain for signal coming from various angle θ . consequently by linearly uniting the signals, we can synthesize the beampattern $B(\theta)$ as displayed in Eq. (1.20). Note that this beampattern $B(\theta)$ can be managed by the weighting coefficients ω_n .

To modify the beampattern, we do not require to mechanically spin the antenna. We can just switch the weighting coefficients ω_n and this should be possible through utilizing electronic gadgets. This technique is named digital beamforming and the weighting coefficients ω_n are called beamformer coefficients. We can express the beampattern as

$$\begin{aligned} B(\theta) &= \sum_{n=0}^{N-1} \omega_n e^{j\frac{2\pi}{\lambda} d_n \sin\theta} \\ &= \sum_{n=0}^{N-1} \omega_n e^{-j\omega n} \Big|_{\omega=\frac{2\pi}{\lambda} d \sin\theta} \\ &= W(e^{j\omega}) \Big|_{\omega=\frac{2\pi}{\lambda} d \sin\theta}. \end{aligned} \quad (1.21)$$

Where $W(e^{j\omega})$ is the Fourier transform of ω_n . Hence, the beamformer design issue can be behaved as an FIR filter design issue. Ordinary FIR filter design methods like Parks-McClellan method can be applied to beamformer design. Note that in filter design issue, the frequency resolution of a filter relies on the filter order. Comparably, the spatial resolution of the beamformer relies on the count of antennas in the uniform linear antenna array ULA array. Note that we have $\omega = \frac{2\pi}{\lambda} d \sin\theta$ in the upper formula. If $d > \frac{\lambda}{2}$, there will be numerous amounts of θ projection to the same ω . This is equal to the aliasing result in sampling. To keep away from this, one chooses $d \leq \frac{\lambda}{2}$. In

practice, the distance among antennas is nearby half of the wavelength. In this situation,

$$-\pi \leq \omega = \frac{2\pi}{\lambda} d \sin\theta = \pi \sin\theta \leq \pi. \quad (1.22)$$

Thus there will not be aliasing in the beam pattern. Beamforming has long been utilized in numerous fields, for instance radar, sonar, medical imaging, seismology, wireless communications, and speech processing.

1.4 Radar classification

Various forms of antennas, receiver, transmitter structures and processing module are exploited in radars according to their operations and on which stage the radar is installed. The partition of antennas is also specified by radar's function. Routine radar structures can be categorized into three classes based on the number of antennas the system has and the interval between them. These are named monostatic, bistatic and multistatic radars [4]. Greater part of radar systems are monostatic. In monostatic radars, receiver and transmitter antennas are co-located and usually there is only one antenna operating both receiving and transmitting functions in a period multiplexed design. In bistatic radars, there are one receiver and one transmitter antenna, but they are considerably separated [1]. Multistatic systems have more than two receiving or transmitting antennas with all antennas separated by large distances when contrasted to the antenna sizes [5].

Newly, a field of radar investigate called Multiple Input Multiple Output (MIMO) radar has been expanded, which can be thought as a speculation of the multistatic radar systems. MIMO radar has multiple receive and transmit multiple antennas as its name represents [6]. The receive and transmit antennas can be in the form of an array and the receive and transmit arrays may be widely separated or co-located as phased array radars. Although some forms of MIMO radars seems phased array radars, but there is a basic conflict between phased array system and MIMO system. The difference is that phased array systems send scaled versions of a singular waveform which are entirely correlated, whereas MIMO system all the time sends various probing signals, through its transmit antennas, that uncorrelated with each other. The multiple receive and transmit antennas of a MIMO radar may also be broadly separated as radar networks.

The basic conflict between a MIMO radar and multistatic radar network is that independent radars that shape the network operate a serious level of local processing and there exists a central processing unit that fuses the results of central processing in a sensible route. For instance, each radar perform detection decisions locally then the central processing unit cumulates the local detection decisions. While MIMO radar make a single decision about the existence of the target by utilize all of the obtainable data and jointly processes received numerous signals [37].

Abbreviation **MISO** signifies Multiple Input Single Output. It explains the radar systems with multiple transmitters and a single receiver antenna.

Abbreviation **SIMO** signifies Single Input Multiple Output. It explains the radar systems with a single transmitter and multiple receiver antennas.

Abbreviation **MIMO** signifies Multiple Input Multiple Output. It explains the radar systems with multiple transmitters and multiple receiver antennas.

An array is called **Uniform Linear Array (ULA)** if the separation between the elements is uniform.

An array is called **filled array** if the spacing between antennas is half of the wavelength.

An array is called **Sparse array** if the spacing between array elements is greater than half of the wavelength.

In the next two subchapter we briefly explain both multistatic and phase radars and discuss about MIMO radar with details in chapter 2.

1.4.1 Multistatic Radar Systems

Radar systems that have more than two receiving or transmitting elements with all elements distributed by large spacing when compared to the elements sizes are generally named multistatic radars. Although there is no a sole determination of multistatic radar systems.

Radar communities define the radar systems that have several spatially separated receiving antennas and only one transmitter as in Fig. 1.9 as multistatic radar systems.

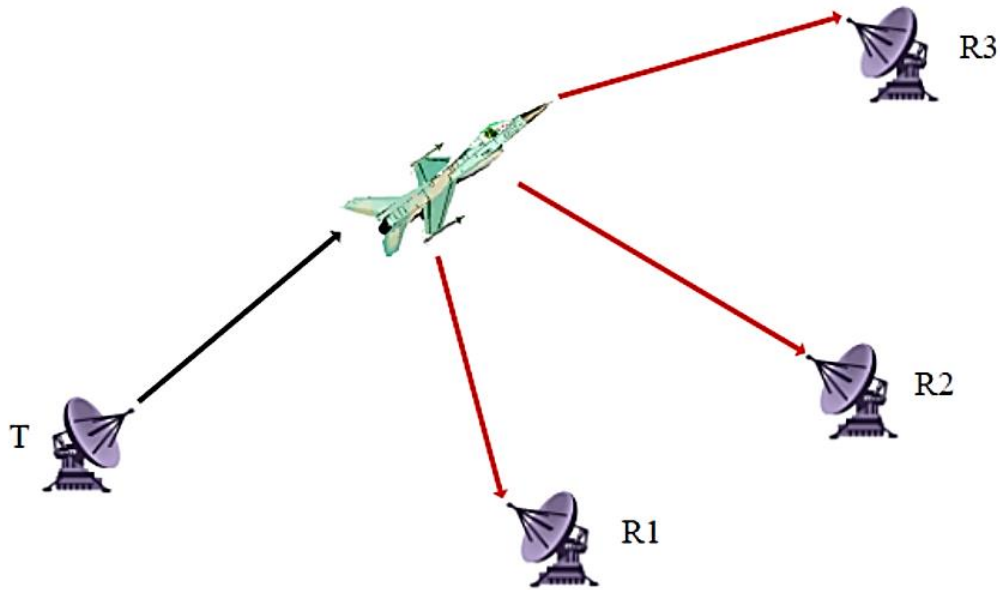


Figure 1.9: Configuration of Multistatic Radar System [37].

On the other hand multiradar (Netted Radar) system is defined radar that have arbitrary systems of broadly distributed radars where all the acquired information is fused and jointly processed as [5]. Each of these broadly distributed radars may run in monostatic mode as in Fig. 1.10 or in a full multistatic mode as in Fig. 1.11. Multisided radar systems are defined radar systems including both the netted radar and multistatic systems. A large amount of information about multisided radar systems and multistatic radar can be obtained in [5] and [7].

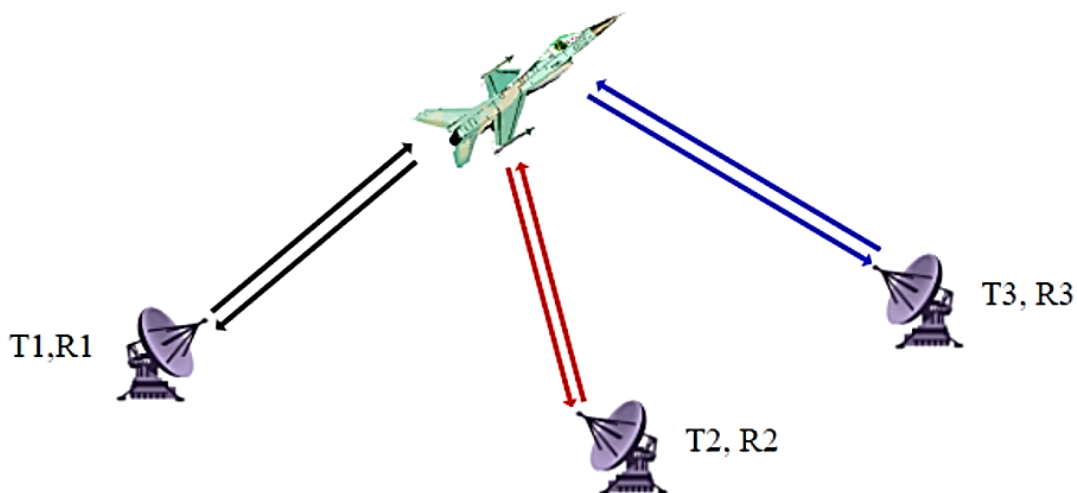


Figure 1.10: Configuration of Multistatic Radar (Multiple Monostatic) [37].

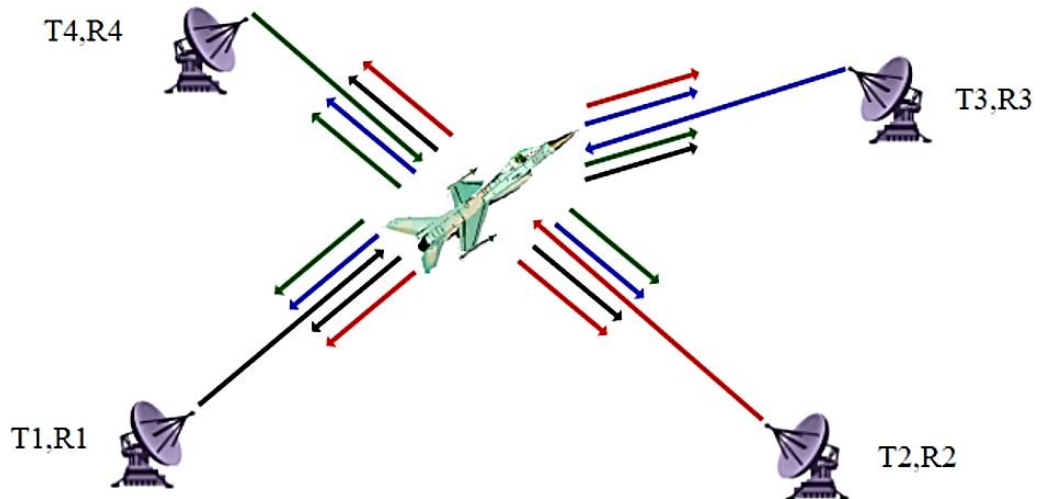


Figure 1.11: Configuration of Multistatic Radar (Fully Multistatic) [37].

In systems like multistatic radar, all transmit receive couples may operate as independent radars. Each couple may process the received data individually and discovery determinations and estimated parameters like velocity and range are fused in a processing center (PCU). This is so called distributed (decentralized) detection. As inverse to this design, all the received data, may be forwarded to a processing center without any prior processing. For this purpose Data transmission lines like fiber cables or copper cables are exist between units and PCU [5].

For joint processing, forwarding of received data is not enough. A common frequency and time reference ascertaining the synchronization between units and PCU should exist. Since the distance between units and PCU may be enormous, establish and maintain this synchronization might be troublesome. This is the major disadvantage of multistatic radar systems.

There are many favors of multistatic systems [5]. First of all, attaching extra receiver and transmitter elements to a monostatic radar boosts the total power and sensitivity of the system and reduces the signal power losses. If sufficiently separated transmitting units illuminate the target, fluctuations of reflected signals are statistically independent at various receiving units. When the received data are jointly processed, these fluctuations are flattened and correspondingly performance of the detection enhances at high possibilities. At the same time detection from different directions increases detection probabilities of secret target. While the angle among, directions from a secret

target to a receiving unit nears 180 degrees, the scattered sign energy dramatically increase at the input of the receiver antenna and this increase cannot be decreased by stealth methods like radar absorbing material coating and body shaping.

High accuracy of location and position estimation of an objective is further benefit of multistatic radar systems. Range estimations of monostatic radars are generally more accurate than angle estimations because angle measurements are related to antenna beamwidth. In monostatic systems accuracy of angle estimations also decreases with increasing range. On the other hand, multistatic radars can utilize range measurements of numerous receivers and special methods such as triangulation and extract angle of achievement data from these range measurements increasing the accuracy of the position and location estimation [37].

Another advantage of multistatic radar systems is increased resolution proficiency. Resolution proficiency defines as the detection probability and measurement accuracy of the system in the presence of extra objects and other interference causes. Presume there are two objects at the equal range in the resolution cell of a monostatic radar receiver. These two targets might be at various ranges to a various radar receiver in the multistatic radar system so that the targets may be determined in the range.

Another advantage of multistatic radar systems appears when transmitters and receivers of multistatic systems are widely distributed so intersection of their main beams may be smaller than a monostatic system resulting diminution in the power echoing from the clutter.

The last benefit of multistatic radar systems to be mentioned in this chapter is their resistance to jamming and augmented survivability. When multistatic radar systems run in bistatic type, it is hard to locate the exact positions of receiver units and this makes the receiver units less vulnerable to jamming and direct physical attack by missiles [37].

1.4.2 Phased Array Radar

Phased Array Radar utilizes antenna arrays for transmitting and receiving waveforms. These arrays may be planar or linear. The interval between the elements is usually uniform in both the planar and linear arrays. These arrays may be co-located and even transmit and receive operations can be executed by the same array. The two arrays may also be widely distributed allowing the radar system to perform in bistatic model. In Fig. 1.12 we give an example configuration of a phased array radar system.

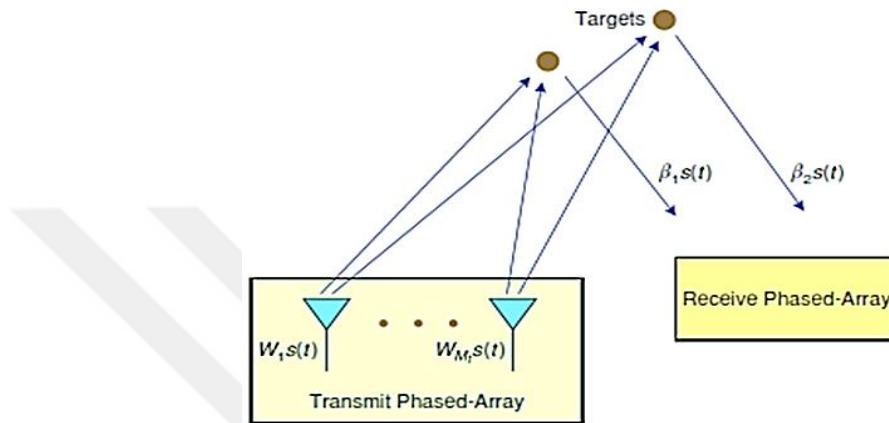


Figure 1.12: Phased Array Radar.

Since the distance between of phased array radar elements is small, the bistatic RCS seen by each transmit-receive couple in a phased array radar system is presumed to be equal.

In phased array radar systems, each of the elements of the transmit array send a scaled copy of the same waveform. Although the elements gradually being omnidirectional, a directive antenna with a high gain can be achieved by accurately adjusting these scale components. By altering these scale components in time, we can steer the beam in space toward any arbitrary direction like as a conventional radar with a directional beam. Even the technology of scaling waveforms can be operated on the signals received by the received elements. This produces the result of using a directional antenna at the receiver. For this reason phased array radars are also named beamformers. Since this beamforming operation is performed electronically, the look direction of the beam may alter so rapidly and the location of interest can be probe very fast without any mechanical progress. Beamforming is the major advantage of phased array radar systems.

Using adequate large number of elements in an array allowing to steer numerous independent beams simultaneously. We can utilize these beams to track numerous targets or probing different areas of the space at once. Also performing time multiplexed fashion to probe and track function may in the same radar system allowing the use of phased array radar as a multi-function radar [4]. Versus these benefits, its complexity, difficulties in the manufacture stages of phased array elements and unaffordable are its major disadvantages.

To indicate signal model of phase radar assume a phased array system that has M_r receive elements and M_t transmit. Consider that receive and transmit arrays are uniform linear arrays with spacing between elements is d_r and d_t respectively.

We can denote the discrete time baseband signal transmitted by the transmit antenna elements as $\sqrt{E_t/M_t} x(t)$ where E_t is the total average transmitted energy.

If the array antennas operate transmit beamforming in the direction of $\tilde{\theta}$ the transmitted signal model can be written in the vector form as

$$\mathbf{x}(t) = \mathbf{a}(\tilde{\theta}) \sqrt{E_t/M_t} x(t). \quad (1.23)$$

Where $\mathbf{a}(\tilde{\theta})$ is the transmitter steering vector. If the transmit array is scaled $\mathbf{a}(\tilde{\theta})$ is in the form of (1.24)

$$\mathbf{a}(\tilde{\theta}) = \begin{bmatrix} 1 \\ e^{j2\pi f_0 d_t \sin(\tilde{\theta})/c} \\ \vdots \\ e^{j2\pi f_0 (M_t-1) d_t \sin(\tilde{\theta})/c} \end{bmatrix}. \quad (1.24)$$

Where c is the speed of light and f_0 is the carrier frequency of the radar. Consider there is a motionless target at the far field of the radar in the direction of θ . Under the consideration of the propagation is nondispersive and transmitting narrowband signal the signal model $x^t(t)$ at the target location can be written as:

$$x^t(t) = \mathbf{a}^H(\theta) \mathbf{x}(t - \tau_t) = \mathbf{a}^H(\theta) \mathbf{a}(\tilde{\theta}) \sqrt{E_t/M_t} x(t - \tau_t). \quad (1.25)$$

Where τ_t is the time interval among the transmit antenna array and the target, H is the Hermitian transpose or conjugate transpose of a matrix and $\mathbf{a}(\theta)$ is

$$\mathbf{a}(\theta) = \begin{bmatrix} 1 \\ e^{j2\pi f_0 d_t \sin(\theta)/c} \\ \vdots \\ e^{j2\pi f_0 (M_t-1) d_t \sin(\theta)/c} \end{bmatrix}. \quad (1.26)$$

Since the array elements of the phased array system are nearly spaced, all transmit receive couples get the same bistatic RCS. Consider that α expresses this backscattering effect. If the objective is at the direction of θ' with respect to the receive antennas then the signal at the receiver array $\mathbf{y}^r(t)$ can be formed as

$$\mathbf{y}^r(t) = \alpha \mathbf{b}(\theta') \mathbf{a}^H(\theta) \mathbf{a}(\tilde{\theta}) \sqrt{E_t/M_t} x(t - \tau) + \mathbf{w}(t). \quad (1.27)$$

Where τ represents the total time interval among transmitter and receiver ($\tau = \tau_t + \tau_r$) and $\mathbf{b}(\theta')$ is

$$\mathbf{b}(\theta') = \begin{bmatrix} 1 \\ e^{-j2\pi f_0 d_r \sin(\theta')/c} \\ \vdots \\ e^{j2\pi f_0 (M_r-1) d_r \sin(\theta')/c} \end{bmatrix}. \quad (1.28)$$

$\mathbf{w}(t)$ is a zero mean vector of complex random procedures which is in the form of

$$\mathbf{w}(t) = \begin{bmatrix} w_1(t) \\ w_2(t) \\ \vdots \\ w_{M_r}(t) \end{bmatrix}. \quad (1.29)$$

1.4.3 Phased-MIMO Radar Systems [8]

Phased MIMO radar systems is a novel conception which efforts to bring excellent perspective of both MIMO radar and phased array jointly in a single radar system. This radar system engages transmit and receive antenna arrays which has nearly spaced antenna elements as Coherent MIMO radar. Transmit array is divided into a number of subarrays. Every subarray coherently transmits signals and operates beamforming towards a definite point in space. By this way like a phased array radar system we can achieve a coherent processing gain. Signals transmitted by each transmit subarray are orthogonal to each other to obtain benefits of waveform diversity like a MIMO radar system.

We can summarize the advantages of Phased MIMO radar system as:

- It benefits from all advantages of the MIMO radar systems. Improved parameter identifiability and angular resolution, Increase the number of target detection.

- It is possible to perform the conventional beamforming techniques at both transmitter and receiver sides
- It provides robustness against strong interference, jammer or clutter
- It provides a tradeoff among angular resolution and robustness toward beam-shape loss

To present a better understanding, the transmitter antenna array construction of phased-MIMO radar is shown in Fig. 1.13.

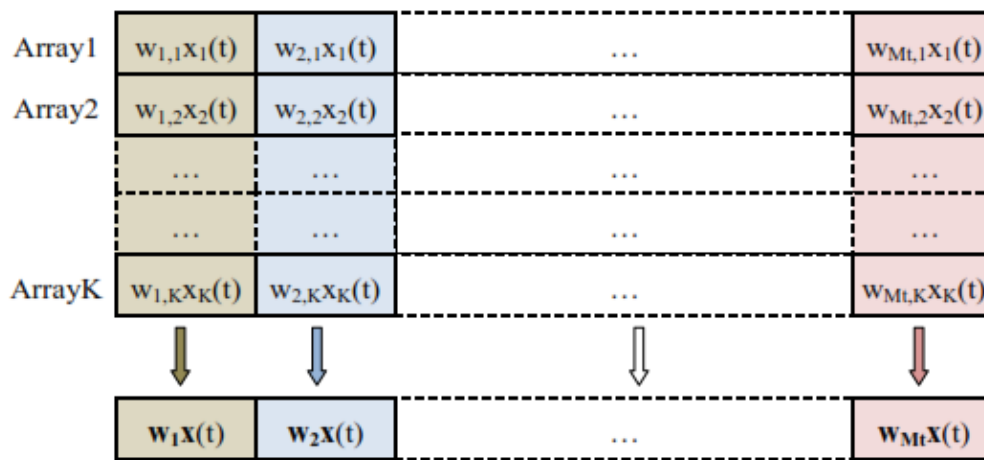


Figure 1.13: Transmitter antenna Array construction Of Phased-MIMO Radar.

In the figure1.13 a transmitter antenna array has M_t elements and divided to K subarrays as shown. Every transmitter antenna belongs to at least one subarray. Every subarray may comprise from one up to M_t elements and generally no two subarrays overlap thoroughly. If a $w_{m,K}$ (weight coefficient) is equal to zero, it implies that the m th transmit element does not belong to k th subarray. The nonzero weight coefficients of a subarray calibrates the same signals to shape and navigate a beam in space and the waveforms $x_m(t)$ and $x_l(t)$ are perpendicular if $\neq l$.

2. MIMO RADAR

In the traditional phased array radar, the system can only transmit scaled versions of a single waveform. Because only a single waveform is used, the phased array radar is also called SIMO (single input multiple-output) radar in contrast to the MIMO radar. We will use “SIMO radar” or “phased array radar” alternatively throughout the thesis.

MIMO Radar system utilizes multiple transmit and receive antennas for sending and receiving waveforms. These antennas may be in the form of an array being and closely spaced or be separately spaced constructing like a netted radar system structure.

Each antenna element in a MIMO radar system propagates various waveforms. These may be orthogonal, simply linearly independent or mutually uncorrelated (Orthogonality always implies Linear Independence but not vice-versa). This is named waveform diversity and it is a characteristic of MIMO radar system. Correlation of waveforms may also be applied to some steps for some operations. Hence performing mutually orthogonal signals with favorable autocorrelation and crosscorrelation effects is one of the growing research fields of MIMO radar [9], [10].

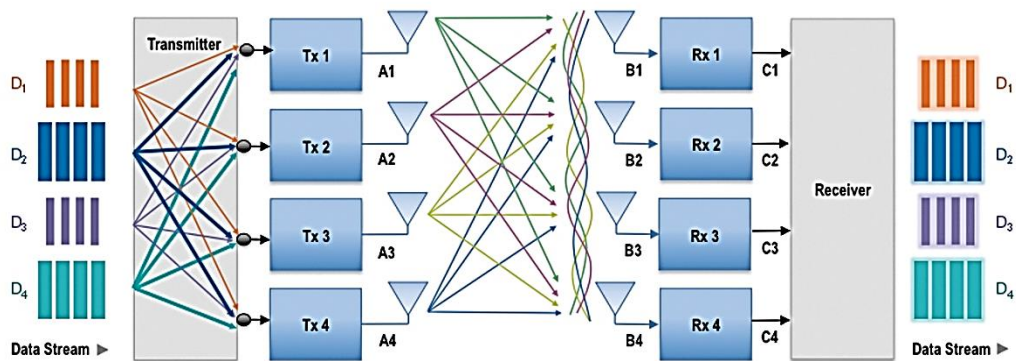


Figure 2.1: 4 x 4 MIMO and channel between the transmitter and the receiver example.

To benefit from this waveform diversity, in each MIMO radar receiver units, there are as many matched filters as the number of transmitted waveforms. The target backscatters are passed through these matched filters compared to every transmitted

waveform. If the number of transmitter array elements is M_t and the number of receiver array elements is M_r , there are totally $M_t M_r$ outcomes of these matched filters. MIMO radar system processes these outputs all together to detection a target. An illustration of a MIMO radar receiver unit is shown in Figure 2.2.

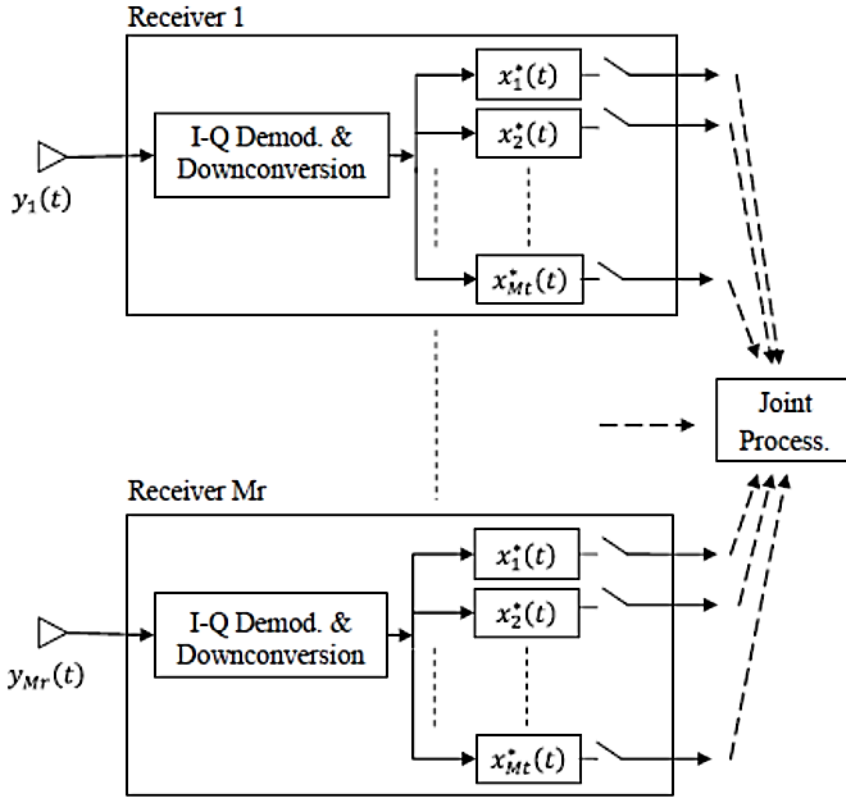


Figure 2.2: Receiver configuration of MIMO Radar system.

In [37], the two models of MIMO radar systems, namely coherent MIMO radar and non-coherent (statistical) MIMO radar are explored. The similarities and differences of these two type of radar configuration from traditional radar systems are investigated. The performance developments obtained by each type of MIMO radar system are described. Here we only briefly explore coherent MIMO radar.

2.1 Coherent MIMO Radar

Coherent MIMO radar system utilizes antenna arrays for transmitting and receiving waveforms. These arrays may be separated or co-located and even transmit and receive operation can be performed by the same array. The interelement spacing can be uniform or non-uniform. Depending on the system application, the arrays may be

sparse or filled. But every time the separation is short compared to the range extent of the target. An illustration allocation of linear arrays of coherent MIMO radar antennas is displayed in Figure 2.3.

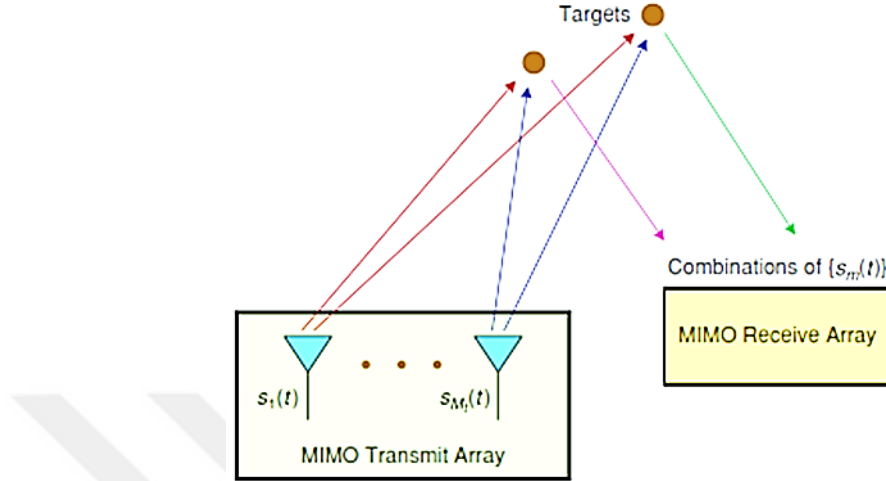


Figure 2.3: Configuration of Coherent MIMO Radar system.

Whatever the interelement spacing is, the most important issue in coherent MIMO radar. If the array elements are located enough closely to each other so that every element observes the same feature of the target i.e. the same RCS. As a result, we generally utilize point target assumption in coherent MIMO radar applications.

Coherent MIMO radar system resembles the phased array radar because of this distributed arrangement of antenna elements. But differently from phased array radar, each antenna element of a Coherent MIMO radar transmits various waveforms.

2.1.1 Signal Model

Assume a MIMO radar system with M_t transmitter and M_r receiver antennas. Let $x_m(n)$ signify the discrete-time baseband signal which emitted by the m th transmit element. Also, let θ signify the location parameter(s) of a typical target, for example, its range and its azimuth angle. Then, under the consideration that the propagation is nondispersive and the transmitted exploring signals are narrowband, we can illustrate the baseband signal at the target location by the expression

$$\sum_{m=1}^{M_t} e^{-j2\pi f_0 \tau_m(\theta)} x_m(n) \cong \mathbf{a}^H(\theta) \mathbf{x}(n), \quad n = 1, \dots, N. \quad (2.1)$$

Where $\tau_m(\theta)$ is the time required by the signal sent via the m th transmit antenna to reach the target, f_0 is the carrier frequency of the radar, $(\cdot)^H$ denotes the conjugate transpose, N signify the number of samples of each transmitted signal pulse,

$$\mathbf{x}(n) = [x_1(n) \ x_2(n) \ \dots \ x_{M_t}(n)]^T. \quad (2.2)$$

And

$$\boldsymbol{\alpha}(\theta) = [e^{j2\pi f_0 \tau_1(\theta)} \ e^{j2\pi f_0 \tau_2(\theta)} \ \dots \ e^{j2\pi f_0 \tau_{M_t}(\theta)}]^T. \quad (2.3)$$

While $(\cdot)^T$ signify the transpose function. By considering that the transmit array of the radar is scaled, $\boldsymbol{\alpha}(\theta)$ is a known function of θ .

When $y_m(n)$ signify the signal received by the m_r th receive element, let

$$\mathbf{y}(n) = [y_1(n) \ y_2(n) \ \dots \ y_{M_r}(n)]^T, \quad n = 1, \dots, N. \quad (2.4)$$

And

$$\mathbf{b}(\theta) = [e^{j2\pi f_0 \tilde{\tau}_1(\theta)} \ e^{j2\pi f_0 \tilde{\tau}_2(\theta)} \ \dots \ e^{j2\pi f_0 \tilde{\tau}_{M_r}(\theta)}]^T. \quad (2.5)$$

When $\tilde{\tau}_m(\theta)$ is the time required by the signal backscattered from the target located at θ to reach at the m th receive element. So, under the simplifying consideration of point targets, we can describe the received data vector by the equation ([5] and [10])

$$\mathbf{y}(n) = \sum_{k=1}^K \beta_k \mathbf{b}^c(\theta_k) \boldsymbol{\alpha}^H(\theta_k) \mathbf{x}(n) + \epsilon(n), \quad n = 1, \dots, N. \quad (2.6)$$

While K is the number of targets that scattered the waveforms back to the radar receiver element, $\{\beta_k\}$ denote complex amplitudes relative to the radar cross sections (RCSs) of those targets, $\{\theta_k\}$ denote their location parameters, $(\cdot)^c$ is the complex conjugate and $\epsilon(n)$ signify the interference plus noise pert. The anonymous parameters, to be measured are $\{\mathbf{y}(n)\}_{n=1}^N$, are $\{\beta_k\}_{k=1}^K$ and $\{\theta_k\}_{k=1}^K$.

2.1.2 Improvements That Coherent MIMO Radar Systems Offer

Waveform diversity makes MIMO radar achieve better performance in several application areas compared to standard phased array radar and is the key of performance improvement for many MIMO radar applications. In the following chapters these improvements offered by Coherent MIMO radar systems will be described.

2.1.2.1 Higher Resolution

At first we describe The “Phantom” Antenna Element to the understanding of within aperture MIMO radar. Consider the simple bistatic antenna pair shown in Fig. 2.4. The geometry shows how, for far-field targets, signals from the bistatic pair would be identical to signals received from a monostatic TRx element positioned mid point between the transmit and receive elements of the bistatic pair. It is clear that a reflected signal arriving with a specific delay must have arisen from some point on the surface of an ellipsoid with foci at the Tx and Rx element positions. It is also clear that for very distant targets the ellipsoid converges to a sphere centered on the mid-point between the elements, forming the phantom TRx element.

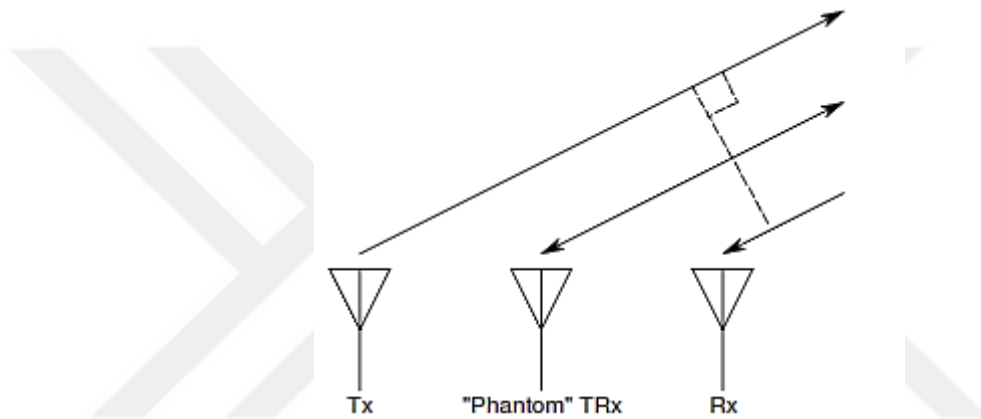


Figure 2.4: Round trip delays are the same for the Tx/Rx pair and the phantom element.

We can extend this idea to show how M transmitters and N receivers can be used to synthesis apertures of various geometries comprising $M \times N$ phantom elements, allowing the formation of $M \times N$ directional beams [11]. The physical elements may be configured to synthesis a one-dimensional (Fig. 2.5), two-dimensional (Fig. 2.6), or even three-dimensional (Fig. 2.7) phantom element array, with the phantom elements being synthesised midway between each transmitter-receiver pair. With there being $M \times N$ pairwise combinations, we show $M \times N$ phantom elements can be synthesised.

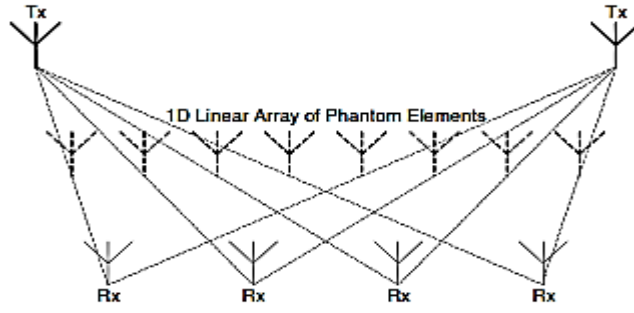


Figure 2.5: One dimensional synthesised linear array of phantom elements.

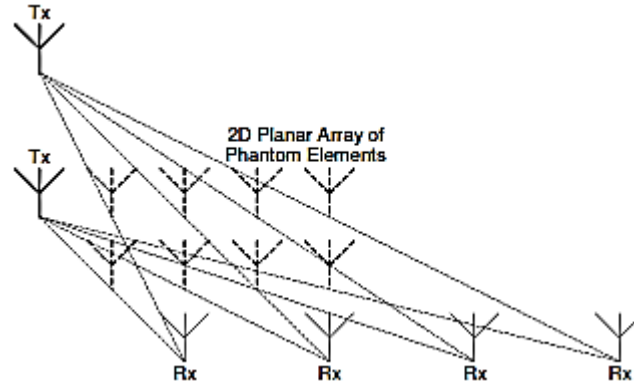


Figure 2.6: Two dimensional synthesised planar array of phantom elements.

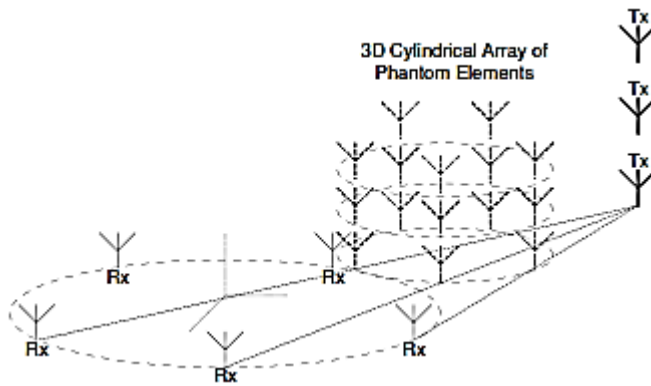


Figure 2.7: Three dimensional synthesised cylindrical array of phantom elements.

At the MIMO radar receiver units the corresponding receiver steering vector for orthogonal waveform is the Kronecker product of transmit and receive steering vectors and is named MIMO steering vector [12]. It can be shown as

$$V_{MIMO} = b^*(\theta') \otimes a^*(\theta). \quad (2.7)$$

The MIMO steering vector is equivalent to a receiver array which performs the same efficiency as the MIMO radar and it involves all attainable transmit receive phase

difference compositions. To present a better perception two examples are given in subsequent paragraphs.

For a MIMO radar which transmit receive array element is uniform linear spaced but each element simultaneously transmit and receive waveform, in this case the MIMO steering vector has $M_t + M_r - 1$ distinct components. This is the minimum achievable number of components which defines the worst case scenario [6], [13]. An illustration of this worst case scenario is shown In Figure 2.8. On the left side of this figure MIMO radar structure with four transmit and four receive elements is given where transmit antenna is also the receive antenna. On the right side the corresponding virtual receiver array equivalent to MIMO radar steering vector is shown. We can see in the virtual array seven (7) distinct elements formed and the other ten elements are duplication of appointed array elements.

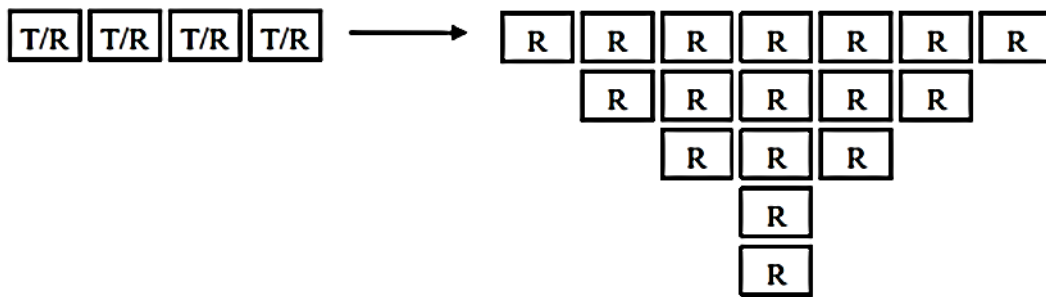


Figure 2.8: Configuration of Virtual Receiver Array – The Worst Case [12].

Figure 2.9 depicts the best case scenario which the MIMO system steering vector has distinct components [6], [13]. This corresponds to the condition where arrays share few or no element to transmit and receive waveforms. In the figure a sparse uniform linear of two elements performs as a transmitter array and a filled uniform linear of four elements performs as a receiver array. The outcome virtual array has eight distinct elements and no duplication of array elements formed in the outcome.

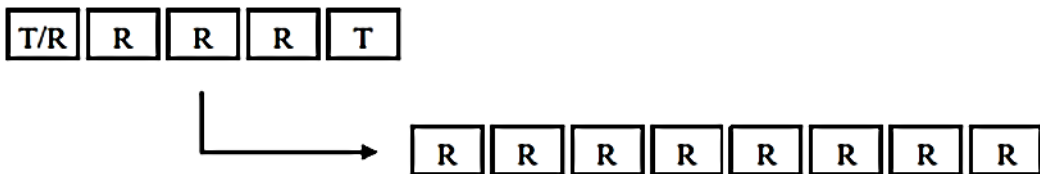


Figure 2.9: Configuration of Virtual Receiver Array – The Best Case [12].

As can be viewed from the images, even in the worst case scenario the numbers of distinct elements in virtual arrays are greater than the number of receiver elements in the real configuration. Consequently, the array aperture is virtually stretched. This stretch results in better angular resolution and higher detection execution. Better angular resolution assists to enhance the characterization of a target and to enhance the refusal ability of the jamming and other interfering causes [12].

Since phased array radar systems transmit coherent waveform, there is no any chance of creation an extended virtual array.

2.1.2.2 Parameter Identifiability

Another fields that MIMO radar system improves performance is the parameter identifiability [14], [13], [15]. In radar community parameter identifiability is defined as the maximum number of objectives that can be uniquely detected by the radar. as reported by [13], the maximum number of objectives that can be uniquely detected by the MIMO radar system - K_{max} - stands in the interval

$$K_{max} \in \left[\frac{2(M_t + M_r) - 5}{3}, \frac{2M_t M_r}{3} \right). \quad (2.8)$$

Where M_t and M_r signifies the number of transmit and receive elements respectively. The quantity K_{max} in (2.8) is directly have connection with the distinct number of components in MIMO steering vector and varies according to

- the arrays being linear or nonlinear,
- the interelement spacing being uniform or non-uniform
- the number of elements being shared between the transmit and receive arrays.

The minimum number in (2.8) related to the worst case scenario where the same filled uniform linear element is utilized simultaneously for both transmitting and receiving. However, the maximum number in the same equation can be obtained when the receive array and the transmit array share no element to operate [15].

In addition, for a phased array radar system, for which all the degree of freedom even containing the total transmitted power are the same as for the MIMO radar system except that, $M_t = 1$, K_{max} can be written as

$$K_{max} \in \left[\frac{2M_r - 3}{3} \right]. \quad (2.9)$$

Where $\lceil \cdot \rceil$ signifies the minimum integer bigger than or equal to a given number [13].

When we compare (2.8) and (2.9), we notice that the highest number of objects that can be uniquely detected by MIMO radar system is up to M_t times bigger than its phased array match and even at the worst case scenario this number is twice bigger than its phased array radar match.





3. STAP IN MIMO RADAR

Space Time Adaptive Processing (STAP) is a modern signal processing method that can enhance target detection capability in the presence of an intense clutter. In this chapter only short summary of this subject is presented, more comprehensive analysis of this technique can be obtained in a book written by Richard Klemm [16].

3.1 Overview of STAP and Airborne Clutter

In airborne radar Moving Target indication operation, we face the problem that reflected signals approaching from motionless ground objects (ground clutter) contain non-zero Doppler bandwidth [17] (Fig.3.1). This is an outcome of relative speed between radar platform (aircraft) and ground area probed by the radar system. As a consequence, target signal can drop within the clutter spectrum and may be invisible under the clutter (Fig. 1 depicts simpler model, where target signal is out of the clutter bandwidth). In this case, clutter elimination will also eliminate target data. STAP technique is to Filter-out ground clutter, while preserving signal reaching from real target.

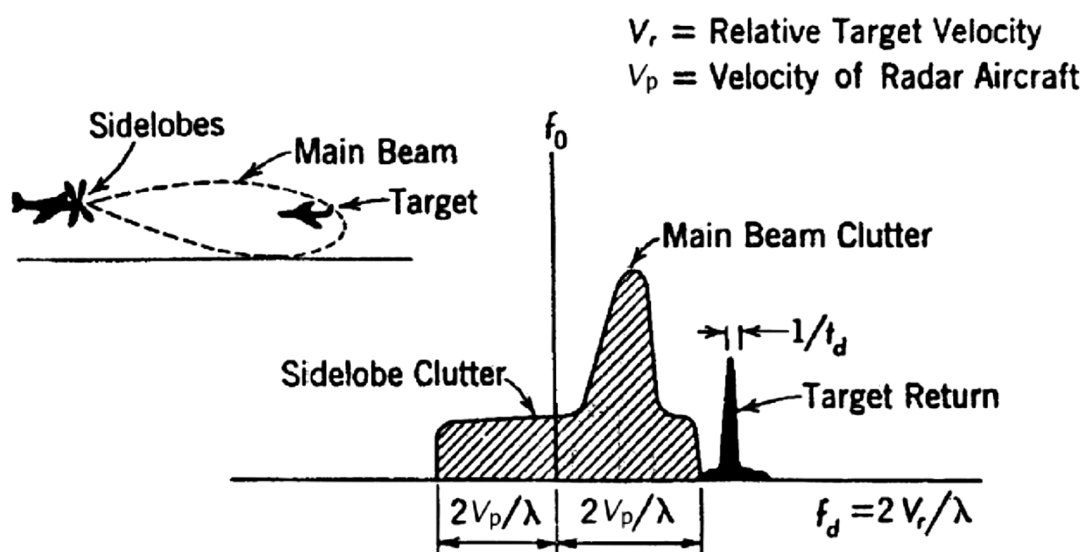


Figure.3.1: Airborne clutter [17].

In order to benefit its advance, STAP performs antenna array, which allows direction of arrival filtering. We can view the geometry of airborne antenna arrays In Fig. 3.2. Axis V_p indicate flight direction. There are practical two original configurations: forward-looking and side-looking.

For side-looking model, receiving antennas are implanted along the flight direction. For forward looking type, receiving antennas are implanted along an axis perpendicular to the flight direction, but parallel to the ground surface. Side-looking model is simpler to explain, hence we consider this configuration only. Also for simplification, we consider that receiving antennas are ULA, with interelement spacing is equal to $\lambda/2$ (λ , denotes wavelength). Antenna array is performed cone-angle (α in Fig. 3.2) filtering. Receiving signal from point P (Fig. 3.2) on the ground is sampled in space by array antennas. Waveforms approaching from point P are received to receiving elements at various moments in time. As a consequence there is a phase difference between array channels. This phase difference is depend on cone angle α . In forward looking configurations (with slant angle), analysis is more complicated, but qualitative outcomes are similar.

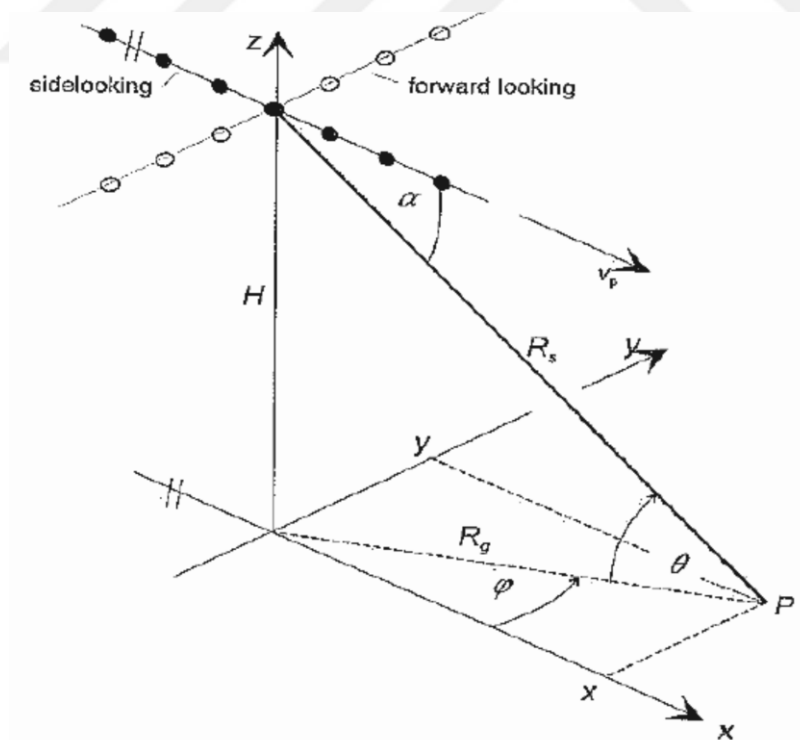


Figure.3.2: Geometry of airborne antenna arrays [16].

It can be viewed that Doppler shift of reflected signals from motionless objectives depends on cone angle [16]. Every point in space, viewed by the radar system under angle α is receiving to the radar at the equal velocity. More precisely, this velocity is related to the radar platform speed and to the cosines of the angle α . Therefore, all such points with same speed in angle α have the same Doppler frequency. Therefore the cone is surface of constant Doppler frequency. But experimentally, airborne radar reflections is not from the whole space but only from the ground surface (excluding object target). Therefore, to access the set of points with the same Doppler frequency we should intersect the ground plane with cone surface. Result of this intersection is a hyperbola. Therefore hyperbola is a set of all points in the ground which have the same Doppler frequency. Lines on the ground of constant Doppler frequency are called isodops. In our case a single hyperbola is exactly an isodop.

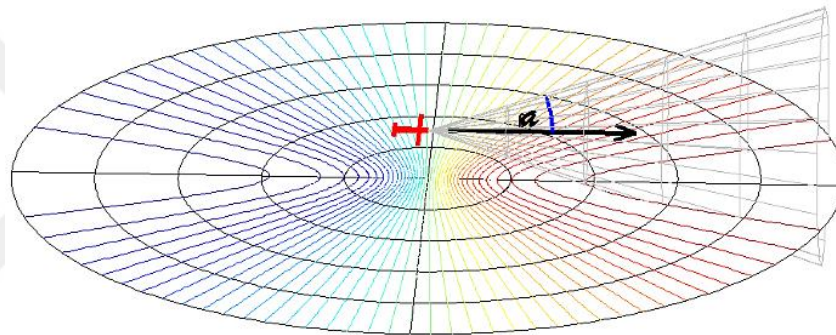


Figure.3.3: Isodops [16].

Each Doppler frequency is depend on a single isodop (hyperbola). Cluster of isodops is depicted in Fig.3.3. In this figure it can be viewed that zero Doppler isodop ($f_r = 0$) is vertical line to the flight path. On the right hand of zero Doppler line, positive Doppler isodops are located. The last one is a maximum Doppler isodop ($f_r = 1$). On the left hand negative Doppler isodops are located. We are generally interested in target indication, and range information simultaneously. A line which has constant range to the radar is called Isorange line. It is a circle on the ground surface, which is an intersection of a ground surface and a sphere with the radius which equals to our range of interest (Fig.3.4).

Considering isodops and isorange lines, we figure out that for the particular range and for the particular Doppler frequency, we receive reflected signal from particular areas on the ground. This can be explained: clutter of the particular Doppler frequency and

from the particular range is coming from particular angles only. This connection is applied with STAP.

In view of the relation between the clutter Doppler frequency and the cone angle, it is obvious that a good spacetime filtering is needed for efficient clutter mitigation. This is also depicted in Fig.3.5, which shows the clutter spectral power (for a side looking array antenna) plotted over the cosine of the look direction azimuth $\cos \alpha$ and the Doppler frequency f_D . The clutter spectrum extends along the diagonal of this plot; it is modulated by the transmit beam.

- Conventional temporal processing means that the projection of the clutter spectrum onto the f_D axis is suppressed via an inverse filter. The clutter canceled this filter is determined by the projected clutter main beam, which is a Doppler effect of the transmit beam. Slow objectives are attenuated.
- For spatial processing, as used for jammer suppression, the clutter spectrum is projected onto the $\cos \alpha$ axis. However, performing an inverse spatial clutter filter forms a broad stop band in the look direction, so that the radar becomes blind. Both fast and slow targets fall into the clutter notch.
- Space-time processing exploits the fact that the clutter spectrum is originally a narrow ridge. A space time clutter filter therefore has a narrow clutter notch, so that even slow targets fall into the pass band.

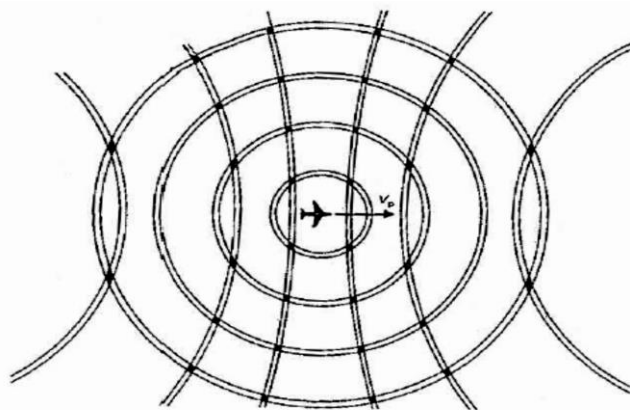


Figure.3.4: Isorange circles and isodops [17].

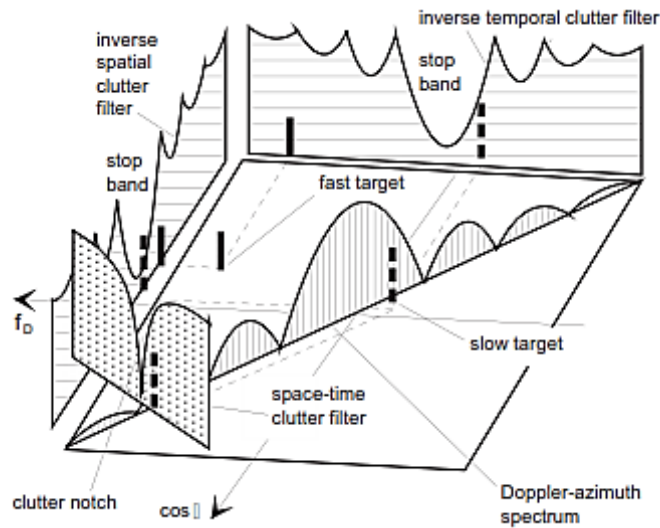


Figure.3.5: Space-time structure of clutter [37].

The MIMO radar space time adaptive processing (STAP) for multipath clutter mitigation can be found in [18]. However, in the MIMO radar system, the STAP technique appeared even more challengeable because of the extra dimension appeared by the orthogonal signals. On one hand, the additional dimension increases the rank of the interference subspace, especially the jammer and clutter subspace. This becomes the STAP more conflicted. On the other hand, the extra degrees of freedom generated by the MIMO radar system allow us to suppress more clutter subspace with minimum effect on signal-to-interference-plus-noise ratio (SINR).

In the next subsection, using the geometry of the MIMO system we will explain the clutter subspace and its rank in MIMO radar system. Practically, the clutter subspace may alter because of such effects like velocity misalignment, array manifold misfit, internal clutter motion (ICM), and channel misfit [19]. In our thesis, an “ideal model” is considered which does not take into account these effects in computation. When this assumption is not reliable, the performance of the outcome will Drop-off. One way to overcome this may be to approximate the clutter subspace by utilize a mixture of both the received data and the assumed geometry. Another way may be to expand a more powerful processing technique versus the clutter subspace misfit. These concepts will be analyzed later.

3.2 STAP in MIMO Radar System

In this part, the STAP issue in MIMO radar is formulated. The MIMO radar generalization for this technique first manifested in [20]. We will concentrate on the concept of utilizing the additional degrees of freedom to boost the spatial resolution of clutter.

3.2.1 Signal Model

Fig.3.6 depicts the simple construction of the MIMO radar system with uniform linear arrays (ULAs), where:

- 1) d_T signifies the transmitter interelement spacing;
- 2) M signifies the number of transmitting elements;
- 3) d_R signifies the receiver interelement spacing;
- 4) N signifies the number of the receiving elements;
- 5) T signifies sending pulse period;
- 6) l represents the index of sending pulse (slow time);
- 7) τ indicates the time within the pulse (fast time);
- 8) v_t is the target velocity toward the radar platform;
- 9) v is the velocity of the radar platform.
- 10) x is the range of the target

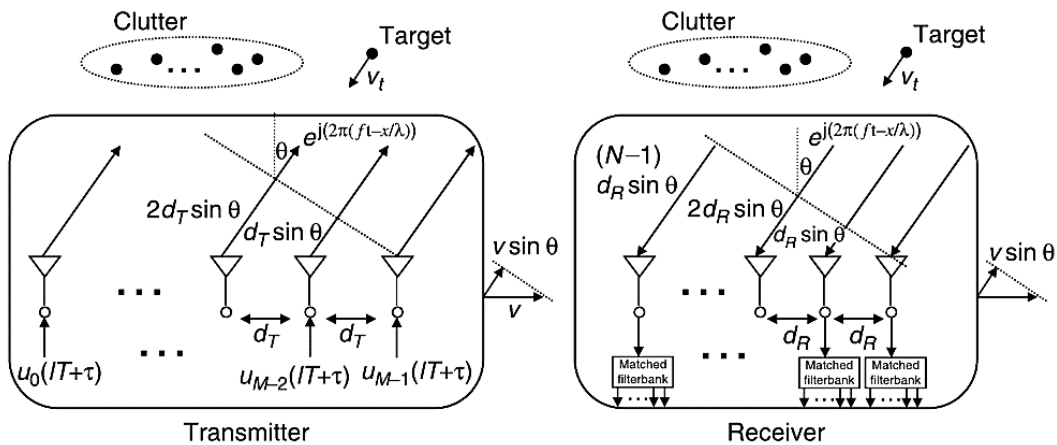


Figure.3.6: MIMO radar system with M transmitting and N receiving antennas. The radar platform is moving with velocity v .

The radar platform motion is considered to be parallel to the linear antenna array. This consideration has been applied in most of the airborne ground moving target indicator (GMTI) radars. Attention that the two antenna arrays are linear and parallel in this model. The distance between transmitter and the receiver arrays are close enough so that they see the same angle value θ . Every array is constructed of omnidirectional antennas. We can express the transmitted signals of the m th element as

$$x_m(lT + \tau) = \sqrt{E}\phi_m(\tau)e^{j2\pi f(lT + \tau)} \quad (3.1)$$

For $m = 1, 2, \dots, M - 1$, where $\phi_m(\tau)$ denote the baseband pulse waveform, E denote the transmitted energy for the pulse and f is the carrier frequency. Now we can express the demodulated received signal of the n th element as

$$\begin{aligned} y_n \left(lT + \tau + \frac{2r}{c} \right) & \approx \sum_{m=0}^{M-1} p_t \phi_m(\tau) e^{\frac{j2\pi}{\lambda}(\sin\theta_t(2vTl + d_r n + d_r m) + 2v_t T l)} \\ & + \sum_{i=0}^{N_c-1} \sum_{m=0}^{M-1} p_i \phi_m(\tau) e^{\frac{j2\pi}{\lambda}(\sin\theta_i(2vTl + d_r n + d_r m))} \\ & + y_n^{(j)} \left(lT + \tau + \frac{2r}{c} \right) + y_n^{(w)} \left(lT + \tau + \frac{2r}{c} \right). \end{aligned} \quad (3.2)$$

For convenience, all of the arguments used in the signal model are summarized in Table.3.1. The first term in (3.2) expresses the signal received from the target. The second term is the signal received from the clutter. The last two terms expresses the jammer signal and white noise. We consider there is no ICM or antenna array misalignment [19]. The phase differences in the received signals are caused by the Doppler effect, the differences of the transmitting element locations and the differences of the receiving element locations. In the MIMO radar system, the transmitting waveforms $\phi_m(\tau)$ satisfy orthogonality:

$$\int \phi_m(\tau)\phi_k^*(\tau)d\tau = \delta_{mk}. \quad (3.3)$$

A bank of matched filters apply to obtain the adequate data as depicted in Fig.3.6. We can rewrite the obtained signals as

TABLE.3.1: roster of the arguments utilize in the signal model.

d_T	Interelement space of the transmitter antennas
d_R	Interelement space of the receiver antennas
M	number of transmitter elements
N	number of the receiving elements
T	Pulse signal period
l	indicates the index of radar pulse (slow time)
τ	time within the pulse (fast time)
v_t	target speed toward the radar station
x_m	transmitted signal in the m th antenna.
Φ_m	baseband pulse waveforms
y_n	demodulated received signal in the n th antenna
v	speed of the radar station.
r	distance of the range bin of interest
c	speed of light
p_t	amplitude of the signal reflected by the target
p_i	amplitude of the signal reflected by the i th clutter
θ_t	looking direction of the target
θ_i	looking direction of the i th clutter
N_c	number of clutter signals
$y_n^{(j)}$	jammer signal in the n th antenna output
$y_n^{(w)}$	white noise in the n th antenna output

$$\begin{aligned}
y_{n,m,l} &\cong \int y_n \left(lT + \tau + \frac{2r}{c} \right) \Phi_k^*(\tau) d\tau \\
&= p_t e^{\frac{j2\pi}{\lambda} (\sin\theta_t (2vTl + d_r n + d_T m) + 2v_t Tl)} \\
&\quad + \sum_{i=0}^{N_c-1} p_i e^{\frac{j2\pi}{\lambda} (\sin\theta_i (2vTl + d_r n + d_T m))} \\
&\quad + y_{n,m,l}^{(J)} + y_{n,m,l}^{(w)}. \tag{3.4}
\end{aligned}$$

For $n = 0, 1, 2, \dots, N - 1$, $m = 0, 1, 2, \dots, M - 1$, and $l = 0, 1, 2, \dots, L - 1$ where $y_{n,m,l}^{(J)}$ is the intended jammer signal, $y_{n,m,l}^{(w)}$ is the intended white noise, and L is the number of the pulses in a coherent processing interval (CPI). To abbreviate the previous equation, we define the following normalized spatial and Doppler frequencies:

$$\begin{aligned}
f_s &\cong \frac{d_R}{\lambda} \sin\theta_t, \quad f_{s,i} \cong \frac{d_R}{\lambda} \sin\theta_i \\
f_D &\cong \frac{2(v \sin\theta_t + v_t)}{\lambda} T. \tag{3.5}
\end{aligned}$$

One can notice that the normalized Doppler frequency of the target is a function of both target velocity and location angle. Throughout this thesis we shall make the assumption $d_R = \lambda/2$ so that spatial aliasing is avoided. Profit the above description, we can simplify the extracted signal in (3.4) as

$$\begin{aligned}
y_{n,m,l} &= p_t e^{j2\pi f_s (n + \gamma m)} e^{j2\pi f_D l} \\
&\quad + \sum_{i=0}^{N_c-1} p_i e^{j2\pi f_{s,i} (n + \gamma m + \beta l)} \\
&\quad + y_{n,m,l}^{(J)} + y_{n,m,l}^{(w)}. \tag{3.6}
\end{aligned}$$

For $n = 0, 1, 2, \dots, N - 1$, $m = 0, 1, 2, \dots, M - 1$, and $l = 0, 1, 2, \dots, L - 1$ where

$$\gamma = d_T / d_R \quad \text{and} \quad \beta = 2vT / d_R$$

3.2.2 Fully Adaptive MIMO STAP

The purpose of space time adaptive processing (STAP) is to discover a linear combination of the obtained data in the way that maximize the SINR. Hence, the target data can be distinguished from the interferences, clutter, and noise to decide the detection. Stacking the obtained data in (3.6), we acquire the NML vector

$$y = (y_{0,0,0} \ y_{1,0,0} \ \dots \ y_{N-1,M-1,L-1})^T. \quad (3.7)$$

Here we can express the linear combination as $w^H y$, where w indicate the weight vector for the equation. To obtained the optimal weight vector w must maximize the SINR such as

$$SINR = \frac{E[|w^H y^t|^2]}{E[|w^H (y^c + y^n)|^2]} = \frac{\sigma_s^2 |w^H s(f_s, f_D)|^2}{w^H R w} \quad (3.8)$$

Where $\sigma_s^2 = E[|y^t|^2]$ is the desired signal power, R interference plus-noise covariance matrix, $s(f_s, f_D)$ is the size NML- MIMO space-time steering vector and $E[.]$ denotes the expectation operator.

The SINR maximization can be obtained by minimizing the denominator of (3.8), i.e., minimizing the variance/power of interference and noise at the output of the adaptive beamformer, while keeping the numerator (3.8) fixed, i.e., ensuring the distortionless response of the beamformer towards the direction of the desired source.. It can be expressed as the following optimization problem:

$$\begin{aligned} & \min_w w^H R w. \\ & \text{subject to } w^H s(f_s, f_D) = 1. \end{aligned}$$

Where $R \cong E[yy^H]$, and $s(f_s, f_D)$ is the size NML- MIMO space-time steering vector, which consists of the elements

$$e^{j2\pi f_s(n+\gamma m)} e^{j2\pi f_D l}. \quad (3.9)$$

For $n = 0,1,2, \dots, N-1$, $m = 0,1,2, \dots, M-1$, and $l = 0,1,2, \dots, L-1$. This w is called minimum variance distortionless response (MVDR) beamformer [21]. The optimal STAP weight vector maximizing the signal to noise plus interference ratio (SINR) [22] is given by

$$w_{opt} = \alpha R^{-1} y^t. \quad (3.10)$$

Where α is a scalar constant which does not affect the SINR, R is the clutter plus noise covariance matrix and

$$y = y^t + y^c + y^n . \quad (3.11)$$

Where y^t , y^c and y^n denote the vectors of the desired signal, interference, and noise, respectively

$$R = E[(y^c + y^n)(y^c + y^n)^H] . \quad (3.12)$$

The output of the filter is $r = w_{opt}^H y$. (3.13)

Weight approximating (r) is digital beamforming, or an inner product, application. The output values is then compared to a threshold value to figure out existence of a target at the determined Doppler and angle. The result of the process function is a separate quantity (decision) for each angle, range, and velocity at which target existence is to be ambiguous. Preferably, the space time adaptive processor supplies coherent gain on target while applying angle and Doppler response suppress to mitigate clutter and jammer.

The extension from the SIMO to the MIMO system is trivial, matrix R and weight vector w_{opt} being of dimension $MNL \times MNL$ and $MNL \times 1$ in the latter case instead of $NL \times NL$ and $NL \times 1$ in the first case, respectively. It is well known that the localization of sources by an antenna array is improved when the number of receiving elements of the array increases. In the case of MIMO STAP, a better estimation of the clutter spectrum is thus expected yielding a better rejection of it when constructing the weight vector (3.10). Indeed, in this case, it has been seen that the number of elements is virtually MN for a number of physical elements of $N+M$ instead of N in the case of SIMO. However this is only true in the theoretical (optimal) case.

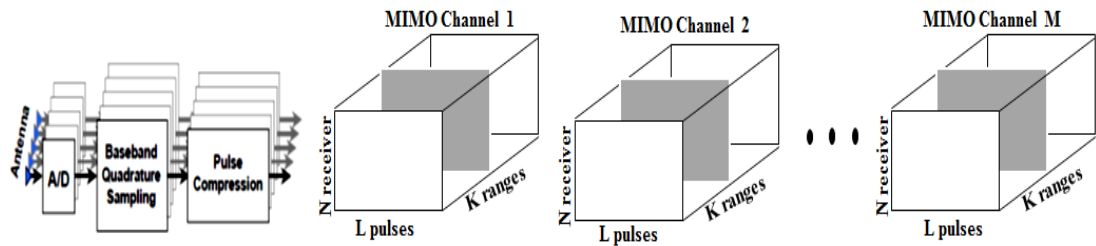


Figure.3.7: MIMO Data cube in a CPI.

In figure 3.7 we see obtained data of MIMO radar in a CPI. Thus a MIMO STAP processor will operate on a four dimensional data hypercube that encompasses the transmit elements M, slow time Doppler pulses L, receive elements N and fast time range sample K. To make it simple we can unify this data cubes as illustrated in Figure 3.8.

In practice, neither R or x^t are known. R may be estimated from K secondary snapshots around the range cell under test as follows. Fig.3.9. The maximum likelihood estimate of the covariance matrix is given by

$$\hat{R}(k_0) = \frac{1}{K-1} \sum_{\substack{k=1 \\ k \neq k_0}}^K (x^c(k) + x^n(k))(x^c(k) + x^n(k))^H. \quad (3.14)$$

The target component x^t is replaced by a steering vector of the form (3.15) computed for a candidate couple of Doppler and spatial frequencies (f_D, f_s).

$$s(f_D, f_s) = b(f_D) \otimes a_R(f_s) \otimes a_T(\gamma f_s). \quad (3.15)$$

Where $b(f_D)$, $a_R(f_s)$ and $a_T(\gamma f_s)$ are temporal and receiving and transmitting spatial steering vectors of dimensions L, N and M, respectively. The suboptimal sample matrix inversion (MIMO) STAP weight vector then consists in [19-16-23]

$$w_{SMI}(k_0, f_D, f_s) = \hat{R}(k_0)^{-1} s(f_D, f_s). \quad (3.16)$$

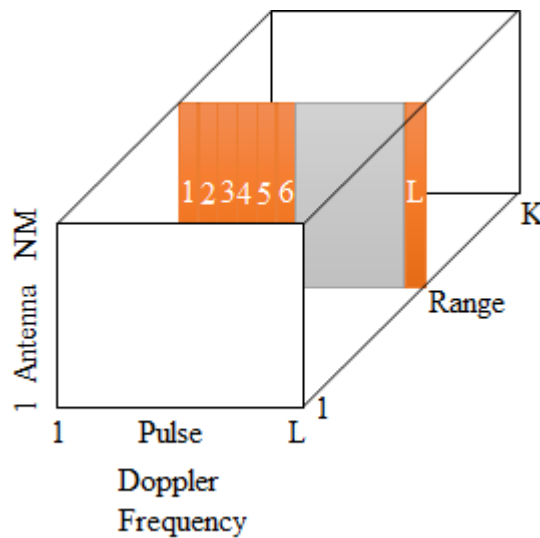


Figure3.8: MIMO STAP Data cube and Range cell of interest.

Note that a weight vector is computed for each range cell and each couple of Doppler and spatial frequencies. It is known in the STAP literature [24] that the “convergence“ of the SMI defined as the number of snapshots necessary to achieve a SINR loss performance of 3 dB compared to the optimal STAP in the absence of clutter, is twice the dimension of the received vector. It follows that the convergence for the SIMO and the MIMO cases is obtained for $K=2NL$ and $K=2NML$ snapshots, respectively. In the same way, the larger the size of the covariance matrix, the more complex the computational load required for the inversion in (3.16). It follows that $O((NML)^3)$ and $O((NL)^3)$ are necessary to compute the SMI weight vectors in the MIMO and SIMO cases, respectively. The theoretical interest of the MIMO system becomes thus limited in practice.

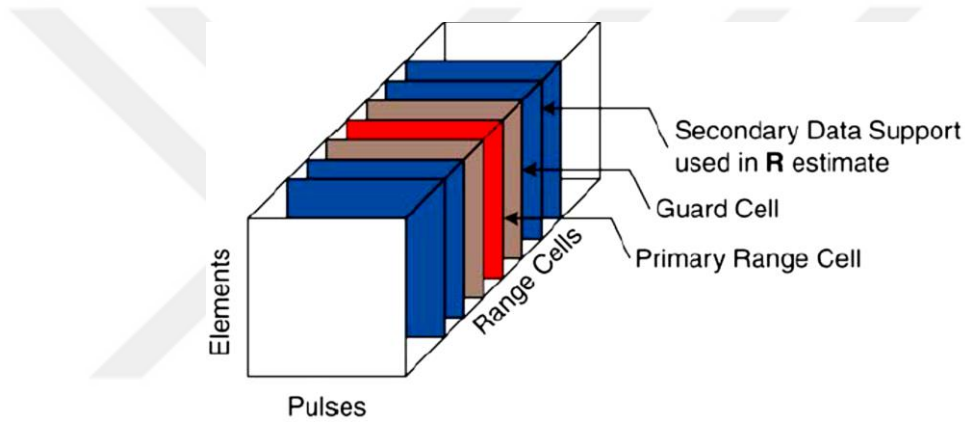


Figure3.9: Estimating the space-time interference covariance matrix.

An alternative approach proposed in the literature for reducing the convergence is based on rank reduction. For example, the eigencanceller (EC) method that we will study in next section.

3.2.3 Clutter Subspace in MIMO Radar System

In this subsection, we explain the subspace and rank of clutter space in the MIMO radar scheme. We can express the covariance matrix R in (3,8) as $R = R_t + R_c + R_j + \sigma^2 I$, where R_t indicates the covariance matrix of the target data, R_c determines the covariance matrix of the clutter data, R_j indicates the covariance matrix of the jammer data, and σ^2 is the variance of the white noise. In STAP literature researcher denoted The clutter subspace as the range space of R_c and denoted the clutter rank as the rank of R_c . In the space time adaptive processing (STAP) investigations, it is a principle

knowledge that the clutter subspace generally has a small rank. Klemm was the first one who illustrated in [25], that the clutter rank is roughly $N+L$ where N and L indicate the number of receiving elements and number of pulses in a coherent processing interval (CPI) Respectively. In [23] and [26], a method for computing the clutter rank was advised. The computed rank is roughly

$$N + \beta(L - 1). \quad (3.17)$$

Where $\beta = 2vT/d_R$. This is named Brennan's rule. In [27], this method has been extended to the models with arbitrary antenna arrays. Using benefits of the low rank feature, the STAP can be applied in a lower dimensional area so that the convergence and the complexity can be highly improved [28]–[16]. This outcome will now be extended to the MIMO radar system. These approaches are often named partially adaptive techniques or subspace techniques.

To approximate the clutter rank in MIMO radar system we describe the clutter term in (3.6) which is displayed as

$$y_{n,m,l}^{(c)} = \sum_{i=0}^{N_c-1} p_i e^{j2\pi f_{s,i}(n+\gamma m+\beta l)}. \quad (3.18)$$

For $n = 0,1,2, \dots, N-1$, $m = 0,1,2, \dots, M-1$, and $l = 0,1,2, \dots, L-1$. Note that $-0.5 \leq f_{s,i} \leq 0.5$ because $d_R = \lambda/2$.

Define
$$C_{i,m,n,l} = e^{j2\pi f_{s,i}(n+\gamma m+\beta l)}. \quad (3.19)$$

And
$$C_i = (C_{i,0,0,0}, C_{i,1,0,0}, \dots, C_{i,N-1,M-1,L-1})^T. \quad (3.20)$$

By stacking the $\{y_{n,m,l}^{(c)}\}$ signals into a vector, one can obtain

$$y^{(c)} = \sum_{i=0}^{N_c-1} p_i C_i. \quad (3.21)$$

Assume that p_i are zero-mean independent random variables with variance $\sigma_{c,i}^2$. The clutter covariance matrix can be expressed as

$$R_c = E \left[y^{(c)} y^{(c)\dagger} \right] = \sum_{i=0}^{N_c-1} \sigma_{c,i}^2 C_i C_i^\dagger. \quad (3.22)$$

Therefore, $\text{span}(R_c) = \text{span}(C)$ where

$$C \triangleq (C_0, C_1, \dots, C_{N_c-1}). \quad (3.23)$$

The vector c_i contain the samples of $e^{j2\pi f_{s,i}x}$ at points $\{n + \gamma m + \beta l\}$, while γ and β are denoted in (3.6). Usually c_i , is a random sampled type of the band limited sinusoidal signal $e^{j2\pi f_{s,i}x}$. If both of γ and β are integers, then the sampled points can only be integers in $\{0, 1, \dots, N + \gamma(M - 1) + \beta(L - 1)\}$.

If $N + \gamma(M - 1) + \beta(L - 1) \leq NML$, then there will be duplications in the results. In simple words, some of the row vectors in C will be completely the same and there will be maximum $N + \gamma(M - 1) + \beta(L - 1)$ separate row vectors in C . Hence, the rank of C is smaller than $N + \gamma(M - 1) + \beta(L - 1)$. So the rank of R_c is.

$$\text{rank}(R_c) \approx [N + \gamma(M - 1) + \beta(L - 1)]. \quad (3.24)$$

This outcome can be thought as a generalization of Brennan's rule [23], given in (3.17), to the MIMO radar system model.

In the SIMO radar system model, applying Brennan's rule, the ratio of the clutter rank and the total dimension of the space time processing steering vector can be obtained as

$$\frac{N + \beta(L - 1)}{NL} = \frac{1}{L} + \frac{\beta(L - 1)}{NL}. \quad (3.24)$$

In the MIMO radar system model with $\gamma = N$ (best case scenario in Figure 2.9), the corresponding ratio becomes

$$\frac{N + N(M - 1) + \beta(L - 1)}{NML} = \frac{1}{L} + \frac{\beta(L - 1)}{NML}. \quad (3.25)$$

We can view that the clutter rank now is smaller than the total data dimension because of the additional dimension originated by the MIMO radar system. So the MIMO radar receiver can mitigate the clutter subspace with little impression on signal-interference noise-ratio. Therefore, a superior spatial resolution for clutter can be accessed.

It is thus worth noting that the convergence speed is no longer proportional to the product of the number of transmitting and receiving elements but a linear combination of them (3.24). Moreover it is also worth noting that if you compare a SIMO antenna array of $N' = MN$ physical elements you can find a MIMO system of N and M physical receiving and transmitting elements, so that by choosing adequately γ ($\gamma < N$) the

rank r_{MIMO} is smaller than the rank of r_{SIMO} the corresponding SIMO. It then follows that with the EC approach, the MIMO STAP system can converge faster than its SIMO counterpart. This was not the case for the SMI algorithm.

3.2.4 Data-Independent Estimation of the Clutter Subspace with PSWF

In this subsection, we analyze a technique which figure out the clutter subspace by utilizing the geometry of the system rather than the received data. The major excellence of this technique is that it is independent from data type. The clutter subspace acquired by this technique can be utilize to enhance the convergence of the space time processing. Analyzes also show that the obtained subspace is more reliable than the ideal case (without ICM and array misalignment).

The vector c_i which is obtained in (3.20) can be noticed as a randomly sampled model of the truncated sinusoidal function

$$c(x; f_{s,i}) \triangleq \begin{cases} e^{j2\pi f_{s,i}x}, & 0 \leq x < X \\ 0, & \text{otherwise.} \end{cases} \quad (3.26)$$

Where $X \triangleq N - 1 + \gamma(M - 1) + \beta(L - 1)$. In addition $-0.5 \leq f_{s,i} \leq 0.5$, because d_R is mostly chosen $\lambda/2$ as in (3.5) to prevent aliasing. So, the power of these signals is often limited to a specified time-frequency space. Fig.3.10 displays a model of such a signal. This kind of signals can be well estimated by linear combinations of $[2WX + 1]$ orthogonal functions [29], where W indicates the one-sided bandwidth and X denotes the duration of the time-limited functions. Hence, we have $W = 0.5$ and $[2WX + 1] = N - 1 + \gamma(M - 1) + \beta(L - 1)$. The vectors c_i can be also estimated by a linear combination of the randomly sampled versions of these $[N - 1 + \gamma(M - 1) + \beta(L - 1)]$ orthogonal functions.

To estimate the subspace that contains this kind of signals, there is a root functions which are limited in time and centralize their power on the matching bandwidth. This kind of original functions are the answers of the following integral equation [29].

$$\mu\psi(x) = \int_0^X \text{sinc}(2W(x - \zeta))\psi(\zeta)d\zeta. \quad (3.27)$$

Where μ denotes a scalar to be found. There are infinite number of solutions $\psi_i(x)$ to this integral equation and μ_i for $= 0, 1, \dots, \infty$. The approximation of $\psi_i(x)$ is called

Prolate Spheroidal Wave Functions (PSWF). By the maximum principle [30], the solution satisfies

$$\begin{aligned} \psi_0(x) &= \arg \max_{\|\psi\|=1} \int_0^X \int_0^X \psi^*(x) \text{sinc}(2W(x-\zeta)) \psi(\zeta) d\zeta dx \\ \psi_1(x) &= \arg \max_{\|\psi\|=1} \int_0^X \int_0^X \psi^*(x) \text{sinc}(2W(x-\zeta)) \psi(\zeta) d\zeta dx \\ &\text{subject to } \int_0^X \psi(x) \psi_k^*(x) dx = 0 \\ &\text{for } k = 0, 1, \dots, i-1. \end{aligned} \quad (3.28)$$

For $i = 0, 1, \dots, \infty$

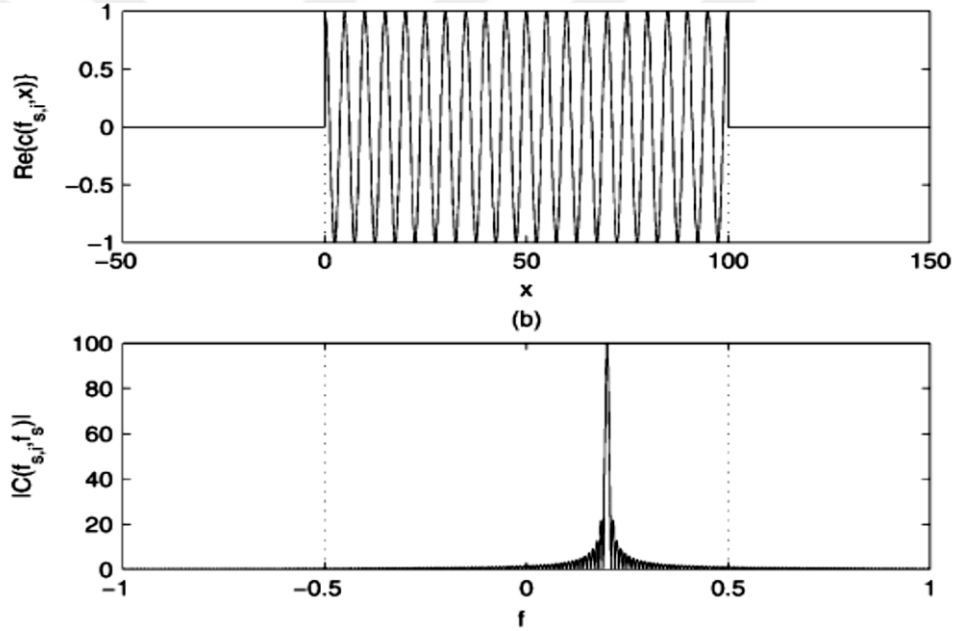


Fig.3.10: (a) Real part and (b) Magnitude response of Fourier transform of Instance of the signal $c(x; f_{s,i})$.

The operation $\psi_i(x)$ is orthogonal to the prior root elements $\psi_k(x)$, for $k < i$ while centralize most of its power on the bandwidth $[-W, W]$. Furthermore, only the first $[2WX + 1]$ eigenvalues μ_i are important [29]. Therefore, the function $c(x; f_{s,i})$ in (3.26) which is limited in time and bandwidth can be truly estimated by linear combinations of $\psi_i(x)$ for $i = 0, 1, \dots, [2WX + 1]$. In this case, $W = 0.5$ and $[2WX + 1] = N - 1 + \gamma(M - 1) + \beta(L - 1)$. So, the randomly sampled versions of $c(x; f_{s,i})$, specifically $c_{i,n,m,l}$, can be estimated by the linear combination

$$C_{i,m,n,l} \triangleq e^{j2\pi f_{s,i}(n+\gamma m+\beta l)} \approx \sum_{k=0}^{r_c-1} \alpha_{i,k} \psi_k(n + \gamma m + \beta l). \quad (3.29)$$

for some $\{\alpha_{i,k}\}$, where

$$r_c \triangleq [N + \gamma(M - 1) + \beta(L - 1)]. \quad (3.30)$$

Stacking the above components into vectors, we have

$$c_i \approx \sum_{k=0}^{r_c-1} \alpha_{i,k} u_k. \quad (3.31)$$

Where u_k is a vector that consists of the elements $\psi_k(n + \gamma m + \beta l)$. Finally, we have

$$\text{span}(R_c) = \text{span}(C) \approx \text{span}(U_c). \quad (3.32)$$

Where $U_c \triangleq (u_0; u_1; \dots; u_{r_c-1})$. Notice that in spite of being Orthogonality of the operation $\psi_k(x)$, the vectors $\{u_k\}$ are usually not orthogonal. This is result of the reality that $\{u_k\}$ are acquired by random sampling which damages orthogonality. In real operation, the PSWF $\psi_i(x)$ can be approximated off-line and saved in the memory. When the elements alter, one can acquire the vectors u_k by resampling the PSWF $\psi_k(n + \gamma m + \beta l)$ to approximate the new clutter subspace. In this way, we can acquire the clutter subspace by utilizing the geometry of the issue. Note that, unlike the eigendecomposition technique, the proposed method based on PSWF does not need the information of R_c .

3.3 PSWF STAP Technique for MIMO Radar System

In this subsection, we explain PSWF STAP technique for MIMO radar which uses the clutter subspace approximation method described in the last section. Because the clutter subspace can be acquired by using the parameter knowledge, the performance and complexity can both be improved.

The target-free covariance matrix can be signified as $R = R_c + R_j + \sigma^2 I$, while R_j indicates the covariance matrix of the jammer signals, R_c indicates the covariance matrix of the clutter signals, and σ^2 denotes the variance of the white noise. Considering (3.32), there is a $r_c \times r_c$ matrix A_c so that $R_c \approx U_c A_c U_c^\dagger$. Where U_c is the square matrix whose i th column is the eigenvector of R_c and A_c is the diagonal

matrix whose diagonal components are the corresponding eigenvalues. Thus, the covariance matrix can be approximated by

$$R \approx R_J + \sigma^2 I + U_c A_c U_c^\dagger. \quad (3.33)$$

$$\text{Define } R_v = R_J + \sigma^2 I.$$

The jammer signals $\mathbf{y}_{n,m,l}^{(J)}$ which figure out in (3.6) are statistically independent in different pulses and different orthogonal waveform components [19]. Therefore, they satisfy

$$E \left[\mathbf{y}_{n,m,l}^{(J)} \cdot \mathbf{y}_{n',m',l'}^{(J)\dagger} \right] = \begin{cases} r_{J,n,n'}, & m=m', l=l' \\ 0, & \text{otherwise.} \end{cases} \quad (3.34)$$

for $n, n' = 0, 1, 2, \dots, N$, $m, m' = 0, 1, 2, \dots, M$, and $l, l' = 0, 1, 2, \dots, L$. Using this fact, the jammer-plus-noise covariance matrix R_v defined in (3.33) can be expressed as

$$R_v = \text{diag}(R_{v_s}, R_{v_s}, \dots, R_{v_s}). \quad (3.35)$$

Where R_{v_s} is an $N \times N$ matrix with elements $[R_{v_s}]_{n,n'} = r_{J,n,n'} + \sigma^2$ for $n, n' = 0, 1, 2, \dots, N$. Hence, the covariance matrix R_c which shown in (3.33) include a block-diagonal jammer-pulse-noise and a low-rank clutter covariance matrix. By performing the matrix inversion lemma [31], we can acquire

$$R^{-1} \approx R_v^{-1} - R_v^{-1} U_c (A_c^{-1} + U_c^\dagger R_v^{-1} U_c)^{-1} U_c^\dagger R_v^{-1}. \quad (3.36)$$

Note that calculation of the block-diagonal matrix R_v^{-1} inversion is simple $R_v^{-1} = \text{diag}(R_{v_s}^{-1}, R_{v_s}^{-1}, \dots, R_{v_s}^{-1})$, and the multiplication of this block-diagonal matrix with another matrix is easy.

3.3.1 Complexity of the New Method

The complexity of directly inverting the $NML \times NML$ covariance matrix R is $O(N^3 M^3 L^3)$. Taking advantage of the block-diagonal matrix and the low rank matrix, in (3.36), the complexity for computing R_v^{-1} is only $O(N^3)$ and in computing A_c^{-1} and $(A_c^{-1} + U_c^\dagger R_v^{-1} U_c)^{-1}$ the complexity just is $O(r_c^3)$, while r_c is indicated in (3.30). The whole complexity for calculating (3.36) is thus diminished from $O(N^3 M^3 L^3)$ to $O(r_c N^2 M^2 L^2)$. This is the complexity of the two $(r_c \times NML)$ matrix multiplication.

The matrix U_c in (3.36) can be acquired by the random sampling of the PSWF as expressed in the last subsection. The noise -pulse- jammer covariance matrix R_v and the matrix A_c both need further approximation from the received data. By reason of the block-diagonal structure, one can approximate the covariance matrix R_v by approximate its submatrix R_{vS} determined in (3.35). The matrix R_{vS} can be approximated when there are no target signals and clutter echo. For this operation, the radar system work in passive mode so that the receive elements can gather the signals with only jammer signals and white noise [16]. The submatrix R_{vS} can be expressed as

$$\hat{R}_{vS} = \frac{1}{K_v} \sum_{k=0}^{K_v-1} r_k r_k^\dagger. \quad (3.37)$$

While r_k is $N \times 1$ vector and indicates the target free and clutter free data collecting by N receiving elements and K_v denotes the number of snapshot in passive mode. By (3.33), one can express A_c as

$$A_c = (U_c^\dagger U_c)^{-1} U_c^\dagger (R - R_v) U_c (U_c^\dagger U_c)^{-1}. \quad (3.38)$$

Therefore, one can estimate A_c by using

$$\hat{A}_c = \frac{1}{K} \sum_{k=0}^{K-1} x_k x_k^\dagger - (U_c^\dagger U_c)^{-1} U_c^\dagger \hat{R}_v U_c (U_c^\dagger U_c)^{-1}. \quad (3.39)$$

Where $x_k = (U_c^\dagger U_c)^{-1} U_c^\dagger y_k$ and y_k is the MIMO space time processing data vector illustrated in (3.7). Substituting (3.36), (3.37) and (3.39) into the MIMO space time adaptive beamformer in (3.16), we acquire

$$w \propto (\hat{R}_v^{-1} - \hat{R}_v^{-1} U_c (\hat{A}_c^{-1} + U_c^\dagger \hat{R}_v^{-1} U_c)^{-1} U_c^\dagger \hat{R}_v^{-1}) s(f_s, f_d). \quad (3.40)$$

3.3.2 Zero-Forcing Technique

Instead of approximating A_c and calculating the Minimum variance distortionless response (MVDR) by (3.40), it is possible straightly “null out” the whole clutter subspace as explain next. Consider that the clutter-to-noise ratio is adequately large and in result whole of the eigenvalues of A_c reach infinity. We acquire $A_c^{-1} \approx 0$. Applying it into (3.40), we can acquire the MIMO space time beamformer as

$$w \propto (\hat{R}_v^{-1} - \hat{R}_v^{-1} U_c (U_c^\dagger \hat{R}_v^{-1} U_c)^{-1} U_c^\dagger \hat{R}_v^{-1}) s(f_s, f_d). \quad (3.41)$$

So we acquire a “zero-forcing” beamformer that mitigate the whole clutter subspace. Because it is no longer necessary to approximate A_c in this method the benefit of this zero-forcing technique is distinguished. Here, we only require to estimate R_{vs} . The technique is no related to the range bin. The matrix R^{-1} calculated by this technique can be utilized for whole range bins. As a result of extra additional dimensions in MIMO STAP, removing the whole clutter subspace will decrease just a small portion of the total dimension. Hence, it will not impress the signal interference plus noise ratio performance importantly, as we shall illustrate. Thus, this technique can be very impressive in multiple input multiple output radar systems.

3.4 Range Recursive Space Time Adaptive Processing (STAP)

From the computational complexity point of view the EC STAP algorithm encounters the same drawbacks as the SMI algorithm, it is to say that it is increased by a multiplicative factor of $O((M)^3)$ because of the eigendecomposition of the clutter plus noise covariance matrix. It is why in this section we explore a range recursive EC-based STAP algorithm. It takes benefit of the abovementioned rank reduction property and consequently convergences faster than the SMI and has a computational load of only $O(NL)$ and $O(MNL)$ for the SIMO and the MIMO cases, respectively.

Here we explain a range recursive subspace-based algorithm in order to construct the STAP filter. Traditionally used in spectral analysis and antenna processing as time-recursive adaptive algorithms [32], adaptive recursive subspace-based algorithms such as FAPI have been more recently used in STAP for airborne radar [33]. In this case of STAP, the recursion relates to the distance instead of time. The classical subspace tracking algorithm on which FAPI is established considers the following scalar function [34]

$$J(W) = E(\|x - WW^H x\|^2). \quad (3.42)$$

Where x is the observed data vector of covariance matrix R and W is the matrix argument. This cost function possesses just a global minimum [34] which is attained only if $W = U_c Q$ where U_c the clutter subspace basis defined in (3.33) and Q is a

unitary matrix. The original algorithm which considered this abovementioned criterion is the projection approximation subspace tracking (PAST) algorithm [34] replacing the expectation by an exponentially weighted sum and supposing an approximation of the clutter ($W(i-1) \approx W(i)$ where i was time in the original version of PAST and that we transpose to range in the proposed STAP version). Thus a basis of the clutter subspace is obtained as the solution of the unconstrained minimization problem:

$$J(W(k)) = \sum_{i=1}^k \beta^{k-i} \|x(i) - W(k)W(i-1)^H x(i)\|^2. \quad (3.43)$$

Where $x(i)$ is the observed data vector at range i and $W(k)$ is the estimated interference (clutter plus noise) subspace basis at range k and β a forgetting factor, $0 < \beta < 1$. This exponentially least square problem is solved by a recursive computation. We here are more interested by the FAPI algorithm [33] which is based on the previous approach with a less restrictive approximation: the projection on the clutter subspace at range i is approximated by the projection on the clutter subspace at range $i-1$.

$$W(i)W(i)^H \approx W(i-1)W(i-1)^H. \quad (3.44)$$

The obtained subspace is found to be orthonormalized. The details of this algorithm are given in table.3.2. The corresponding STAP filter computed for each snapshot is obtained through

$$w_{FAPI}(k) = (I - W(k)W(k)^H)v(f_D, f_S). \quad (3.45)$$

3.5 Fast and stable YAST algorithm

In this section we explore another implementation of the YAST algorithm (Yet Another Subspace Tracker) for principal and minor subspace tracking. YAST was initially derived from the Subspace Projection (SP) algorithm by C.E. Davila [38], which was known for its exceptional convergence rate, compared to other classical principal subspace trackers. The novelty in the YAST algorithm was the lower computational cost (linear if the data correlation matrix satisfies a so-called shift-invariance property), and the extension to minor subspace tracking. However, the original implementation of the YAST algorithm suffered from a numerical stability problem (the subspace weighting matrix slowly loses its orthonormality)[35].

TABLE.3.2: the input $\mathbf{x}(k)$ is \mathbf{x} defined in (3.11) at range k .

FAP Algorithm

Initialization : $W(0) \leftarrow I_{M \times N}, Z(0) \leftarrow I_{N \times N}$

For $K = 1$ to *Nbr snapshot* **do**

$$y(k) = W(k-1)^H \cdot x(k)$$

$$h(k) = Z(k-1) \cdot y(k)$$

$$g(k) = \frac{h(k)}{\beta + y^H(k) \cdot h(k)}$$

$$e(k) = x(k) - W(k-1) \cdot y(k)$$

$$\varepsilon^2(k) = \|x(k)\|^2 - \|y(k)\|^2$$

$$\tau(k) = \frac{\varepsilon^2(k)}{1 + \varepsilon^2(k)\|g(k)\|^2 + \sqrt{1 + \varepsilon^2(k)\|g(k)\|^2}}$$

$$\eta(k) = 1 - \tau(k)\|g(k)\|^2$$

$$y'(k) = \eta(k)y(k) + \tau(k)g(k)$$

$$h'(k) = Z(k-1)^H y'(k)$$

$$\epsilon(k) = \frac{\tau(k)}{\eta(k)} (Z(k-1)g(k) - (h'(k)g(k))g(k))$$

$$Z(k) = \frac{1}{\beta} (Z(k-1) - g(k)h'(k)^H + \epsilon(k)g(k)^H)$$

$$e'(k) = \eta(k)x(k) - W(k-1)y'(k)$$

$$W(k) = W(k-1) + e'(k) \cdot g(k)^H$$

End for

Consider a sequence of independent n -dimensional random data vectors $\{x(t)\}_{t \in Z}$, whose $n \times n$ correlation matrix $C_{xx}(t)$ is estimated by applying an exponential window to the data, leading to the update

$$C_{xx}(t) = \beta C_{xx}(t-1) + x(t)x(t)^H. \quad (3.46)$$

Where $0 < \beta < 1$ is the exponential forgetting factor. As mentioned in [35], the generalized Rayleigh quotient is maximized (resp. minimized) when the subspace weighting matrix $W(t)$ spans the principal subspace (resp. the minor subspace) of $C_{xx}(t)$. Unfortunately, implementing this optimization over all orthonormal matrices is computationally demanding, and does not lead to a simple recursion between $W(t)$ and $W(t-1)$. In order to reduce the complexity, the implementation of YAST

proposed below recursively performs this search within the $(r + 1)$ -dimensional subspace spanned by $W(t - 1)$ and $x(t)$.

Let $\Pi(t)$ be the orthogonal projector on the augmented subspace, and $W(t)$ an $n \times (r + 1)$ orthonormal matrix such that

$$\Pi(t) = W(t)W(t)^H. \quad (3.47)$$

Then any r -dimensional subspace of $\text{span}(\Pi(t))$ can be represented by the orthogonal projector

$$\Pi(t) = \Pi(t) - v(t)v(t)^H. \quad (3.48)$$

Where the unitary vector $v(t)$ belongs to the range space of $\Pi(t)$. In particular, $v(t)$ can be written in the form

$$v(t) = W(t)\phi(t). \quad (3.49)$$

Where $\phi(t)$ is an $(r + 1)$ -dimensional unitary vector. Substituting equations (3.47) to (3.49) into *generalized Rayleigh quotient* [35], the criterion to be optimized can be rewritten as

$$\mathcal{J}(\Pi(t)) = \text{trace} \left(C_{yy}(t) \right) - \phi(t)^H C_{yy}(t) \phi(t). \quad (3.50)$$

Where $C_{yy}(t)$ is the $(r + 1) \times (r + 1)$ matrix

$$C_{yy}(t) = W(t)^H C_{xx}(t) W(t). \quad (3.51)$$

According to equation (3.50), \mathcal{J} is maximized (resp. minimized) when $\phi(t)$ is the minor (resp. principal) eigenvector of $C_{yy}(t)$. Finally, given the new data vector $x(t)$, the YAST algorithm updates the previous subspace weighting matrix $W(t - 1)$ by successively computing

- 1) An orthonormal basis $W(t)$ of the augmented subspace;
- 2) The compressed matrix $C_{yy}(t)$ defined in equation (3.51);
- 3) The principal or minor eigenvector $\phi(t)$ of $C_{yy}(t)$ (for MST or PST resp.), and a basis $W'(t)$ of the range space of the projector $\Pi(t)$ defined in equation (3.48);
- 4) The $r \times r$ compressed matrix $C'_{yy}(t)$, defined as

$$C'_{yy}(t) = W'(t)^H C_{xx}(t) W'(t). \quad (3.52)$$

Which will permit a fast calculation of $C_{yy}(t)$ in step 2).

The convergence of this YAST algorithm is proved and a fast implementation is proposed in [35]. The complete pseudo-code of YAST is summarized in table.3.3.

TABLE.3.3: YAST Algorithm

<i>Input: $x(t)$</i>
$y(t) = W(t - 1)^H x(t)$
$e(t) = x(t) - W(t - 1)y(t)$
$\sigma(t) = \ e(t)\ _2$
<i>if $\sigma(t) \neq 0$</i>
$u(t) = e(t) / \sigma(t)$
$x'(t) = C_{xx}(t - 1) x(t)$
$y'(t) = C_{yy}(t - 1) y(t)$
$y''(t) = W(t - 1)^H x'(t)$
$C'_{yy}(t) = \beta C_{yy}(t - 1) + y(t) y(t)^H$
$z(t) = \beta (y''(t) - y'(t)) / \sigma(t) + \sigma(t) y(t)$
$\gamma(t) = \beta \frac{x(t)^H x'(t) - 2\Re(y(t)^H y''(t)) + y(t)^H y'(t)}{\sigma(t)^2} + \sigma(t)^2$
$C_{yy}(t) = \begin{bmatrix} C'_{yy}(t) & z(t) \\ z(t)^H & \gamma(t) \end{bmatrix}$
If Principal Subspace Tracking
$(\emptyset(t), \gamma(t)) = \min\{rig(C_{yy}(t))\}$
Else if Minor Subspace Tracking
$(\emptyset(t), \gamma(t)) = \max\{rig(C_{yy}(t))\}$
End if
$[\varepsilon(t)\phi'(t)^T, \quad \varphi(t)]\theta(t) = \phi(t)^T$
$e_1(t) = -e^{i \text{angle}(\phi'_1(t))} [1, 0 \dots 0]^T$
$a(t) = \frac{\phi'(t) - e_1(t)}{\ \phi'(t) - e_1(t)\ _2}$
$b(t) = W(t - 1) a(t)$
$Q(t) = W(t - 1) - 2b(t)a(t)^H - \varepsilon(t)u(t) e_1(t)^H$
$D(t) = \text{diag}(1/\ q_1(t)\ _2, 1 \dots 1)$
$W(t) = Q(t)D(t)$
$a'(t) = 4C'_{yy}(t)a(t) - 4(a(t)^H C'_{yy}(t)a(t)) a(t)$
$z'(t) = 2z(t) - 4(a(t)^H z(t))a(t) - \varepsilon(t)\gamma(t)e_1(t)$
$C''_{yy}(t) = \text{Herm}(C'_{yy}(t) - a'(t)a(t)^H - \varepsilon(t)z'(t)e_1(t)^H)$
$C_{yy}(t) = D(t)C''_{yy}(t)D(t)$
End if



4. SIMULATION RESULTS

In this chapter, results of the simulations which have been performed in this thesis study are introduced. In this thesis, simulations are performed to present STAP performance of different MIMO radar configurations. At first we compare adapted patterns for optimum STAP of SIMO and MIMO radar. In this comparison we use simple matrix inversion method for different type of MIMO and SIMO radar configuration. Next, we demonstrate adapted pattern of MIMO STAP for the first time using FAPI algorithm which was proposed earlier in [39]. At the end we propose the fast and stable YAST algorithm for STAP in MIMO radar and we compare adapted patterns of FAPI and YAST.

In this section, a model is configured for the waveforms received by an airborne pulsed-Doppler radar antennas. In this model an array antenna is implanted on radar platform and there is an independent receiver channel (match filter) behind each element. The received signals will generally include a factor due to receiver noise and may include factor due to both desired object and undesired interference. Here, interference defines either clutter, jamming, or both. The outcomes engender here form the foundation for the analysis of the different space-time processing technique that are explained in the third chapter of this thesis.

Assumed system is a pulsed Doppler airborne radar. The radar antenna element is a uniformly spaced linear array antenna (ULA) including of M transmitter and N receiver. The radar platform is flying at an altitude h_a with a constant motion velocity vector v_a . The selected coordinate system is depicted in Figure 4.1. The angle variables θ and ϕ refer to true elevation and azimuth, and not the conventional spherical coordinate system angles.

TARGET: A target is determined as a scattered mobile point that must be discovered. The segment of the space time samples at the range gate matching to the target range R_t will be derived. Furthermore the target is specified by its elevation θ_t , azimuth ϕ_t , speed relative to the radar v_t , and radar cross-section (RCS) σ_t .

NOISE: Consider that the only noise origination is internally produced receiver noise, which is generally present on every channel. Because every antenna has its own channel, assume that the noise existent on every antenna are mutually uncorrelated. In addition, consider that the momentary bandwidth is wide compared with the PRF. Hence, noise samples on each antenna derived at time moment distinct by a nonzero multiple of the PRI are temporally uncorrelated.

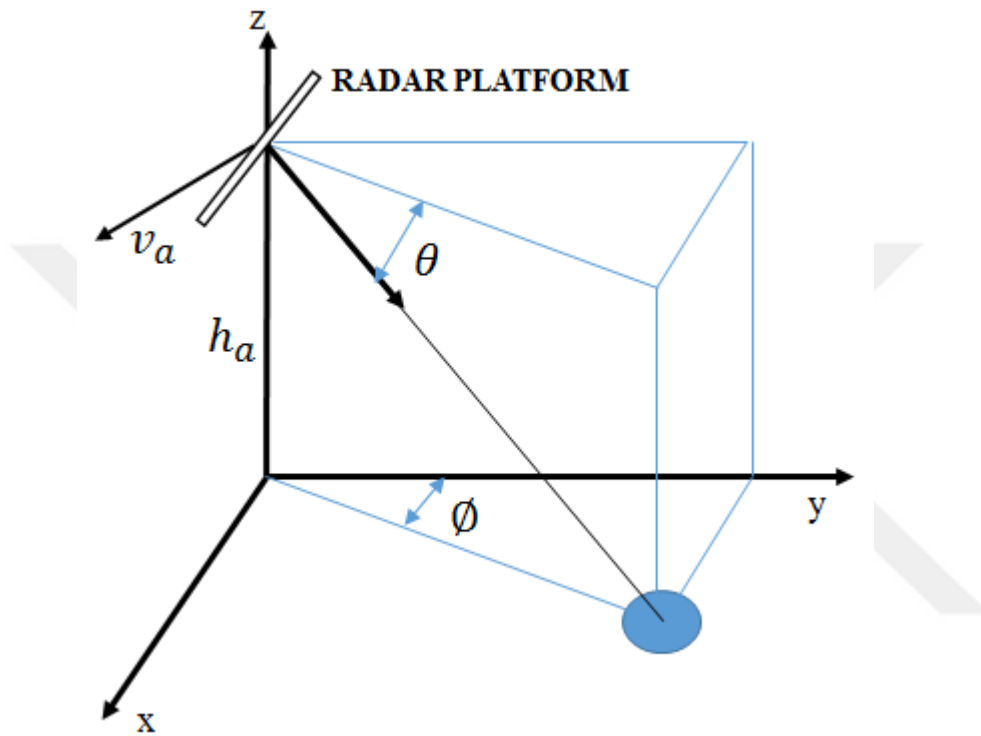


Figure 4.1: Platform geometry.

The noise energy is $\sigma^2 = N_0B$. For goal of this simulation, an appropriate normalization is to set $\sigma^2 = 1$ so that whole signal levels can be cited by their SNR per antenna and pulse.

The noise assumption above is practical only when the prevailing source of noise is internally originated receiver amplifier noise. If sky noise is a main generator, a spatial correlation may require to be applied into the model above.

JAMMING: Just barrage noise jamming which produces from airborne platforms or ground based at far distance from the radar will be considered. The jamming power is considered to fill the radar's momentary bandwidth. The narrowband consideration that a waveform's propagation time among the array (time delay) is small compared to $1/B$, so notice again there is signal correlation among the array. Oppositely, a radar PRF is

considered that is significantly short than the momentary bandwidth therefor the jamming decorrelates from one pulse to the next. In other words, the jamming is temporally uncorrelated from pulse to pulse and spatially correlated from antenna to antenna. Thus, jamming perform like a point target or a discrete clutter source spatially, but like as thermal noise in time domain.

CLUTTER: Radar clutter is usually known as the reflected signals from any scatterers believed to be not of strategic significance. For an airborne radar system, the ground surface is the main source of clutter and is the only type of clutter to be assumed in this simulation. Of the numerous origins of interference, clutter is the most complex because it is distributed in both range and angle and is spread in Doppler frequency because of the platform movement. In this thesis, a scheme is utilized for the ground clutter element of the space time samples for a target range, and the effects of the clutter space time covariance matrix are applied.

Since earth is considered to have zero inherent speed, the velocity of clutter depends only to the radar the platform velocity. Ground clutter is distributed in range unlike a target. It is extended from the platform altitude to the radar horizon over all azimuths.

As an estimation to a continuous form of clutter, the clutter echo from each unclear range will be considered as the overlap of a large number N_c of independent clutter origins that are equally distributed in azimuth about the radar. The energy of each clutter contribution is acquired from the radar equation for ground clutter [36]. Different type of the clutter scattering have been suggested, depending on the radar frequency, terrain type, polarization, etc. For the configuration in this thesis, the constant gamma model [36], $\sigma_0 = \gamma \sin \varphi_c$, is applied, where γ indicates the terrain dependent parameter and φ_c indicates grazing angle created by the ray from antenna to clutter patch and the surface tangent at the clutter patch .

For simplicity, the assumptions made in this simulation are listed in Table 4.1. In Table 4.2, airborne radar system parameters, platform and interference scenario are given. The platform altitude is 9 km, and the range of interest is 130 km. The clutter-to-noise ratio (CNR) is 40 dB. There are two jammers at -40° and 25° . The jammer-to-noise ratio (JNR) for each jammer equals 50 dB.

TABLE.4.1: Assumption in this model.

Model Summarization

Radar System

Constant PRF waveform

Constant platform velocity

Non-relativistic velocities

Array axis and platform velocity vector lie in the horizontal plane

Narrowband waveforms and receivers ($B \ll f_0$)

Uniform linear antenna array (possibly columns of a planar array)

Target Model

Constant velocity

Point target

Noise Model

Noise signals on different elements are mutually uncorrelated

Internally generated receiver noise is dominant source

Noise decorrelates over a PRI ($f_r \ll B$)

Jamming Model

Only continuous barrage noise jamming is considered

Jamming may be assumed stationary over a CPI (coherent processing interval)

Jamming signal decorrelates over a PRI

Clutter Model

Number of independent scatterers

Clutter from a single range approximated by large

Gaussian intrinsic clutter motion spectrum

Constant gamma reflectivity model

ICM (internal clutter motion) spectrum is the same for each clutter patch

TABLE.4.2: airborne radar system parameters, platform and interference scenario.

$M=6, 9$	number of transmitter
$N=3, 6, 9$	number of receiver
$L=18$	number of pulse
$f_0 = 450 \times 10^6$	radar operating frequency
$f_r = 300$	prf in hz
$G_t = 22$	transmit gain in db
$G_r = 10$	column receive gain in db
$N_c = 360$	number of clutter patches
$\lambda = c/f_0$	operating wavelength
$d_r = \lambda/2$	interelement spacing
$h_a = 9000$	platform height in meters
$v_a = 50 \text{ m/s}$	platform velocity
$FF = 3$	receiver noise figure in db
$P_n = N_n \times B$	receiver noise power in watts
$R_{cik} = 130k$	(clutter) range of interest in meters.
$dR = c/2/B$	radar range resolution
$R_e = 6370000$	earth radius in meters.
$L_s = 4$	system losses in db
$G_{el} = 4$	element gain in db
$\gamma = N$	dt/dr spacing of the transmitting antennas/ spacing of the receiver antennas
$\theta_{tj} = [-40 \ 25]$	jamer azimuth angles in degrees.
$\theta_{tt} = 0 \ \phi_{it} = 0$	target azimuth and elevation
$f_{dt} = 100$	target doppler frequency in Hertz.

4.1 Optimum Fully Adaptive STAP

In Figure.4.2 and Figure.4.3 we compare adapted patterns for optimum STAP of SIMO and MIMO radar. The expected target is placed at 0° azimuth with Doppler frequency 100 Hz. in the SIMO context of $N=18$ receiving elements, $M=1$ transmitting elements and $L=18$ pulses, $\beta = 1$. In the MIMO context of $N=6$ receiving elements, $M=3$ transmitting elements and $L=18$ pulses, $\beta = 1$ and $\gamma = N=6$ ($\gamma = d_T/d_R \beta = 2vT/d_R$). The pattern's mainlobe is at the target location. The jamming is suppressed by the deep vertical pattern nulls at the jammer azimuths. These pattern nulls suppress the interference at the output to well below thermal noise.

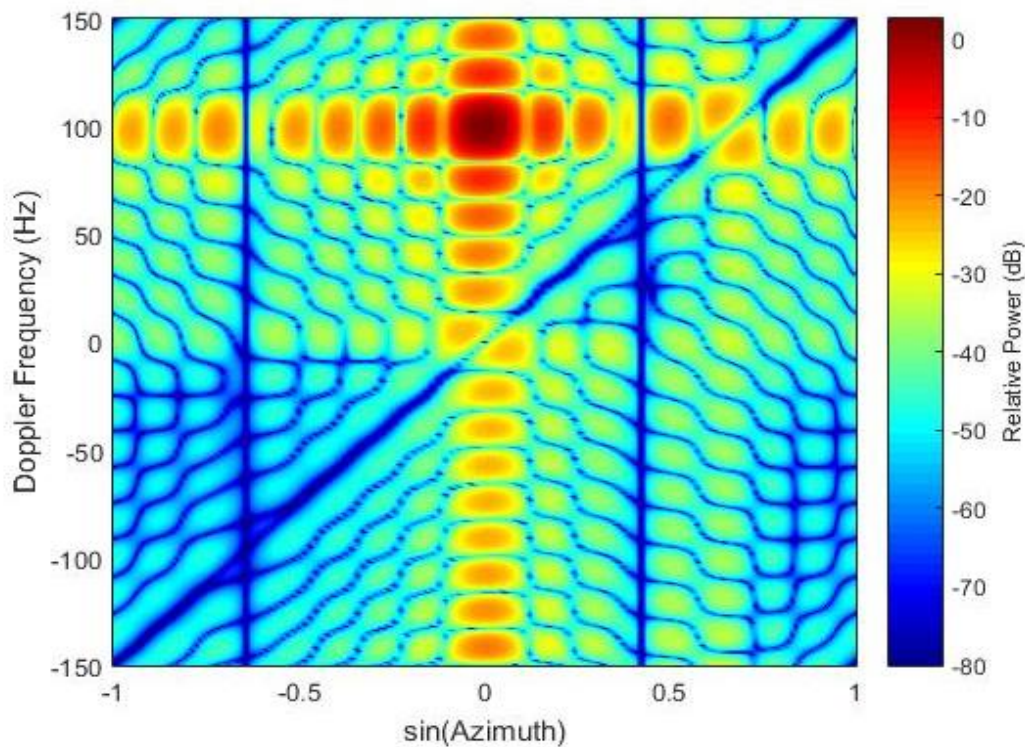


Figure.4.2: optimum fully adaptive STAP of SIMO radar $N=18$, $M=1$, $L=18$.

We can view the adapted pattern of 18 antennas in a SIMO radar system obtain only with 9 antennas in a MIMO radar. The results showed that compared to SIMO radar, MIMO radar could achieve the same STAP performance with fewer physical antennas and we will see when the number of antennas is the same, MIMO radar could obtain more distinct virtual array elements and have better adapted pattern.

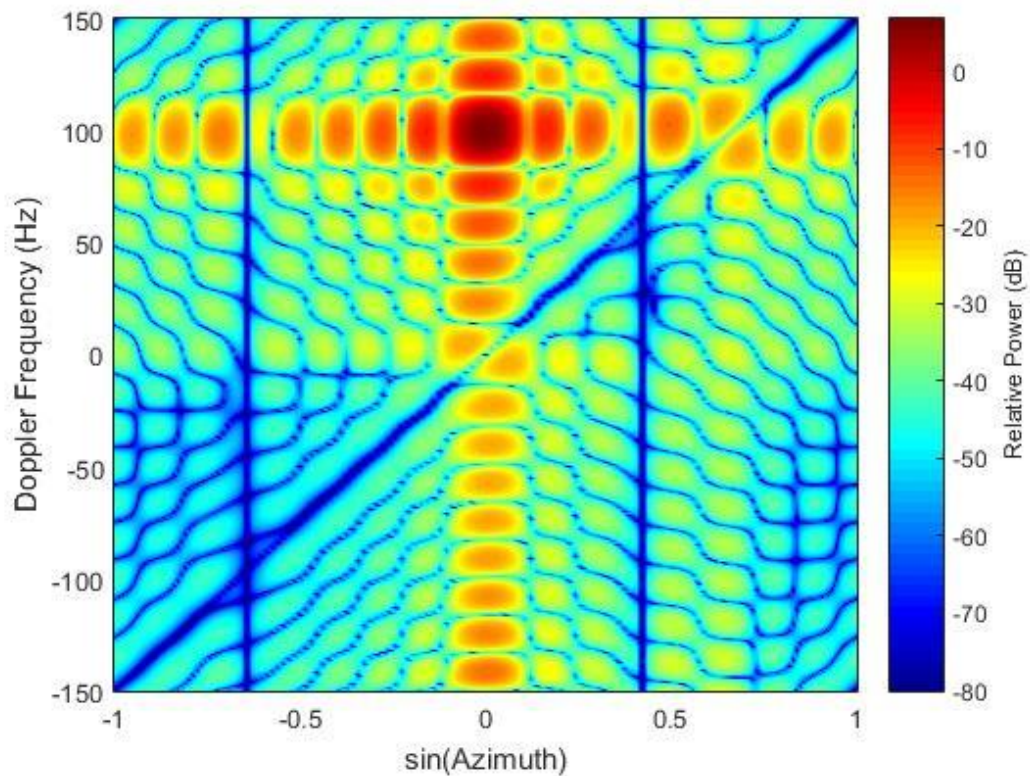


Figure.4.3: optimum fully adaptive STAP of MIMO radar $N=6$, $M=3$, $L=18$.

Figure.4.4 and Figure.4.5 depict the two original cuts of this patterns. The azimuth pattern at the target Doppler illustrates the receive beamformer; it represent nulls at both the jammer azimuths and the azimuth where the sidelobe clutter and target have the same Doppler frequency. The second cut depicts the Doppler Effect at the target azimuth. The intense clutter null appear at zero Doppler mitigates mainlobe clutter. Jammer and clutter nulls exist at other azimuths do not become visible in this pattern cut.

Once again we can see from principal plane cuts at target azimuth and Doppler that the MIMO radar with $M+N$ antenna arrays has the same performance as SIMO radar with $M*N$ antenna arrays and this is due to the advantage of Virtual Receiver Array Configuration in MIMO radar. Note that in this MIMO radar we configure the best scenario corresponds to the case where transmit and receive arrays share no antennas and $\gamma = N$.

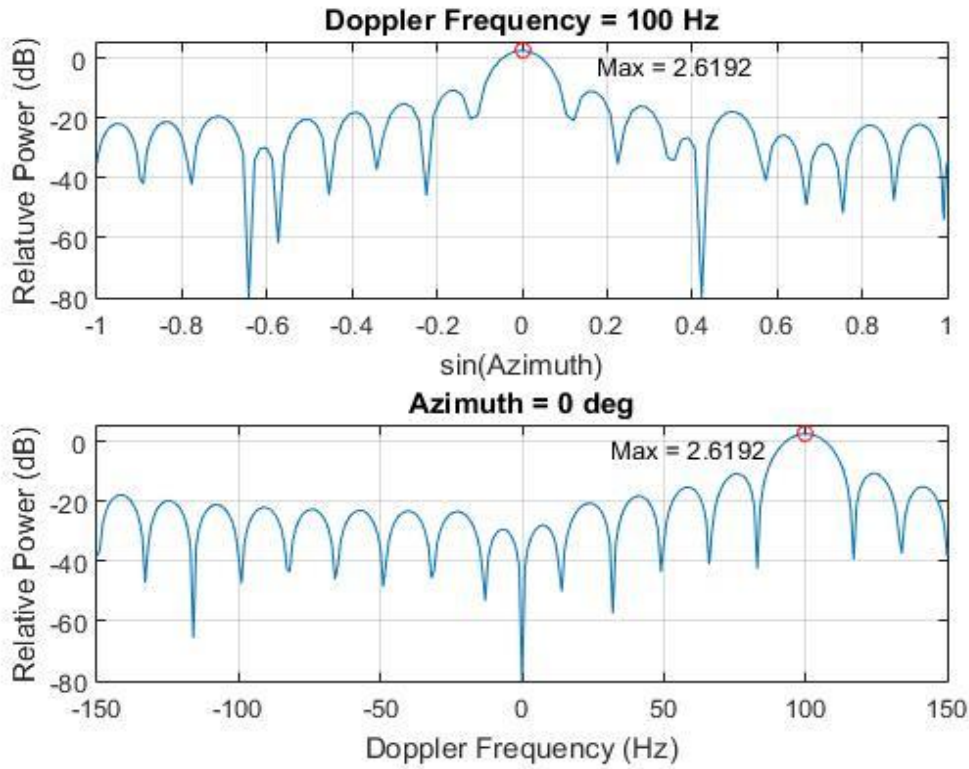


Figure.4.4: Principal plane cuts at target azimuth and Doppler of SIMO radar $N=18$, $M=1$, $L=18$.

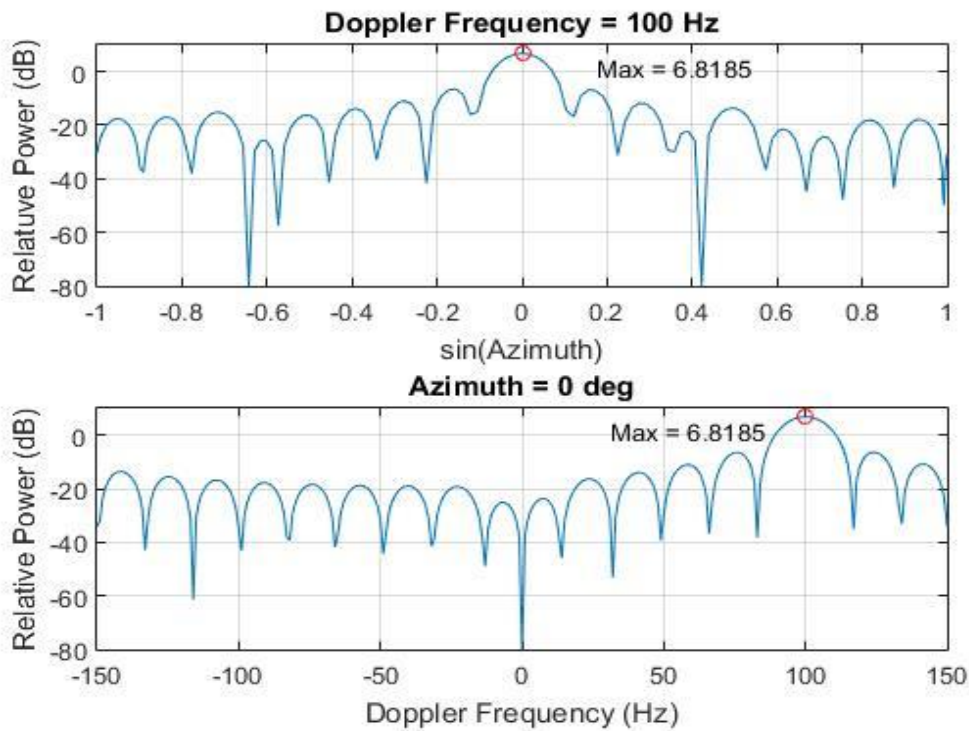


Figure.4.5: Principal plane cuts at target azimuth and Doppler of MIMO radar $N=6$, $M=3$, $L=18$.

The results in Figure 4.6 and Figure 4.7 reveal that while we configure MIMO radar with the same antenna number used in SIMO one, we obtain better angular resolution and higher SNIR. In this MIMO context $N=9$ receiving elements, $M=9$ transmitting elements and $L=18$ pulses, $\beta =1$ and $\gamma =N=9$. Figure 4.6 shows adapted patterns for optimum STAP of MIMO radar and Figure 4.7 depicts the two original cuts of this pattern. The azimuth pattern at the target Doppler illustrates the receive beamformer, it represent nulls at both the jammer azimuths and the azimuth where the sidelobe clutter and target have the same Doppler frequency. The second cut illustrates the Doppler Effect at the target azimuth. The intense clutter null appear at zero Doppler mitigates mainlobe clutter.

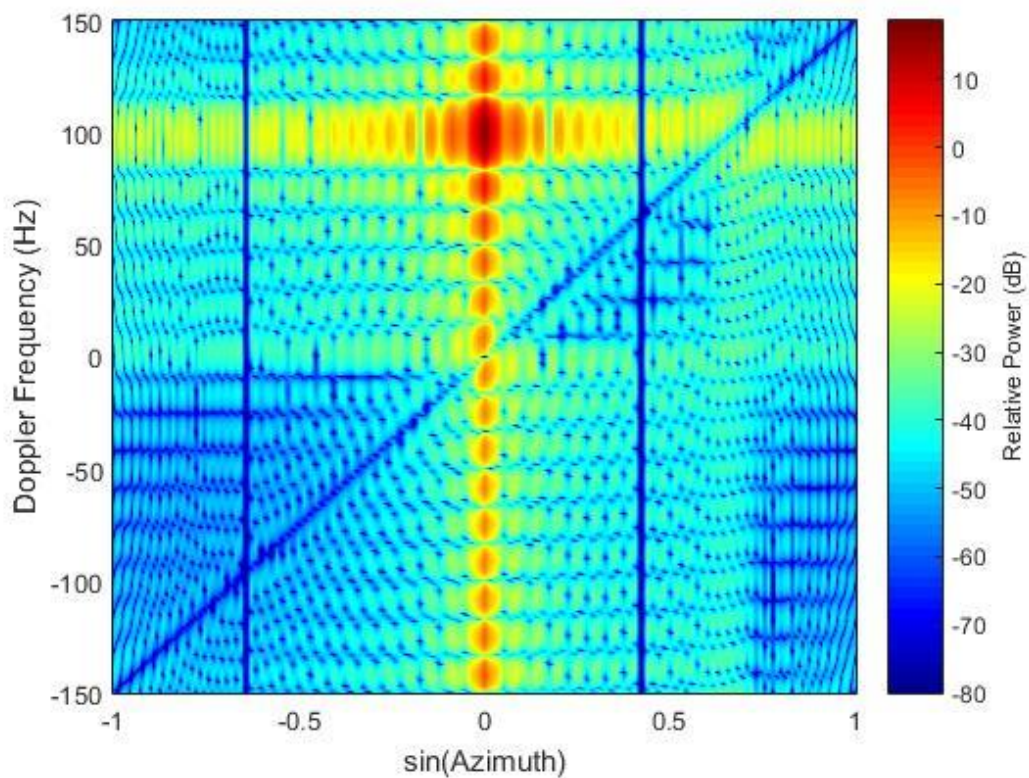


Figure.4.6: optimum fully adaptive STAP of MIMO radar $N=9$, $M=9$, $L=18$.

This time we increase the number of pulses in a CPI in MIMO radar and there is no change in the number of antennas. Figure 4.8 and Figure 4.9 depict adapted patterns for optimum STAP of MIMO radar and two original cuts of this pattern. The azimuth pattern at the target Doppler illustrates the receive beamformer. The second cut presents the Doppler Effect at the target azimuth.

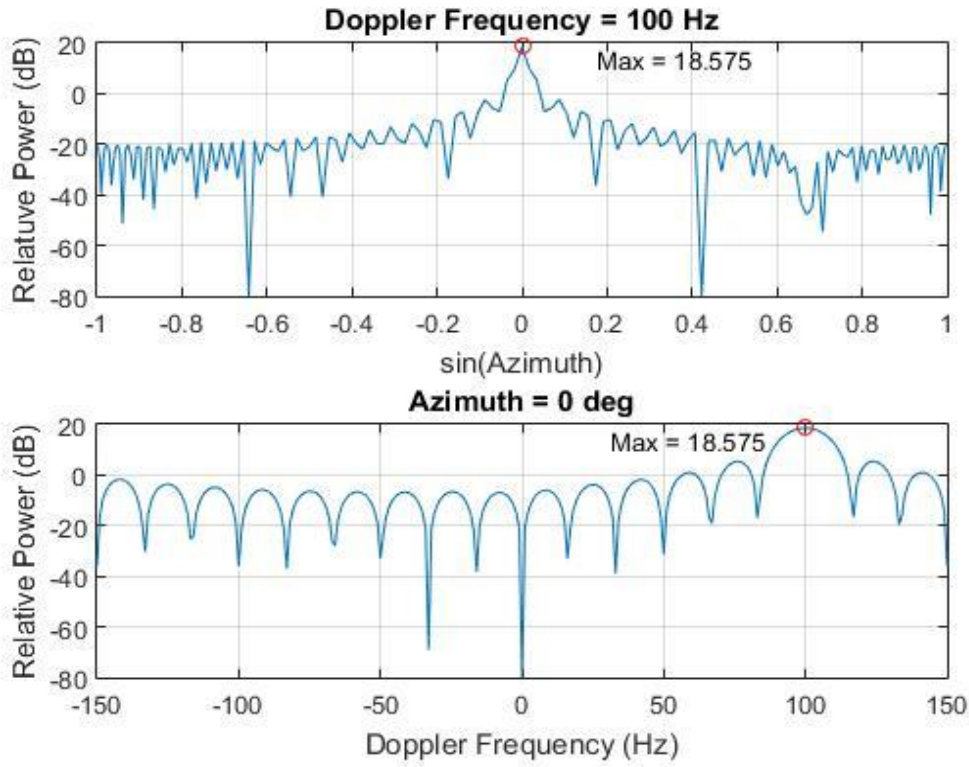


Figure.4.7: Principal plane cuts at target azimuth and Doppler of MIMO radar $N=9$, $M=9$, $L=18$.

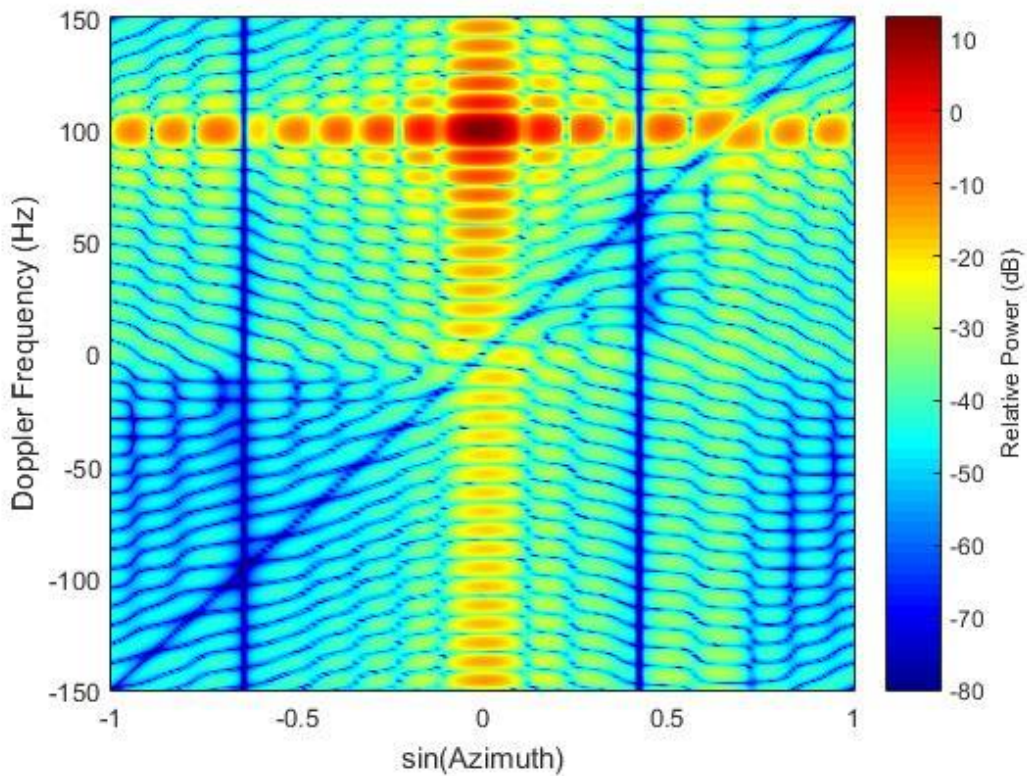


Figure.4.8: optimum fully adaptive STAP of MIMO radar $N=6$, $M=3$, $L=36$.

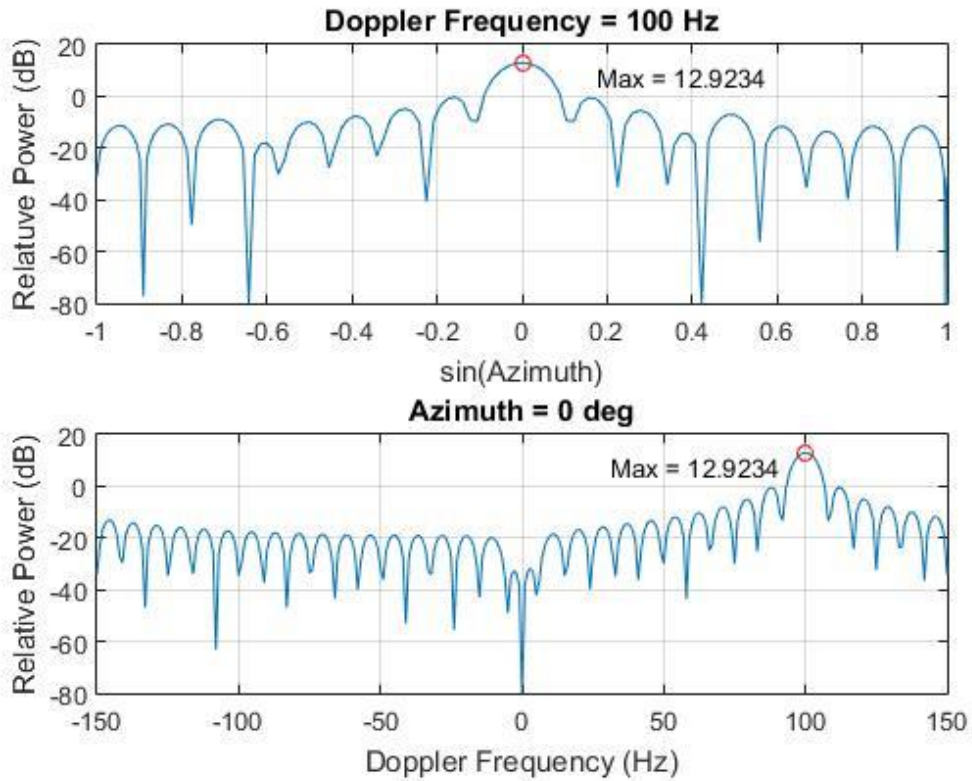


Figure.4.9: Principal plane cuts at target azimuth and Doppler of MIMO radar $N=6$, $M=3$, $L=36$.

4.2 FAPI Algorithm in STAP

In Figure 4.10 and Figure 4.11 the performances of the SIMO and MIMO versions of the FAPI algorithm are illustrated in the same conditions that those of Figures 4.2 and 4.3. Figure.4.12 and Figure.4.13 depict the two original cuts of this patterns. The azimuth pattern at the target Doppler illustrate the receive beamformer. The second cut presents the Doppler Effect at the target azimuth. The intense clutter null appear at zero Doppler mitigates mainlobe clutter. Jammer and clutter nulls exist at other azimuths do not become visible in this pattern cut.

It should be noted that in the case of MIMO radar by choosing adequately r ($r < N$) the rank r_{MIMO} is smaller than r_{SIMO} the rank of the corresponding SIMO. Indeed, while being a reduced rank subspace based technique as the FAPI algorithm, it requires much less training snapshots to converge than the SMI method. Contrarily to the SMI it also has a low computational cost which is a linear function of the dimension of the virtual received signal vector.

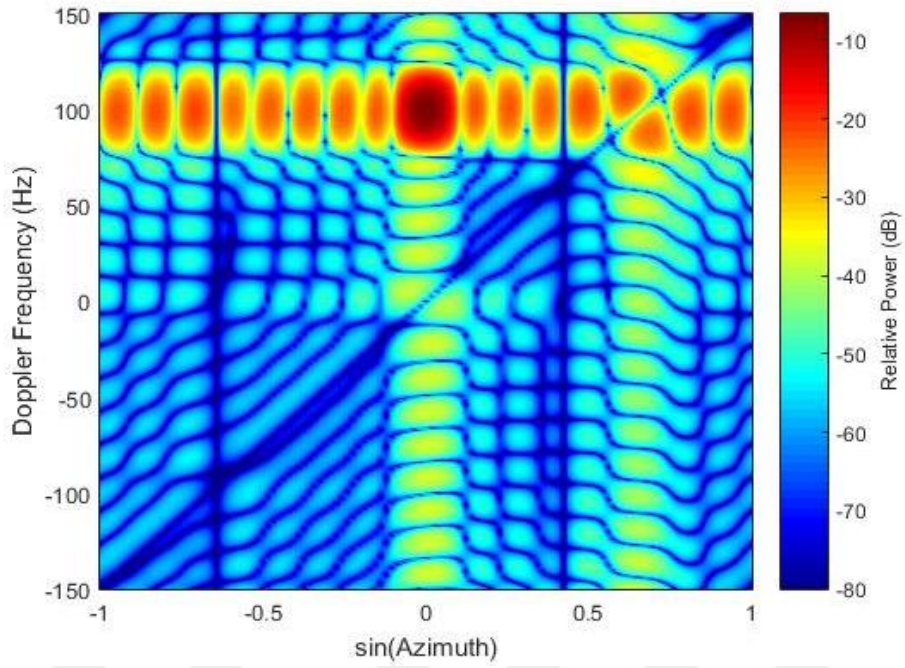


Figure.4.10: FAPI algorithm STAP of SIMO radar $N=18$, $M=1$, $L=18$.

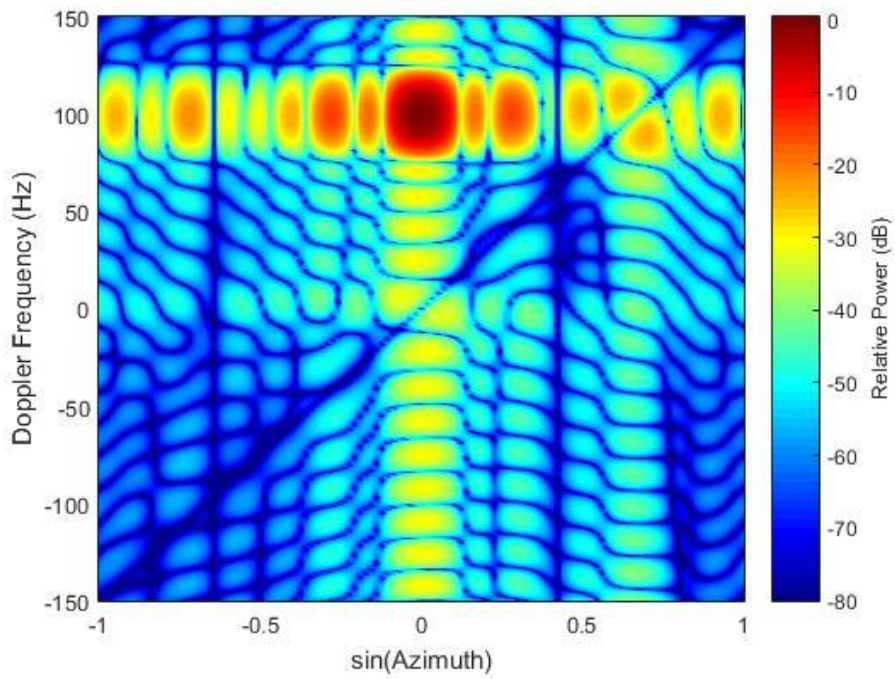


Figure.4.11: FAPI algorithm STAP of MIMO radar $N=6$, $M=3$, $L=18$.

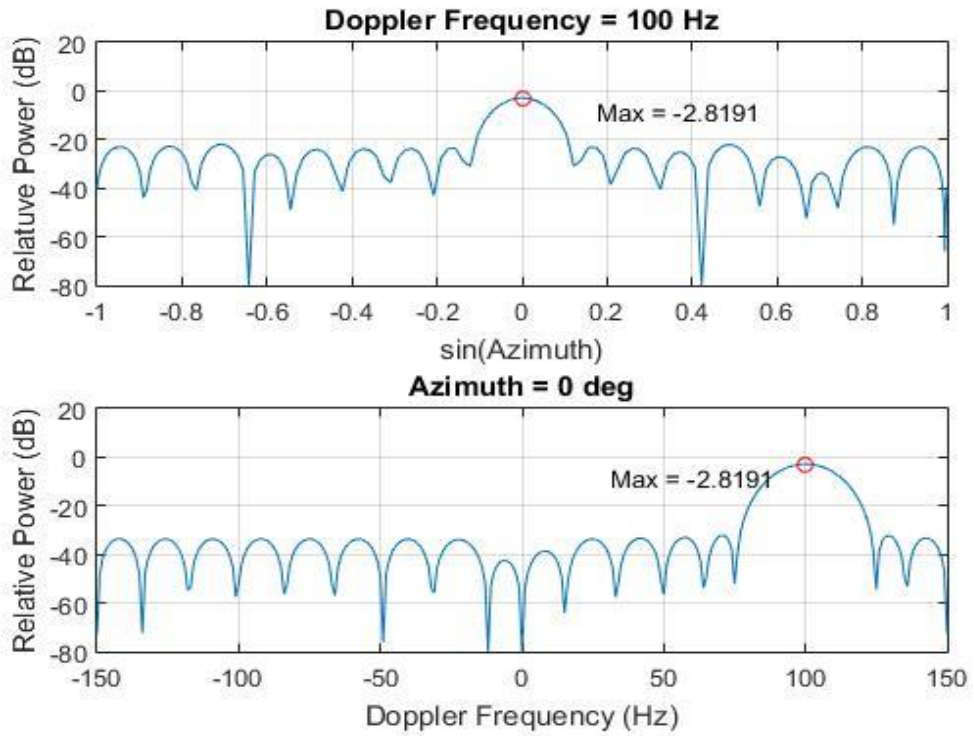


Figure.4.12: Principal plane cuts at target azimuth and Doppler of **FAPI** algorithm SIMO radar $N=18, M=1, L=18$.

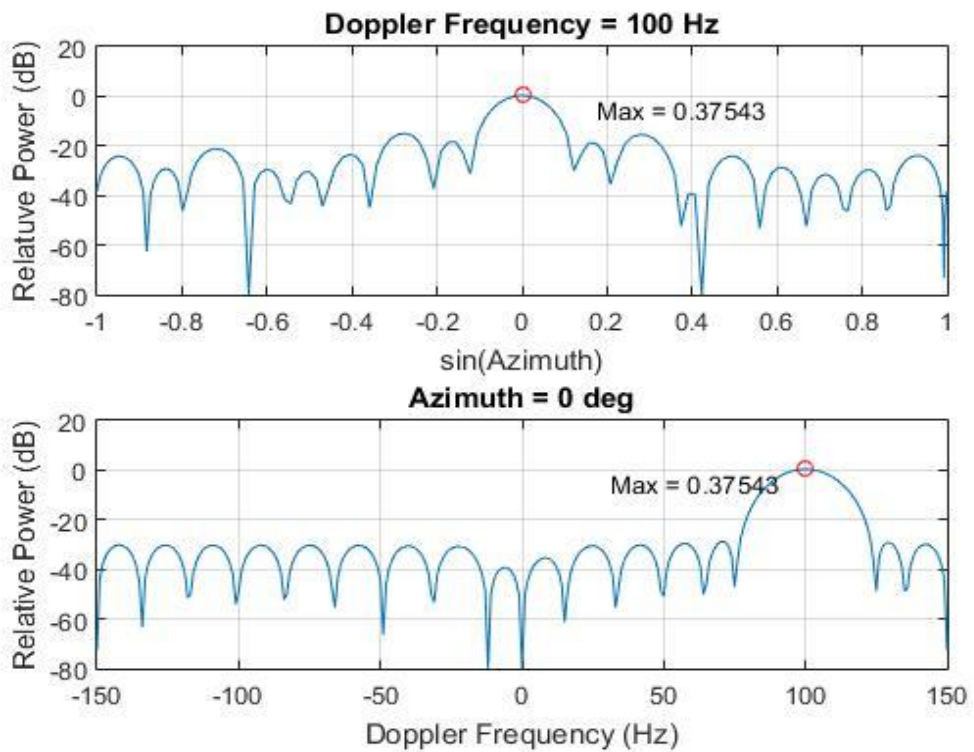


Figure.4.13: Principal plane cuts at target azimuth and Doppler of **FAPI** algorithm MIMO radar $N=6, M=3, L=18$.

Figure 4.14 and Figure 4.15 depicted adapted patterns for FAPI algorithm STAP of MIMO radar with $N+M=18$ (same antennas number with SIMO) and two original cuts of this pattern. The azimuth pattern at the target Doppler illustrates the receive beamformer. The second cut presents the Doppler Effect at the target azimuth.

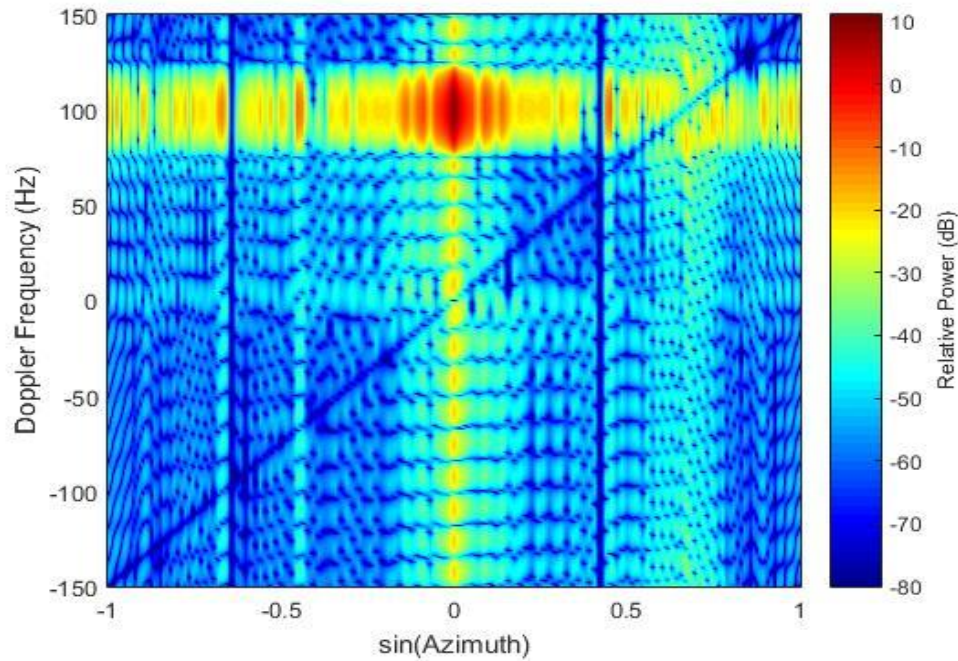


Figure.4.14: FAPI Algorithm STAP of MIMO radar $N=9$, $M=9$, $L=18$.

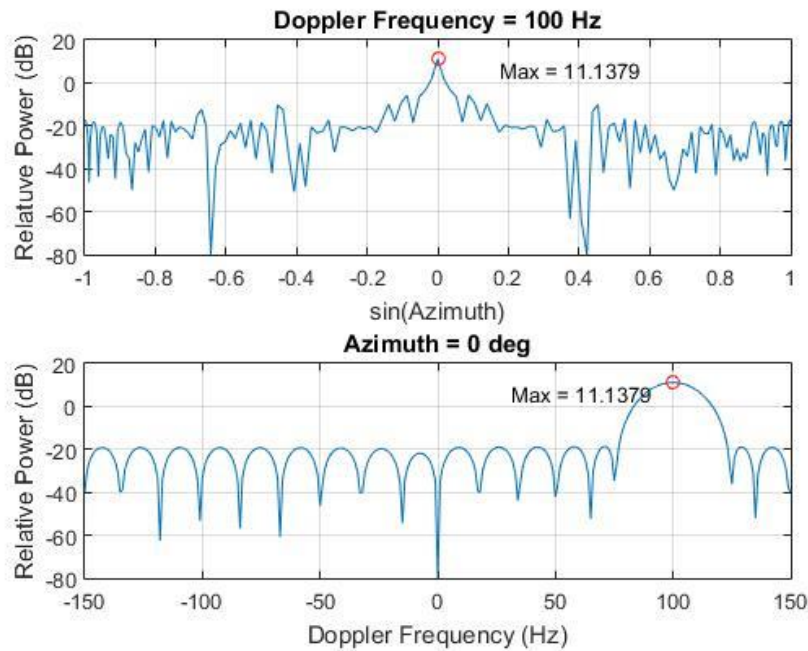


Figure.4.15: Principal plane cuts at target azimuth and Doppler of **FAPI** algorithm MIMO radar $N=9$, $M=9$, $L=18$.

4.3 Fast and stable YAST Algorithm in STAP

In Figure 4.16 and Figure 4.17 the performances of the SIMO and MIMO versions of the YAST algorithm are illustrated in the same conditions that those of Figures 4.2 and 4.3. Figure.4.18 and Figure.4.19 show the two original cuts of this patterns. The azimuth pattern at the target Doppler illustrates the receive beamformer. The second cut presents the Doppler Effect at the target azimuth. The intense clutter null appear at zero Doppler mitigates mainlobe clutter. Jammer and clutter nulls exist at other azimuths do not become visible in this pattern cut.

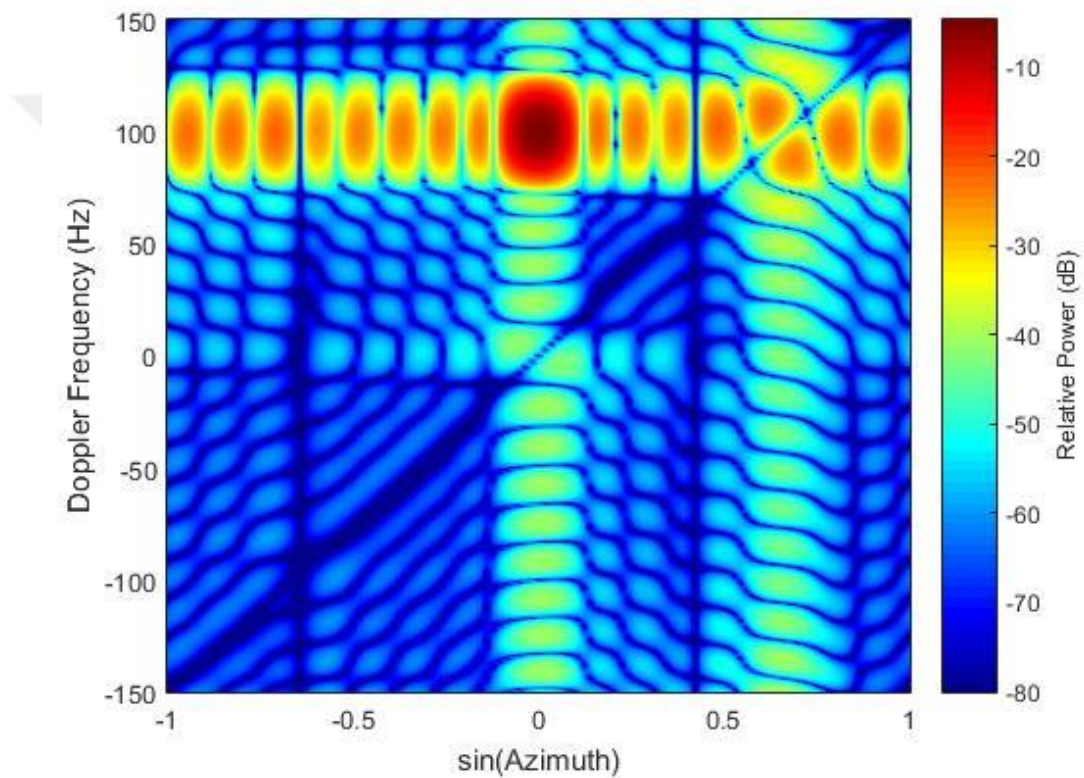


Figure.4.16: fast and stable YAST algorithm STAP of SIMO radar $N=18$, $M=1$, $L=18$.

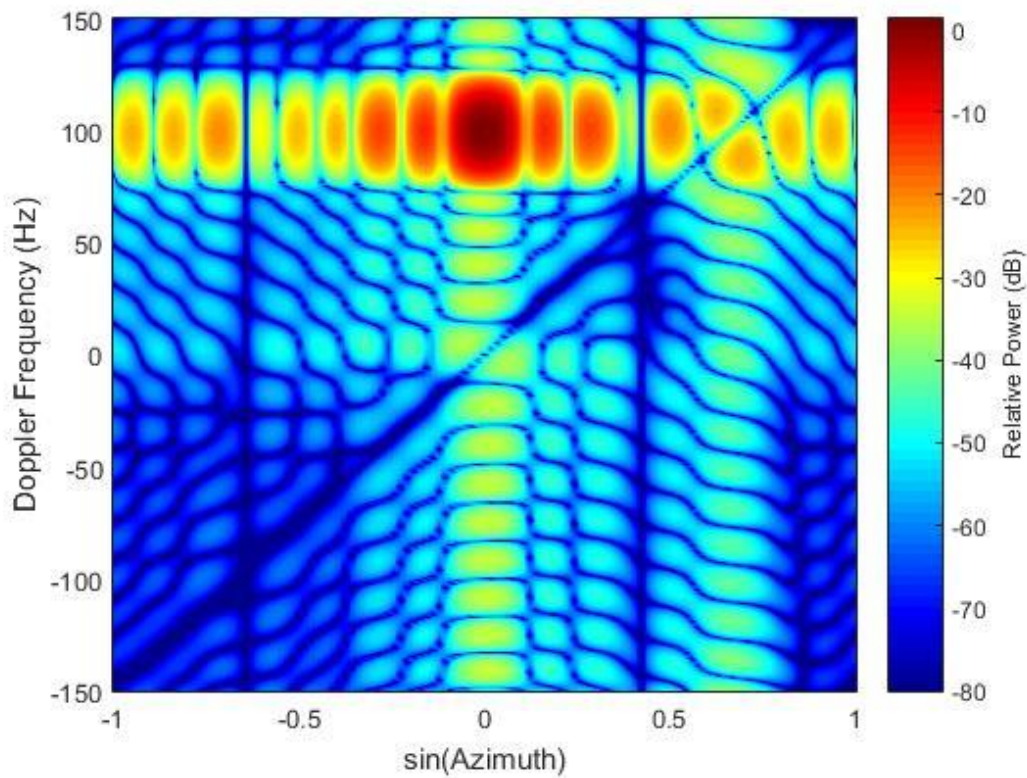


Figure.4.17: fast and stable **YAST** algorithm STAP of MIMO radar $N=6$, $M=3$, $L=18$.

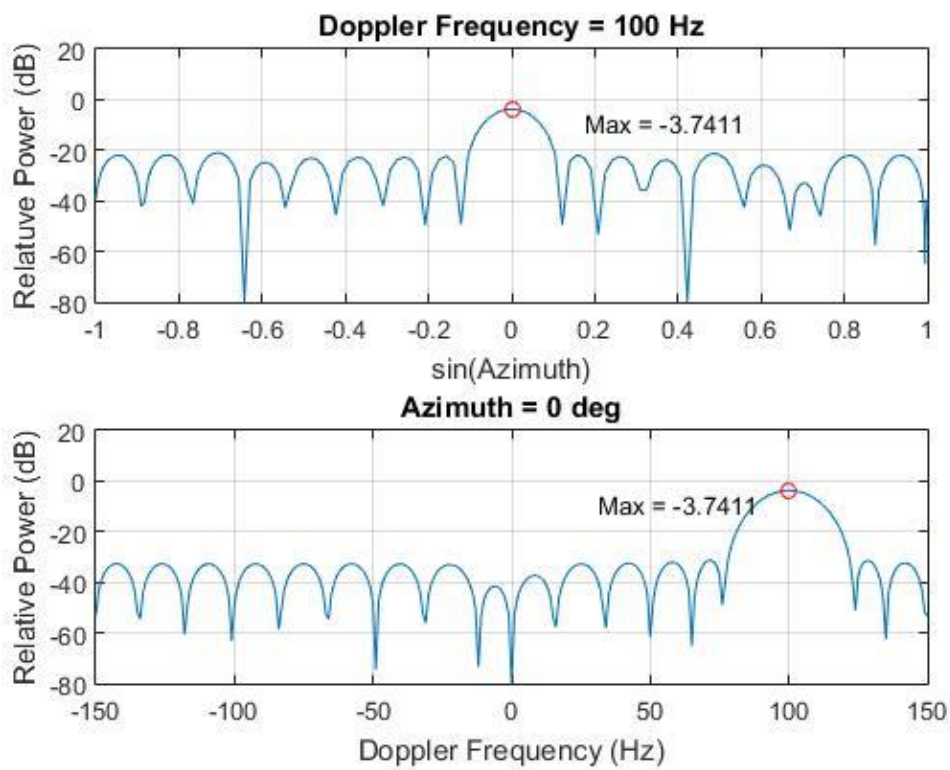


Figure.4.18: Principal plane cuts at target azimuth and Doppler of **YAST** algorithm SIMO radar $N=18$, $M=1$, $L=18$.

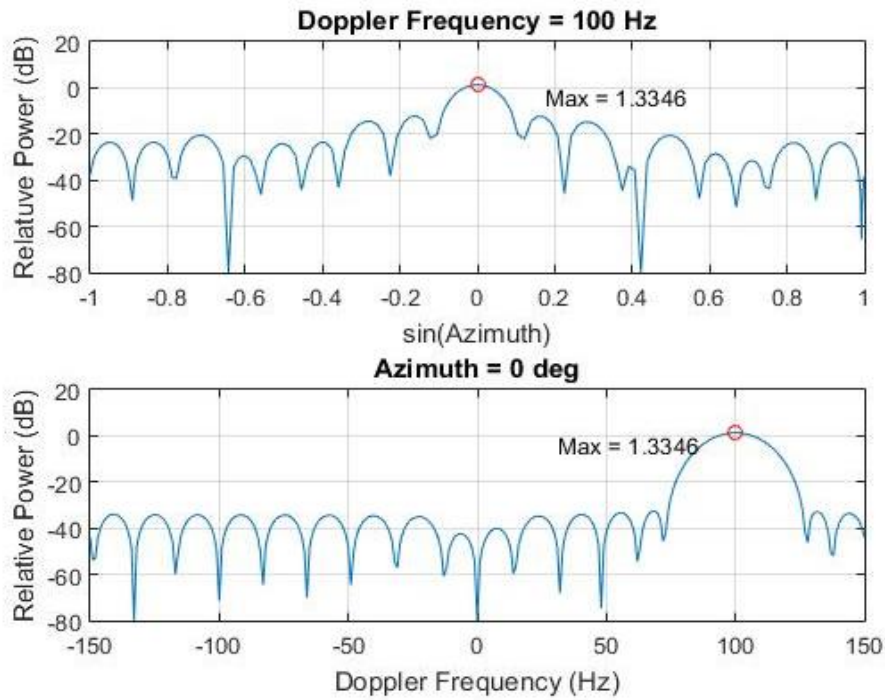


Figure.4.19: Principal plane cuts at target azimuth and Doppler of YAST algorithm MIMO radar $N=6$, $M=3$, $L=18$.

Figure 4.20 and Figure 4.21 show adapted patterns for YAST algorithm STAP of MIMO radar with $N+M=18$ (same antennas number with SIMO) and two original cuts of this pattern. The azimuth pattern at the target Doppler illustrates the receive beamformer. The second cut presents the Doppler effect at the target azimuth.

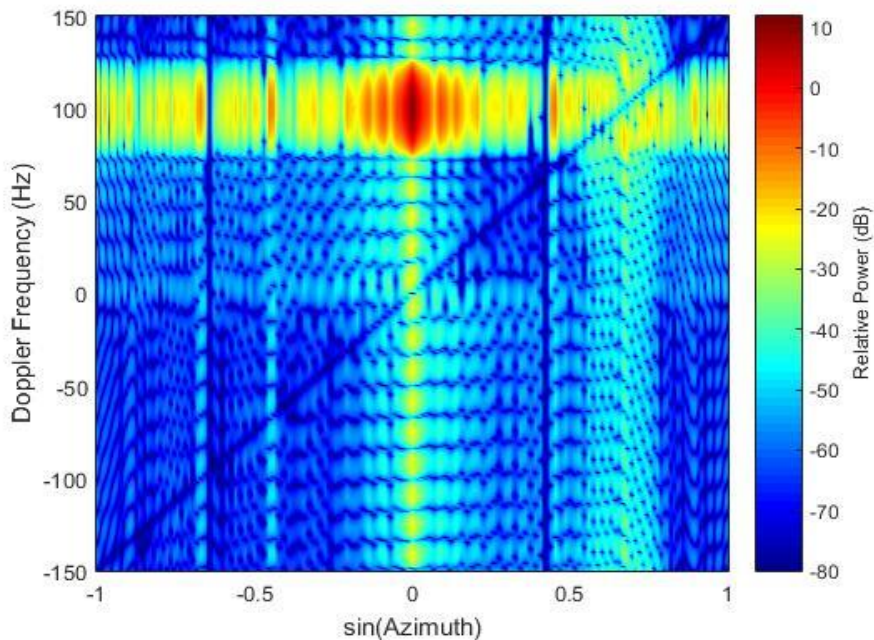


Figure.4.20: YAST Algorithm STAP of MIMO radar $N=9$, $M=9$, $L=18$.

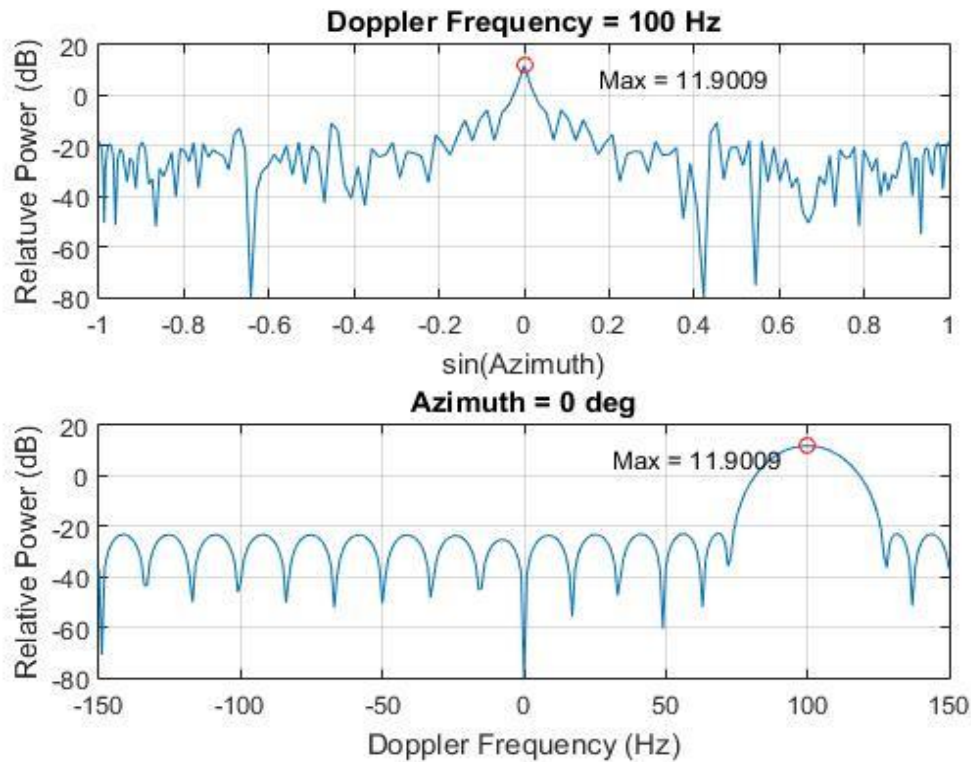


Figure.4.21: Principal plane cuts at target azimuth and Doppler of YAST algorithm MIMO radar N=9, M=9, L=18.

Figure.4.22 and Figure.4.23 compare fully adaptive performance with FAPI and YAST for the example scenario of MIMO radar. Assume SNR 0 dB. Optimum fully adaptive space time processing achieves about 25 dB SINR over the most of the Doppler space. In the existence of interference condition, optimum fully adaptive STAP is granting near maximum gain on target while mitigating both jamming and clutter to well below thermal noise. When the target is near 0 Hz or 300 Hz the SINR is extremely small, because in this condition the target is near the mainlobe clutter in both Doppler and angle. Efficiency decline as the target drop into the corresponding null that the application has appointed on the mainlobe clutter.

The same figures also illustrate the efficiency of FAPI and YAST STAP. The YAST and FAPI efficiency is always a little lower than the optimum. Conversely, the form of the curve is similar to the fully adaptive technique. Over most of the Doppler space, the SINR achieved with FAPI and YAST STAP is about 1.8 dB less than optimum.

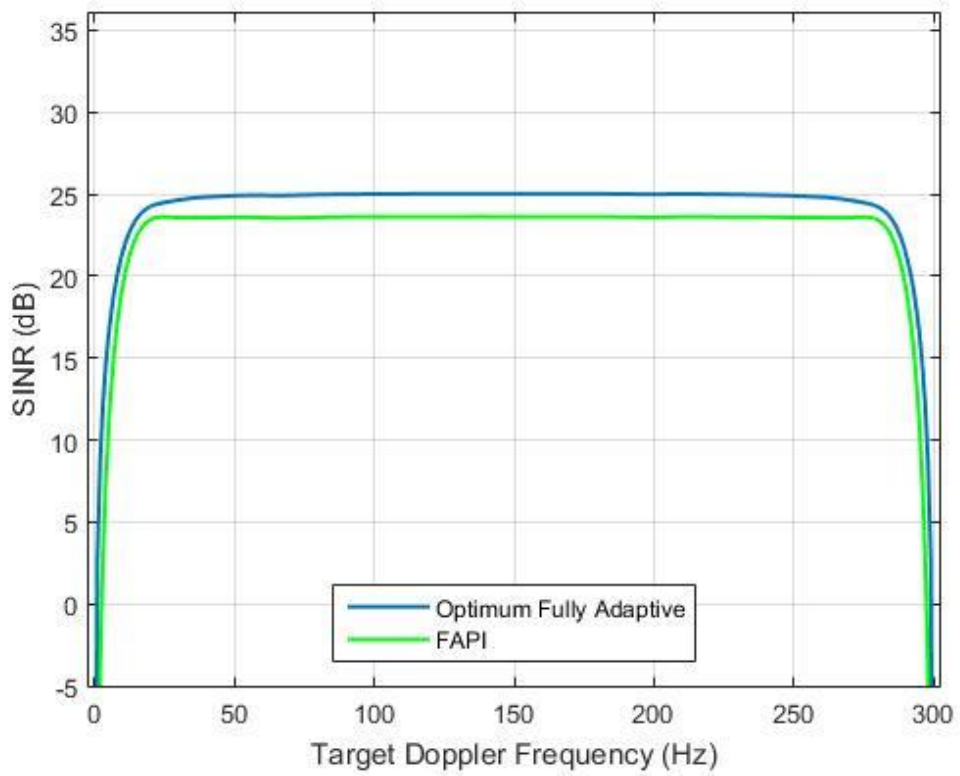


Figure.4.22: SINR for the optimum and FAPI STAPs.

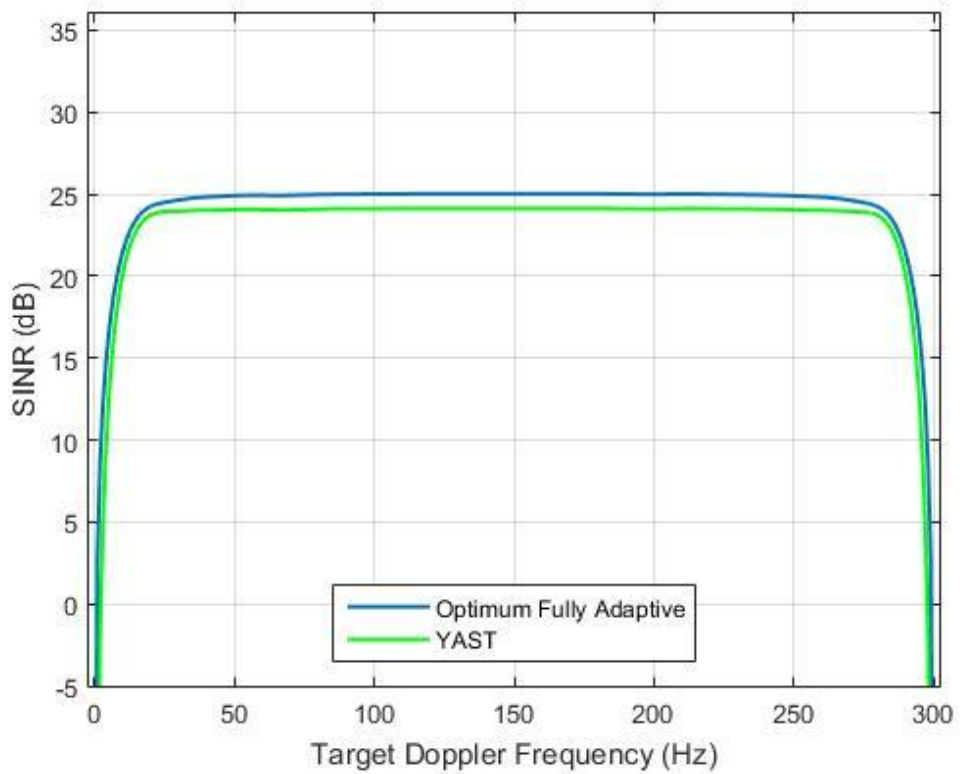


Figure.4.23: SINR for the optimum and YAST STAPs.



REFERENCES

- [1] **M. A. Richards.** (2005). *Fundamentals of Radar Signal Processing*, McGraw-Hill.
- [2] **H. L. Van Tree.** (2001). *Detection, Estimation, and Modulation Theory, Part I*, Wiley-Interscience.
- [3] **N. Levanon and E. Mozeson.** (2004). *Radar Signals*, Wiley-IEEE Press.
- [4] **M. Skolnik.** (2001). *Introduction to Radar Systems*, McGraw-Hill.
- [5] **V.S. Chernyak.** (1998). “*Fundamentals of Multisite Radar Systems : Multistatic Radars and Multiradar Systems*”, Gordon and Breach Science Publishers.
- [6] **J. Li, P. Stoica.** (2009). “*MIMO Radar Signal Processing*”, Wiley,
- [7] **T. Johnsen, K.E. Olsen.** (2006). “*Bi- and Multistatic Radar*”, Nato Documents, RTO-EN-SET-086, Jul.
- [8] **A.Hassanien and S. Vorobyov.** (2010). “*Phased-MIMO Radar: A Tradeoff Between Phased-Array and MIMO Radars*”, IEEE Transactions on Signal Processing, vol. 58, no. 6, pp. 3137-3151.
- [9] **B. Liu, Z. He, J. Zeng and B. Liu.** (2006). “*Polyphase Orthogonal Code Design for MIMO Radar Systems*”.
- [10] **H. Deng.** (2004). “*Polyphase Code Design For Orthogonal Netted Radar Systems*”, IEEE Transactions on Signal Processing, vol. 52, pp. 3126-3135.
- [11] **B. Donnet and I. Longstaff.** (2006). “*MIMO radar, techniques and opportunities*”, Proc. 3rd Eur. Radar Conf., pp. 112-115.
- [12] **F.C. Robey, S. Coutts, D. Weikle, J.C. McHarg, K. Cuomo.** (2004). “*MIMO Radar Theory And Experimental Results*”, Proceedings of the 38th Asilomar Conference on Signals, Systems and Computers, vol. 1, pp. 300-304.
- [13] **J. Li, P. Stoica, L. Xu and W. Roberts.** (2007). “*On Parameter Identifiability Of MIMO Radar*”, IEEE Signal Processing. Letters, vol. 14, no. 12, pp. 968-971.
- [14] **J. Li and P. Stoica.** (2006). “*MIMO Radar – Diversity Means Superiority*”, Proceedings of the 14th Annular Workshop on Adaptive Sensor Array Processing, MIT Lincoln Laboratory, Lexington, MA.
- [15] **J. Li and P. Stoica.** (2007). “*MIMO Radar With Colocated Antennas*”, IEEE Signal Processing. Magazine, vol. 24, no. 5, pp. 106-114.
- [16] **R. Klemm.** (2002). *Principles of space-time adaptive processing*, IEE, London.
- [17] **D. C. Schleher.** (1991). *MTI and Pulsed Doppler Radar*, Artech House.

- [18] **V. F. Mecca, D. Ramakrishnan, and J. L. Krolik.** (2007). “MIMO radar space-time adaptive processing for multipath clutter mitigation,” *Proc. IEEE Workshop Sensor Array Multichannel Signal Processing*, pp. 249–253.
- [19] **J. R. Guerci.** (2003). *Space-Time Adaptive Processing*. Norwood, MA: Artech House.
- [20] **D. W. Bliss and K. W. Forsythe.** (2003). “Multiple-input multiple-output (MIMO) radar and imaging: Degrees of freedom and resolution,” in *Proc. 37th IEEE Asilomar Conf. Signals, Systems, Computers*, vol. 1, pp. 54–59.
- [21] **J. Capon.** (1969). “High-resolution frequency-wavenumber spectrum analysis,” *Proc. IEEE*, vol. 57, no. 8, pp. 1408–1418.
- [22] **H.L.Van Trees.** (2002). “Optimum array processing”, Part IV of “Detection, estimation and modulation theory”, Wiley.
- [23] **J. Ward.** (1994). “Space-time adaptive processing for airborne radar”, Technical report 1015, Lincoln Laboratory.
- [24] **I.S. Reed, J.D. Mallett, and L.E. Brennan.** (1974). “Rapid convergence rate in adaptive arrays,” *IEEE Transactions AES*, Vol. 10, No. 6, pp. 853-863.
- [25] **R. Klemm.** (1983). “Adaptive clutter suppression for airborne phased array radars,” *Proc. Inst. Elect. Eng. F*, vol. 130, no. 1, pp. 125–132.
- [26] **L. E. Brennan and F. M. Staudaher.** (1992) “Subclutter visibility demonstration,” Adaptive Sensors, Inc., Santa Monica, CA, Tech. Rep. RL-TR-92-21.
- [27] **N. A. Goodman and J. M. Stiles.** (2007). “On clutter rank observed by arbitrary arrays,” *IEEE Trans. Signal Process.* vol. 55, no. 1, pp. 178–186.
- [28] **R. Klemm,** (1993). “Adaptive air- and spaceborne MTI under jamming conditions,” in *Proc. IEEE Nat. Radar Conf*, pp. 167–172.
- [29] **D. Slepian and H. O. Pollak.** (1962). “Prolate spheroidal wave functions, Fourier analysis and uncertainty—III: The dimension of the space of essentially time-and-band-limited signals,” *Bell Syst. Tech. J.*, pp. 1295–1336.
- [30] **J. P. Keener.** (1988). *Principles of Applied Mathematics*. Reading, MA: Addison- Welsley.
- [31] **R. A. Horn and C. R. Johnson.** (1985). *Matrix Analysis*. Cambridge, U.K.: Cambridge Univ. Press.
- [32] **R. Badeau, B. David, and G. Richard.** (2005). “Fast approximated power iteration subspace tracking,” *IEEE Trans. On Signal Processing*, vol. 53, pp.2931–2941.
- [33] **H. Belkacemi and S. Marcos.** (2006). “Fast iterative subspace algorithms for airborne STAP radar”, ” in *Journal of Signal Processing Special Issue on Multisensor Processing for Signal extraction and applications*, article ID 37296.
- [34] **B. Yang.** (1995). ”Projection Approximation Subspace Tracking,” *IEEE Trans. On Signal Processing*, vol. 43, pp. 95–107.
- [35] **R. Badeau , G. Richard and B. David.** (2008). "Fast and stable YAST algorithm for principal and minor subspace tracking", *IEEE Trans. Signal Process.*, vol. 56, no. 8, pp. 3437-3446.

- [36] **F.E. Nathanson.** (1991). *Radar Design Principles, Second Edition*, McGraw-Hill, Inc.
- [37] **S.B.AKDEMİR.** (2010). ” *An Overview Of Detection In MIMO Radar*” A Thesis Submitted To Middle East Technical University.
- [38] **R. Badeau , B. David and G. Richard.** (2005). "Yet another subspace tracker", *Proc. IEEE ICASSP\05*, vol. 4, pp. 329-332.





CURRICULUM VITA



Candidate's full name: Meysam Behnam Khajehpasha

Place and date of birth: Iran – Urmia - 13/06/1985

Permanent Address: Iran - Urmia

B.Sc.: Electronic and Communication Engineering
Urmia University (2005-2010)
Electronic Engineering Faculty

Publications: